

國立交通大學

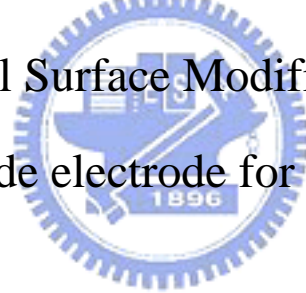
材料科學與工程研究所

碩士論文

奈米碳管化學表面改質應用於直接甲醇燃料電池

陰極電極之研究

Study of Chemical Surface Modifications of CNTs as  
cathode electrode for DMFC



研究生：莊方慈

指導教授：陳家富 教授

中華民國 九十五年 七月

奈米碳管化學表面改質應用於直接甲醇燃料電池  
陰極電極之研究

Study of Chemical Surface Modifications of CNTs as  
cathode electrode for DMFC

研 究 生：莊方慈                      Student:Fang-Tzu Chuang

指 導 教 授：陳家富 教授            Advisor:Prof. Chia-Fu Chen

國立交通大學

材料科學與工程研究所



A Dissertation Submitted to Institute of Material Science and  
Engineer College of Engineering  
National Chiao Tung University

in partial Fulfillment of the requirements for the Degree of  
Master of Science in Material Science and Engineerung

July, 2006

Hsinchu, Taiwan, Republic of China

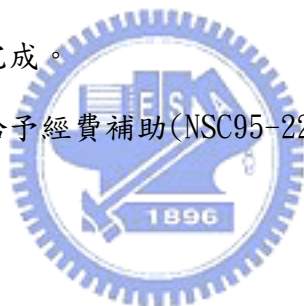
中華民國 九十五年七月

## 誌 謝

很幸運能來到交大材料所研習，並且在學術研究上作出貢獻，當然除了是自己本身要努力外，而身邊的人亦予我許多協助。本論文能順利完成，首先感謝指導教授陳家富老師，感謝老師這二年來，在研究大方向及儀器設備提供指導，且在修課時以予專業知識的教導，故能在研習的領域有所進展。

在實驗部分，則首先感謝陳建仲學長，龔亮仁學長予我在設計實驗的構想及規劃；除此之外，他們不吝與我一同討論分析結果，協助我克服許多實驗上的問題。再來特別感謝清大的陳燦耀學長及實驗室的劉厥揚學長，協助我在實驗中重要部分的製程及試片分析。然而當實驗遇到困境時，陳建銘學長，徐振航學長，羅鴻鈞學長，施騰凱學長，洪淙琦學長以及王瑞豪學長都會適時予我些想法及鼓勵；再加上平日與陳宜輝同學互相勉勵下，督促自己順利將實驗完成。

最後感謝國家科學委員會給予經費補助(NSC95-2218-E-009-009.)



# 奈米碳管化學表面改質應用於直接甲醇燃料電池

## 陰極電極之研究

研究生：莊方慈

指導教授：陳家富 教授

國立交通大學

材料科學與工程研究所

### 摘要

本研究是以多壁奈米碳管作為直接甲醇燃料電池陰極部分的鉑觸媒載體，因此先在碳布上直接生成大量且具方向性的多壁奈米碳管；此方法可以簡化碳管應用於陰極的製程，且碳布上的奈米碳管具有高附著性。

再以高溫條件，使用  $\text{HNO}_3$ 、 $\text{H}_2\text{SO}_4$ 、 $\text{KOH}$  作為多壁奈米碳管的化學表面改質溶液，以產生官能基鍵結在奈米碳管上，促進鉑離子均勻地及高密度地披覆在多壁奈米碳管表面上。並探討溫度、時間、濃度對多壁奈米碳管化學表面改質之效應，而利用 FTIR、XPS、EDX、CV 的分析，我們發現多壁奈米碳管在 6 小時的 14M  $\text{HNO}_3$  處理下，可以產生大量官能基以協助電化學觸媒鉑金屬的披覆，進而提升陰極部分的電池效能。

# **Study of Chemical Surface Modifications of CNTs as cathode electrode for DMFC**

Student: Fang-Tzu Chuang

Advisor: Prof. Chia-Fu Chen

Institute of Material Science and Engineering

National Chiao-Tung University

## **Abstract**

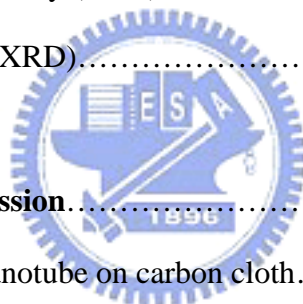
In this study, multi-wall carbon nanotubes (MWNTs) are used as Pt catalyst support for cathode electrode in the direct methanol fuel cell (DMFC). Thus, a lot of well-align MWNTs are fabricated on carbon cloth directly. The method in the cathode electrode of DMFC is easy to constructed and sticking on the carbon cloth tightly.

Then, MWNTs are modified by  $\text{HNO}_3$ ,  $\text{H}_2\text{SO}_4$ , and  $\text{KOH}$  at high temperature may produce different functional groups to attract more Pt ions nucleating uniformly and densely. Moreover, there are the other parameters, temperature, time, and concentration, in the function of chemical modification for MWNTs. In this way, we would find 14M-MWNTs at 6 hours by using FTIR, XPS, EDX, and CV may produce a lot of functional groups to increase Pt anchoring sites. Finally, it could improve the efficiency of half-cell test.

# Contents

Abstract (Chinese).....	I
Abstract (English) .....	II
Contents.....	III
Figure Caption.....	VI
Table Caption.....	X
<b>Chapter 1.Introduction.....</b>	<b>1</b>
1.1 Preface.....	1
1.2 Background of the study.....	5
1.2.1 Pt/Carbon black for DMFC electrode (commerce).....	5
1.2.2 Carbon nanomaterials for DMFC electrode.....	7
1.2.3 Modification of CNTs powder for DMFC electrode.....	8
1.3 Motivation.....	9
<b>Chapter 2.Fundamentals of MEA for DMFC and Modification of CNT.....</b>	<b>10</b>
2.1 Assemble of MEA for DMFC.....	10
2.1.1 Proton Exchange Membrane.....	10
2.1.2 Catalyst Layer.....	10
2.1.3 Gas diffusion layer.....	11
2.2 Principle of DMFC.....	13
2.3 Growth and Characterization of Carbon Nanotube.....	15
2.3.1 Growth Methods.....	15
2.3.2 The growth mechanism of Carbon nanotubes.....	18
2.4 Modification of Carbon Nanotube.....	19

<b>Chapter 3. Experimental Procedures</b> .....	20
3.1 Fabrication of CNT on C Cloth.....	21
3.2 Modification of carbon nanotube on carbon cloth.....	22
3.3 Dispersing of Pt on Prepared Carbon Cloth.....	23
3.4 Analysis Instruments.....	24
3.4.1 Scanning Electron Microscopy (SEM).....	24
3.4.2 Transmission Electron Microscopy (TEM).....	24
3.4.3 X-ray Photoelectron Spectroscopy (XPS).....	25
3.4.4 Fourier Transform Infrared Spectrometer (FTIR).....	26
3.4.5 Cyclic Voltammetry (CV) Potentiostat.....	26
3.4.6 Energy Dispersive X-ray (EDX).....	27
3.4.7 X-Ray Diffraction (XRD).....	28
<b>Chapter 4. Results and Discussion</b> .....	30
4.1 Morphology of carbon nanotube on carbon cloth.....	30
4.2 Multi-wall carbon nanotubes are modified by HNO <sub>3</sub> , H <sub>2</sub> SO <sub>4</sub> , and KOH.....	32
4.2.1 Analysis of functional groups.....	33
4.2.2 Qualitative analysis of Pt on MWNTs.....	37
4.2.3 Analysis of dispersive Pt on MWNTs.....	40
4.2.4 EDX analysis of Pt on MWNTs.....	40
4.2.5 Half-cell test.....	44
4.2.6 Summary.....	44
4.3 Multi-wall carbon nanotubes are modified by HNO <sub>3</sub> with Temperature (T), time (t), and concentration (conc.).....	46
4.3.1.1 Analysis of MWNTs morphology with T.....	47
4.3.1.2 Analysis of functional groups with T.....	47



4.3.2.1 FTIR of 2M HNO <sub>3</sub> -MWNTs with t.....	50
4.3.2.2 EDX analysis of Pt/2M HNO <sub>3</sub> -MWNTs.....	50
4.3.2.3 Half-cell test.....	51
4.3.2.4 Effective activating area.....	51
4.3.3.1 FTIR of 14M HNO <sub>3</sub> -MWNTs with t.....	58
4.3.3.2 EDX analysis of Pt/14M HNO <sub>3</sub> -MWNTs.....	58
4.3.3.3 Half-cell test.....	58
4.3.3.4 Effective activating area.....	59
4.3.4 Summary.....	59
4.4 Analysis of 14M HNO <sub>3</sub> -MWNTs.....	66
4.4.1 Analysis of mean Pt nanoparticle size.....	66
4.4.2 Analysis of MWNTs morphology.....	68
4.4.3 Summary.....	68
<b>Chapter 5. Conclusions</b> .....	<b>72</b>
Reference.....	73





# Figure Captions

## Chapter 1.

Fig.1.1 Fuel cell stack the application on several electronic productions.....	4
Fig.1.2 The development of fuel cell.....	4
Fig.1.3 Thin-film methods for commercial electrode (Pt/C black).....	6
Fig.1.4 PTFE-bound methods and thin-film technique.....	6
Fig.1.5 TEM images of microwave-synthesized Pt nanoparticles supported on different carbon: (a) Vulcan XC-72 carbon; (b) carbon nanotubes.....	7
Fig.1.6 MWNTs are modified by HNO <sub>3</sub> and followed by reduction of metals.....	8

## Chapter 2.

Fig.2.1 The schematic of a unit cell of DMFC.....	11
Fig.2.2 MEA structure.....	12
Fig.2.3 The chemical formula and physical structure of the membrane Nafion®.....	12
Fig.2.4 Illustration of DMFC in Principles.....	13
Fig.2.5 (a)-(c) Schematic experimental setups for nanotube growth methods.....	17
Fig.2.6 Two general growth modes of nanotube in chemical vapor deposition.....	18
Fig.2.7 MWNTs are modified by HNO <sub>3</sub> .....	19

## Chapter 3.

Fig.3.1 Flow chart of experimental procedures.....	20
Fig.3.2 Schematic diagram of the MPECVD system.....	21
Fig.3.3 Schematic diagram of the chemical modification.....	22
Fig.3.4 The experimental procedures of polyol process.....	23
Fig.3.5 Diagram of a Scanning Electron Microscopy.....	24

Fig.3.6 Diagram of a X-ray Photoelectron Spectroscopy.....	25
Fig.3.7 Diagram of a Fourier Transform Infrared Spectrometer.....	26
Fig.3.8 Schematic of a Cyclic Voltammetry (CV) Potentiostat.....	27
Fig.3.9 Elements in an EDX spectrum are identified based on the energy content of the X-rays.....	28
Fig.3.10 Schematic of X-Ray Diffraction.....	29

#### **Chapter 4.**

Fig.4.1 SEM images of pristine carbon cloth with different magnitude.....	31
Fig.4.2 SEM images of MWNTs on carbon cloth with different magnitude.....	31
Fig.4.3 The length of MWNTs is about 20 $\mu\text{m}$ and its diameter is about 20 nm.....	31
Fig.4.4 MWNTs display hollow tubes with amorphous and crystalline layer.....	31
Fig 4.5 The absorption spectra of MWNTs modified by $\text{HNO}_3$ , $\text{H}_2\text{SO}_4$ , and $\text{KOH}$ ...	34
Fig.4.6 XPS survey spectra of MWNTs modified by $\text{HNO}_3$ , $\text{H}_2\text{SO}_4$ , and $\text{KOH}$ .....	35
Fig.4.7 (a) The C 1s spectrum of $\text{HNO}_3$ -MWNTs.....	35
Fig.4.7 (b) The C 1s spectrum of $\text{H}_2\text{SO}_4$ -MWNTs.....	36
Fig.4.7 (c) The C 1s spectrum of $\text{KOH}$ -MWNTs.....	36
Fig.4.8 The mapping of EDX for $\text{HNO}_3$ -MWNTs.....	38
Fig.4.9 The XPS survey spectrum of $\text{HNO}_3$ -MWNTs after the reduction.....	38
Fig.4.10 Chemical shift of binding energy in $\text{Pt}4f_{7/2}$ and $\text{Pt}4f_{5/2}$ with $\text{Ar}^+$ etching.....	39
Fig.4.11 Pt nanoparticles are agglomerated like a larger nanoparticle.....	41
Fig.4.12 Pt nanoparticles disperse uniformly on $\text{HNO}_3$ -MWNTs.....	41
Fig.4.13 The amount of Pt loading on raw MWNTs is 16.88 wt%.....	42
Fig.4.14 The amount of Pt loading on $\text{KOH}$ -MWNTs is 21.23 wt%.....	42
Fig.4.15 The amount of Pt loading on $\text{H}_2\text{SO}_4$ -MWNTs is 22.84 wt%.....	42
Fig.4.16 The amount of Pt loading on $\text{HNO}_3$ -MWNTs is 26.08 wt%.....	43

Fig.4.17 Pt loading on MWNTs with different chemical modification.....	43
Fig.4.18 Electrocatalytic activity is evaluated by the current peaks.....	45
Fig.4.19 Little damage for 14M HNO <sub>3</sub> -MWNTs at 80 <sup>0</sup> C.....	48
Fig.4.20 Little damage for 14M HNO <sub>3</sub> -MWNTs at 90 <sup>0</sup> C.....	48
Fig.4.21 A serious damage for 14M HNO <sub>3</sub> -MWNTs at 100 <sup>0</sup> C.....	48
Fig.4.22 (a) FTIR of 2M HNO <sub>3</sub> -MWNTs with different T.....	49
Fig.4.22 (b) FTIR of 14M HNO <sub>3</sub> -MWNTs with different T.....	49
Fig.4.23 The number of -COOH would increase with t gradually.....	53
Fig.4.24 The amount of Pt loading on raw MWNTs is 14.37 wt%.....	53
Fig.4.25 The amount of Pt loading on 2M HNO <sub>3</sub> -MWNTs at 6 hr is 16.72 wt%.....	54
Fig.4.26 The amount of Pt loading on 2M HNO <sub>3</sub> -MWNTs at 12 hr is 24.38 wt%.....	54
Fig.4.27 The amount of Pt loading on 2M HNO <sub>3</sub> -MWNTs at 18 hr is 28.21 wt%.....	54
Fig.4.28 The amount of Pt loading on 2M HNO <sub>3</sub> -MWNTs at 24 hr is 26.99 wt%.....	55
Fig.4.29 2M HNO <sub>3</sub> -MWNTs from 12 hr to 24 hr may anchor the most Pt.....	55
Fig.4.30 The currents peaks represent the activity of Pt with t.....	56
Fig.4.31 Electrochemically active surface areas of Pt with t.....	57
Fig.4.32 The number of -COOH would increase with t gradually.....	61
Fig.4.33 The amount of Pt loading on raw MWNTs is 15.38 wt%.....	61
Fig.4.34 The amount of Pt loading on 14M HNO <sub>3</sub> -MWNTs at 6 hr is 26.52 wt%.....	62
Fig.4.35 The amount of Pt loading on 14M HNO <sub>3</sub> -MWNTs at 12 hr is 27.94 wt%.....	62
Fig.4.36 The amount of Pt loading on 14M HNO <sub>3</sub> -MWNTs at 18 hr is 25.79 wt%.....	62
Fig.4.37 The amount of Pt loading on 14M HNO <sub>3</sub> -MWNTs at 24 hr is 25.95 wt%.....	63
Fig.4.38 14M HNO <sub>3</sub> -MWNTs from 6 hr to 24 hr may anchor the most Pt.....	63
Fig.4.39 The currents peaks represent the activity of Pt with t.....	64
Fig.4.40 Electrochemically active surface areas of Pt with t.....	65
Fig.4.41 XRD patterns of Pt on raw-MWNTs and 14M HNO <sub>3</sub> -MWNTs.....	69

Fig.4.42 The average diameters for Pt/raw-MWNTs is 5.8802 nm.....70

Fig.4.43 The average diameters for Pt/14M HNO<sub>3</sub>-MWNTs is 7.29 nm.....70

Fig.4.44 (a) raw MWNTs (b) 14M HNO<sub>3</sub>-MWNTs.....70

Fig.4.45 (a) raw MWNTs with Pt (b) 14M HNO<sub>3</sub>-MWNTs with Pt.....71

Fig.4.46 Hypothetical model for stable state of 14M HNO<sub>3</sub>-MWNTs.....71



## Table Captions

### Chapter 1

Table 1.1 Five types of fuel cell characteristics.....	3
--	---

### Chapter 3

Table 3.1 The parameters of the growth of MWNTs.....	21
--	----

### Chapter 4

Table 4.1 MWNTs are modified by HNO <sub>3</sub> , H <sub>2</sub> SO <sub>4</sub> , and KOH.....	32
--	----

Table 4.2 The absorption spectra ranges of several functional groups.....	34
---	----

Table 4.3 The development of the binding energy of Pt4f <sub>7/2</sub> and Pt4f <sub>5/2</sub> with time.....	39
---	----

Table 4.4 HNO <sub>3</sub> -MWNTs with different T.....	46
---	----

Table 4.5 MWNTs are modified by HNO <sub>3</sub> at 90 <sup>0</sup> C for 2M and 14M with t.....	50
--	----

Table 4.6 The value of electrochemically active surface areas of the Pt with the t.....	57
---	----

Table 4.7 The value of electrochemically active surface areas of the Pt with the t.....	65
---	----

Table 4.8 The average size of Pt/raw-MWNTs and Pt/14M HNO <sub>3</sub> -MWNTs.....	69
--	----

# Chapter 1 Introduction

## 1.1 Preface

Over the past few years, the direct conversion of chemical into electrical energy via fuel cells has been at the center of attention of electrochemical research and technology development. This is due not only to the scientifically fascinating complexity of fuel cell reactions and the general awareness of the technological potential of fuel cells, but is also a result of society's strive towards developing environmentally-harmless power generation. **Direct methanol fuel cell (DMFC)** for instance, the product of the reaction is only little water and carbon dioxide and is free of nitrogen oxide, carbon monoxide, sulfite, and hydrocarbon.

W. R. Grove reported that the reaction between hydrogen and oxygen in 1839. However, the first application of fuel cell was in the 1960s as an auxiliary power source in the Gemini space flights. Subsequently, advances in this technology were stagnant until the late 1980s when the fundamental design underwent significant reconfiguration. In the recent years, the new applications are in decentralized power supply systems, in portable products, and in sensor technology. In the quest for a highly efficient, emission-free drive system, the development of mobile automotive fuel cell units is proving to be quite promising.

A variety of fuel cells are in different stages of development. The most common classification of fuel cells is on the basis of the type of electrolyte used in the cells and includes **(1) polymer electrolyte fuel cell (PEFC)**, **(2) alkaline fuel cell (AFC)**, **(3) phosphoric acid fuel cell (PAFC)**, **(4) molten carbonate fuel cell (MCFC)**, and **(5) solid oxide fuel cell (SOFC)**. The basic characteristics of these five types of fuel cell are listed in Table 1.1 and Fig 1.1 show present fuel cell stack application on several electronic productions.

In recent years, the DMFC used for vehicle transportation and local power generation has received increasing attention in Fig 1.2. Due to its high electrochemical performance efficiency, simple stack design, pollution-free, noise-free, and low temperature operation, DMFC has become a promising candidate for portable power source. Besides, DMFC with the promises

such as the elimination of electrolyte leakage and lower corrosion has applications in the areas of military, aerospace and transportation.

The electrode of DMFC is consistent of electro-chemical catalyst Pt / C. Many researches about rising Pt performance efficiency and Pt amount reduction are still facing the challenge the widely application of the membrane and electrode assembly (MEA). In this study, **multi-wall carbon nanotubes (MWNTs)** modified by chemical solution are acted as support instead of commercial carbon black to support and disperse Pt. It is allowed to rise performance efficiency of Pt in the electrode.



**Table 1.1 Five types of fuel cell characteristics**

	PEFC	AFC	PAFC	MCFC	SOFC
Electrolyte	Hydrated Polymeric Ion Exchange Membranes	Mobilized or Immobilized Potassium Hydroxide in asbestos matrix	Immobilized Liquid Phosphoric Acid in SiC	Immobilized Liquid Molten Carbonate in LiAlO <sub>2</sub>	Perovskites (Ceramics)
Electrodes	Carbon	Transition metals	Carbon	Nickel and Nickel Oxide	Perovskite and perovskite / metal cermet
Operating Temperature	40 - 80 °C	65 - 220 °C	205 °C	650 °C	600 - 1000 °C
Charge Carrier	H <sup>+</sup>	OH <sup>-</sup>	H <sup>+</sup>	CO <sub>3</sub> <sup>2-</sup>	O <sup>2-</sup>
Catalyst	Pt	Pt	Pt	Ni	Perovskites/Ni
CO impact	Poison	Poison	Poison	Fuel	Fuel
Product Heat Management	Process Gas + Liquid Cooling Medium	Gas + Electrolyte Circulation	Process Gas + Liquid cooling medium or steam generation	Internal Reforming + Process Gas	Internal Reforming + Process Gas
Efficiency (LHV)	30-45%	30-50%	30-45%	45-60%	45-75%
Major Advantages / Disadvantages	Quick start-up H <sub>2</sub> preferable Heat & water management issues	Pure H <sub>2</sub> Good performance Expensive	Lower performance than AFC Expensive	Wider fuel choices Cogeneration Corrosive liquid electrolyte	All ceramic Wider fuel choices Co-generation Durability
Example of installed units	250 kW (Ballard)	12 kW (for space shuttles) (ZeTek)	1.2 MW 5,000 h (Milan)	2 MW 4,000 h (Fuel Cell Energy)	300, 220 kW; 100kW-17500h (SWPC)
Major Applications	Transportation Stationary	Space Stationary Transportation	Stationary	Stationary Transportation (APU)	Stationary Transportation (APU)

[<http://www.ip3.unipg.it/FuelCells/en/whatisit.asp>]





**Fig 1.1 Fuel cell stack the application on several electronic productions**

[engadget.com ; pr.fujitsu.com ; www.maxmoto.co.uk ; files.automotiveforums.com]

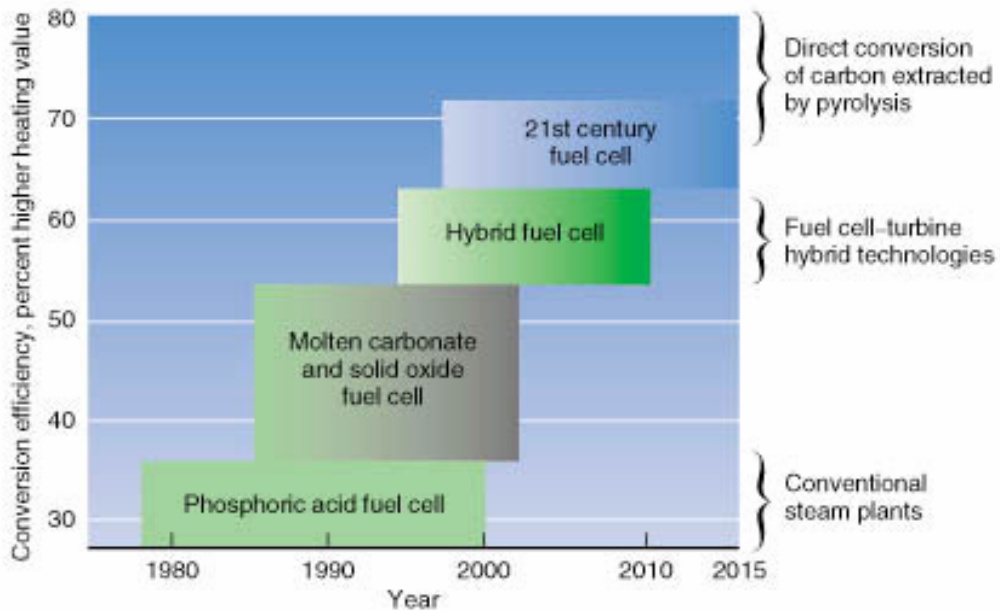


**Fig 1.2 The development of fuel cell**

[www.cms.llnl.gov/s-t/carbon\\_con.html](http://www.cms.llnl.gov/s-t/carbon_con.html)

## 1.2 Background of the Study (Literature Review)

### 1.2.1 Pt/Carbon black for DMFC electrode (Commerce)

Before the development of the thin-film catalyst layer [1], PTFE-bound catalyst layers were the convention [2–5]. In these catalyst layers, the catalyst particles were bound by a hydrophobic PTFE structure commonly cast to the diffusion layer. This method was able to reduce the platinum loading of prior **direct methanol fuel cells (DMFC)** by a factor of 10; from 4 to 0.4 mg/cm<sup>2</sup> [5]. In order to provide ionic transport to the catalyst site, the PTFE-bound catalyst layers are typically impregnated with Nafion by brushing or spraying. However, platinum utilization in PTFE-bound catalyst layers remains approximately 20 wt% [4, 6]. Nevertheless, researchers have continued to work on developing new strategies for Nafion impregnation [3].

The present convention in fabricating catalyst layers for DMFC is to employ thin-film methods in Fig. 1.3. In his 1993 patent, Wilson [1] described the thin-film technique for fabricating catalyst layers for DMFC with catalyst loadings less than 0.35 mg/cm<sup>2</sup>. In this method the hydrophobic PTFE traditionally employed to bind the catalyst layer is replaced with hydrophilic perfluorosulfonate ionomer (Nafion). Thus, the binding material in the catalyst layer is composed of the same material as the membrane. Even though PTFE features effective binding qualities and imparts beneficial hydrophobicity in the gas diffusion layers, there is no particular benefit to its presence in the catalyst layer [7]. Thin-film catalyst layers have been found to operate at almost twice the power density of PTFE-bound catalyst layers. This correlates with an active area increase from 22 to 45.4% when a Nafion-impregnated and PTFE-bound catalyst layer is replaced with a thin-film catalyst layer. Their methodology is schematically described in Fig. 1.4.

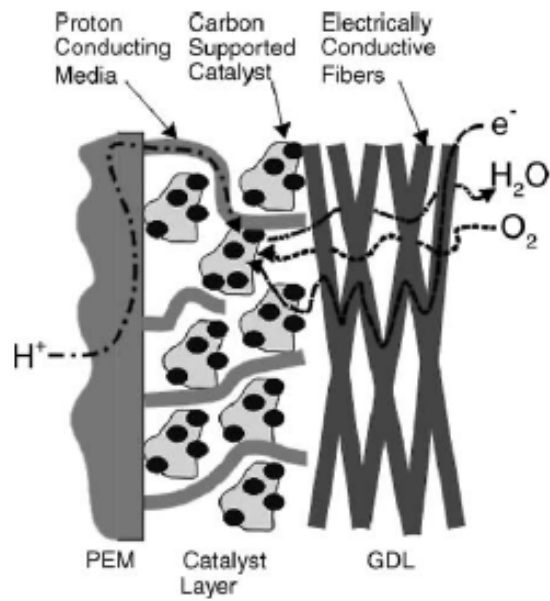


**Fig. 1.3 Thin-film methods for commercial electrode (Pt/C black)**

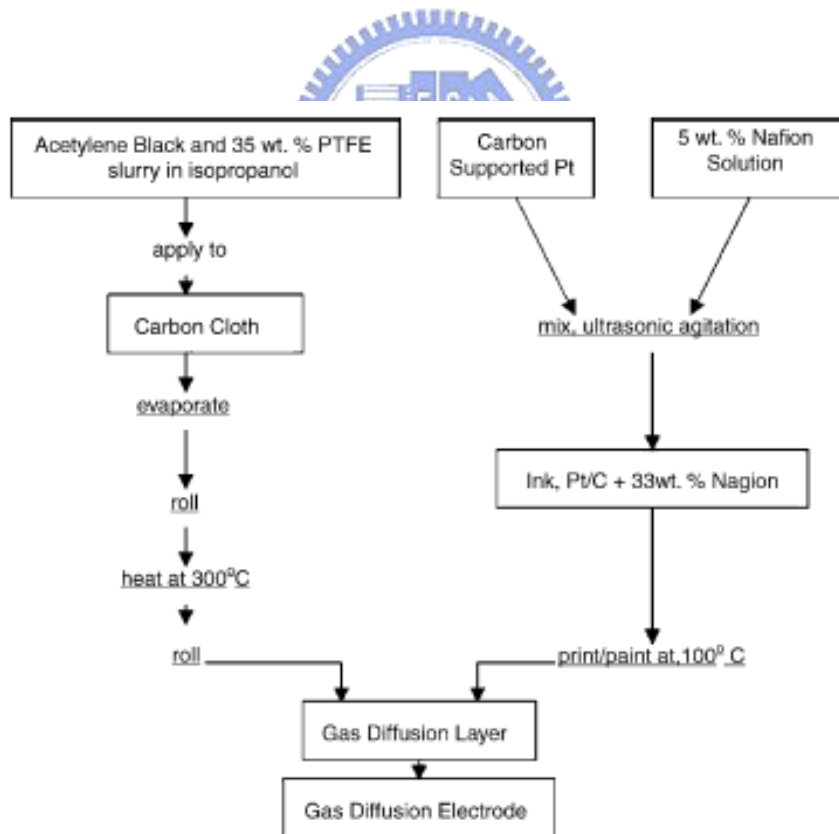


**Fig. 1.4 PTFE-bound methods and thin-film technique**

## 1.2.2 Carbon nanomaterials for DMFC electrode

In the last section, carbon blacks were mainly employed as supporting materials for fuel cell application. Uchida et al. [8] reported the effect of microstructure within various carbon blacks. Recently, nanostructured carbon materials [9], graphite carbon nanofiber [10,11], mesocarbon microbeads [12], and **carbon nanotubes (CNTs)** [13–17] were utilized as supporting materials of catalysts where the dispersion of platinum or platinum-based alloy nanoparticles were affected. Vulcan XC-72 carbon black is commonly used as a carbon supporting materials for electrode catalysts in DMFCs. In this report, CNTs were used as the supporting material.

Fig. 1.5 (a) and (b) are typical TEM images of Vulcan carbon-supported and CNT supported catalysts, showing a remarkably uniform and high dispersion of metal particles on the surface of carbon material.

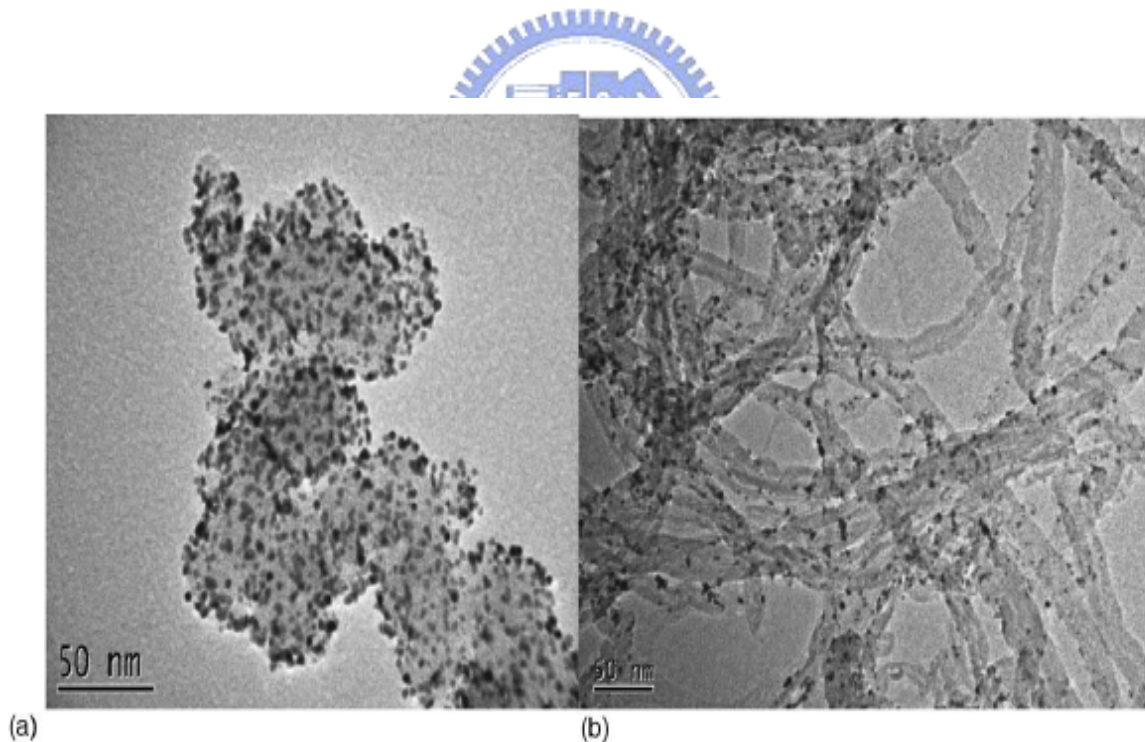


**Fig. 1.5 TEM images of microwave-synthesized Pt nanoparticles supported on different carbon: (a) Vulcan XC-72 carbon; (b) carbon nanotubes**

### 1.2.3 Modification of CNTs powder for DMFC electrode

One method of metal deposition on CNT surface has been introduced: CNTs impregnated with an alcoholic solution of hexachloroplatinic acid was calcinated at high temperature, under nitrogen or hydrogen atmosphere to convert platinum ion to platinum crystallites whose size was dependent on the calcination temperature and time. Che et al. [16] prepared electrocatalysts (i.e., Pt, Ru, and PtRu nanoparticles on CNTs) by this method in Fig. 1.6.

Another general method to obtain a more controlled and specific nucleation of metals and metal compounds on the surface is to modify the multi-wall carbon nanotubes (MWNTs) surface through oxidation to introduce anchoring sites, and then to attach metals on the sites through reduction.

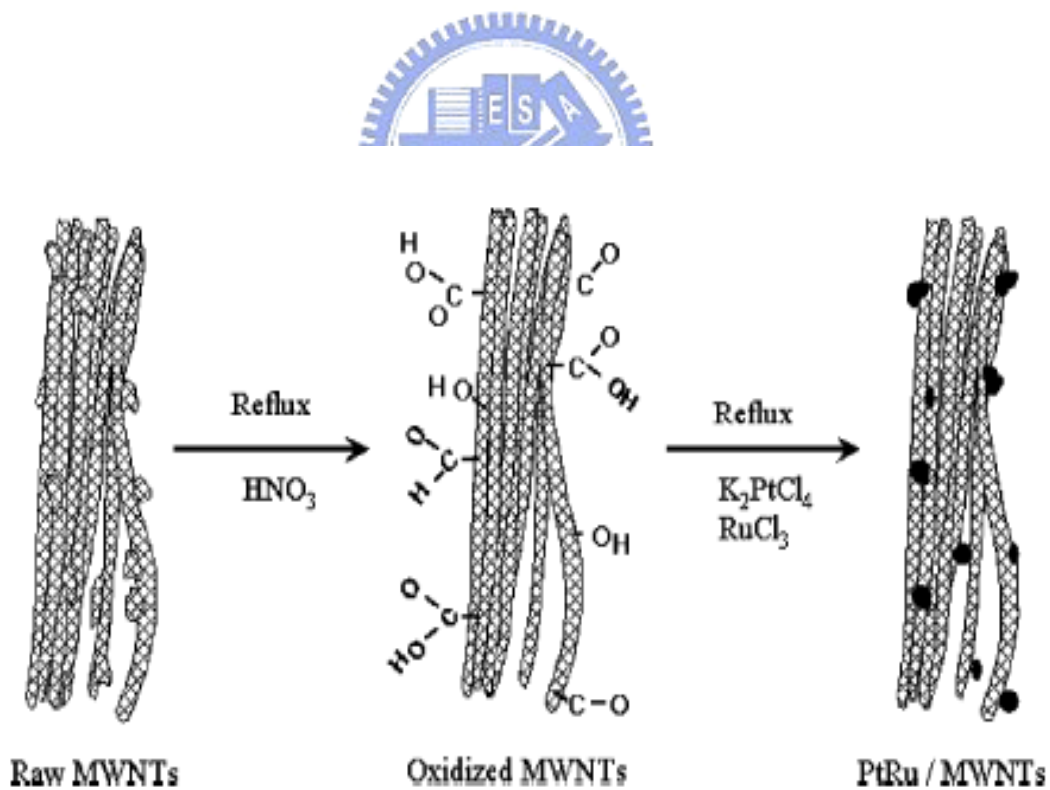


Fig. 1.6 MWNTs are modified by  $\text{HNO}_3$  and followed by reduction of metals

### 1.3 Motivation

In this study, multi-wall carbon nanotubes (MWNTs) are used as catalyst support. Attractive properties of nanotubes related with their good electrical conductivity and high specific surface area have been demonstrated in the electrochemical energy storage systems. Some researches have already used the application of carbon nanotubes powder as electrocatalyst, Pt and Pt/Ru, support for cathodic and anodic reactions in fuel cell [18–28]. However, there was little research that CNTs were fabricated on carbon cloth directly. The method in the electrode of DMFC is easy to constructed and sticking on the carbon cloth tightly.

And then, the other researches were reported that the chemical modifications of the surface of CNTs powder by using  $\text{HNO}_3$  or  $\text{H}_2\text{SO}_4\text{-HNO}_3$  could improve the metal particle dispersion, increase the available metal specific surface area, reduce the amounts of the expensive active metal component, and open the cap of CNTs[29–30]. However, there was a lack of the correlation of the CNTs texture and structure with the chemical and electrochemical analysis. Our purpose is to find which chemical solution, temperature, concentration, and time parameter is the best way to modify CNTs in order to rise the efficiency of cathode in the DMFC.

# Chapter 2 Fundamentals of MEA for DMFC and Modification of Carbon nanotube (CNT)

## 2.1 Assemble of MEA for DMFC

Typically, the DMFC is composed of a membrane electrode assembly (MEA) and two graphite flow-field plates, which are pressed against the MEA. The central component of the DMFC is the MEA composed of membrane, catalyst, and gas diffusion layers. Each of these layers has special functions in the DMFC and follows to explain its functions. For the interaction of the layers in the MEA it is important to define the respective functions of the individual components. Fig. 2.1 shows the description of the components in the DMFC. Fig. 2.2 shows the structure of the MEA.

### 2.1.1 Proton Exchange Membrane

The proton exchange membrane for DMFC is commercially available from DuPont Incorporation and has a commercial name, Nafion®. This organic proton-conductive membrane is a sulfonic acid-based perfluorinated polymer or polystyrene sulfonate polymer. It is used as electrolyte and the protons (cations) are allowed to permeate through it, but anions are rejected. The Nafion® structure is composed of three different parts, namely, rigid hydrophobic backbone, flexible perfluorocarbon, and hydrated ionic cluster region. The chemical formula and physical structure of the membrane is shown in Fig. 2.3.

### 2.1.2 Catalyst Layer

The catalyst layer is in direct contact with the membrane and the gas diffusion layer. It is also referred to as the active layer. In both the anode and cathode, the catalyst layer is the location of the half-cell reaction in a DMFC. The catalyst layer is either applied to the membrane or to the gas diffusion layer. In either case, the objective is to place the catalyst particles,

platinum or platinum alloys, within close proximity of the membrane.

### 2.1.3 Gas diffusion layer

The porous gas diffusion layer in DMFC ensures that reactants effectively diffuse to the catalyst layer. In addition, the gas diffusion layer is the electrical conductor that transports electrons to and from the catalyst layer. Typically, gas diffusion layers are constructed from porous carbon paper, or carbon cloth, with a thickness in the range of 100–300  $\mu\text{m}$ . The gas diffusion layer also assists in water management. In addition, gas diffusion layers are typically wet-proofed and could ensure that the pores of the gas diffusion layer do not become congested with liquid water.

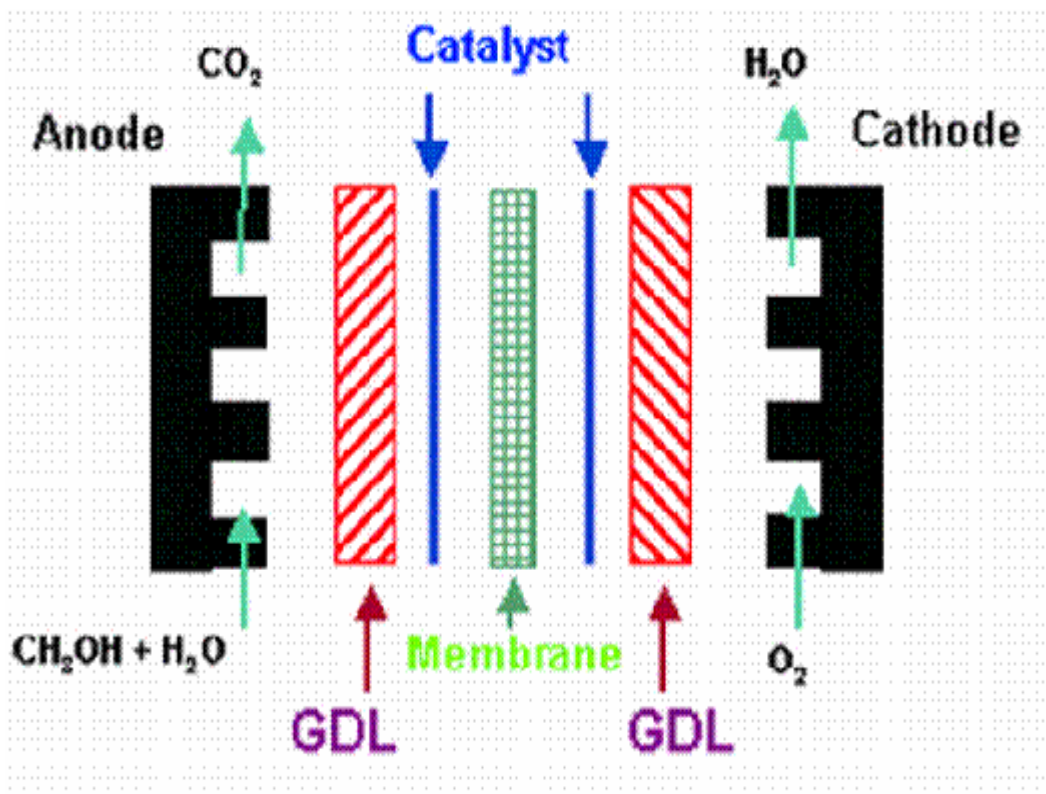


Fig.2.1 The schematic of a unit cell of DMFC

[\[www.eng.wayne.edu/page.php?id=1740\]](http://www.eng.wayne.edu/page.php?id=1740)





Fig.2.2 MEA structure

[www.hidrotec-fuelcell.com.ar/mea\\_esp.htm](http://www.hidrotec-fuelcell.com.ar/mea_esp.htm)

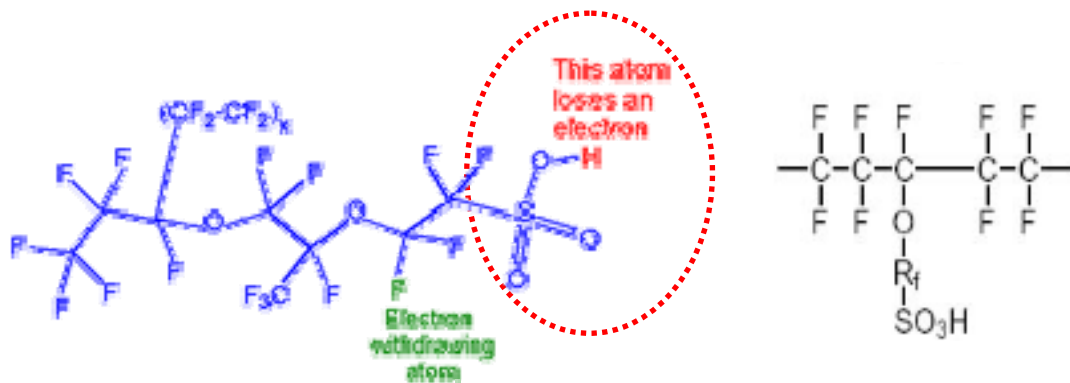
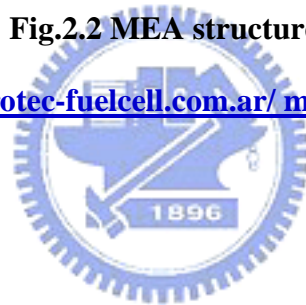


Fig.2.3 The chemical formula and physical structure of the membrane Nafion®

[Dupont Products information about Nafion ]

## 2.2 Principle of DMFC

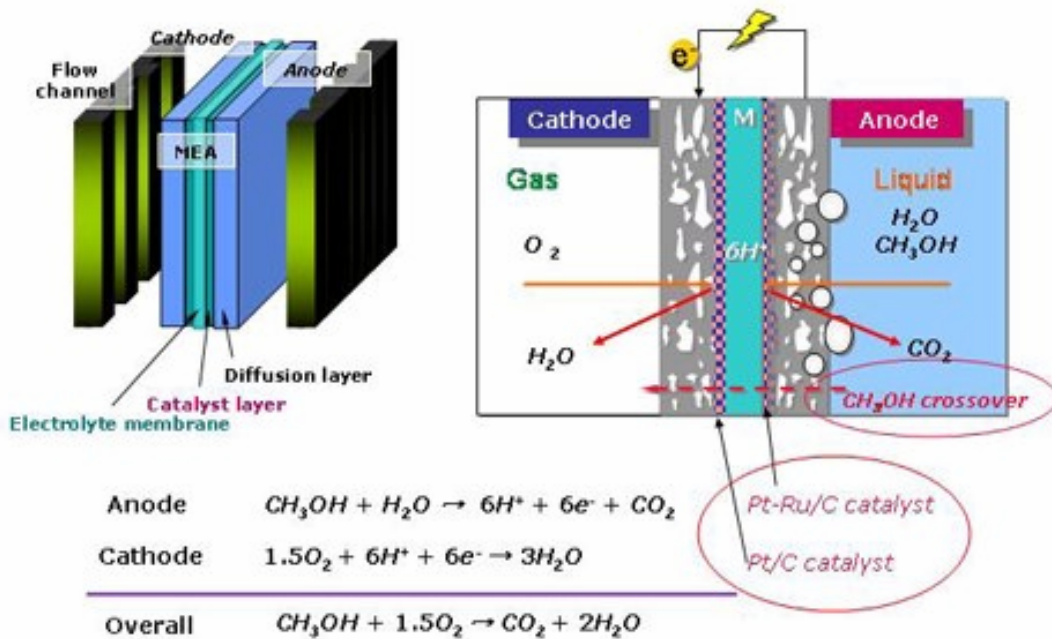


Fig.2.4 Illustration of DMFC in Principles

[www.echem.titech.ac.jp/~dmfc/C01/C01mokuteki.html](http://www.echem.titech.ac.jp/~dmfc/C01/C01mokuteki.html)

The schematic of a unit cell DMFC and its principle are in the Fig. 2.4. As soon as methanol attains to the surface of anode, it may be oxidized by electrocatalyst particle Pt and provide  $CO_2$ ,  $H^+$ , and six electrons. The follow is the location of the half-cell reaction in the anode for DMFC.



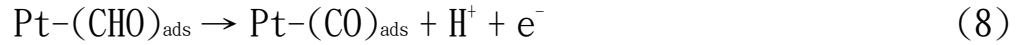
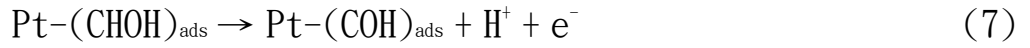
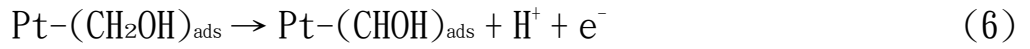
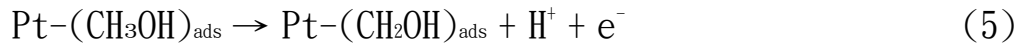
In the other hand, when electrons reach the cathode by external current loop,  $H^+$  ions transfer the proton exchange membrane to the cathode surface and provide water with oxygen from the air. The follow is the location of the half-cell reaction in the cathode for DMFC.



Finally, methanol is oxidized in the overall reaction for DMFC.



As the assumption of the absorption, the detail reaction mechanism on the surface of the electrocatalyst Pt is below the equation.



From all above equations, we could find that it is the complex in this reaction mechanism in the anode. There are many intermedium in the sequence reactions. The intermedium,  $\text{Pt}-(\text{CO})_{\text{ads}}$ , is formed by CO and Pt when all  $\text{H}^+$  leave the surface of Pt. Furthermore, Pt itself gets out of the ability for oxidizing methanol. It is named Poison Effect. In order to solve the problem, the second electrocatalyst, transitional metal (Sn、Ru、Re、Mo), is added to assist water segregate. Then, it allows  $\text{Pt}-(\text{CO})_{\text{ads}}$  to be reduced as Pt.



Furthermore, some researches use three kinds of metal as the electrocatalyst on the anode. In the other hand, the electrocatalyst, Pt, is the single kind of metal on the cathode.

## 2.3 Growth and Characterization of Carbon Nanotube

In 1991, Iijima of the NEC Laboratory in Japan reported the first observation of multi-walled carbon nanotubes (MWNTs) in carbon-soot made by arc-discharge. About two years later, he made the observation of single-walled carbon nanotubes (SWNTs). The past decade witnessed significant research efforts in efficient and high-yield nanotube growth methods. The success in nanotube growth has led to the wide availability of nanotube materials, and is a main catalyst behind the recent progress in basis physics studies and applications of nanotubes.

Nanotubes can be utilized individually or as an ensemble to build functional device prototypes, as has been demonstrated by many research groups. Ensembles of nanotubes have been used for field emission based flat-panel display, composite materials with improved mechanical properties and electromechanical actuators. Bulk quantities of nanotubes have also been suggested to be useful as high-capacity hydrogen storage media. Individual nanotubes have been used for field emission sources, tips for scanning probe microscopy and nano-tweezers. Nanotubes also have significant potential as the central elements of nano-electronic devices including field effect transistors, single-electron transistors and rectifying diodes.

### 2.3.1 Growth Methods

#### Arc-Discharge

In arc-discharge, carbon atoms are evaporated by plasma of helium gas ignited by high currents passed through opposing carbon anode and cathode in Fig. 2.5(a). Arc-discharge has been developed into an excellent method for producing both high quality multi-walled nanotubes and single-walled nanotubes. MWNTs can be obtained by controlling the growth conditions such as the pressure of inert gas in the discharge chamber and the arcing current. In 1992, a breakthrough in MWNTs growth by arc-discharge was first made by Ebbesen and Ajayan who achieved growth and purification of high quality MWNTs at the gram level. The synthesized

MWNTs have lengths on the order of ten microns and diameters in the range of 5-30nm. The nanotubes are typically bound together by strong van der Waals interactions and form tight bundles. MWNTs produced by arc-discharge are very straight, indicative of their high crystallinity. For as-grown materials, there are few defects such as pentagons or heptagons existing on the sidewalls of the nanotubes. The by-product of the arc-discharge growth process is multi-layered graphitic material. Heating the as-grown material in an oxygen environment oxidizes away the graphitic particles. Polyhedral graphitic particles exhibit higher oxidation rates than MWNTs; nevertheless, the oxidation purification process also removes an appreciable amount of nanotubes.

### **Laser Ablation**

The method utilizes intense laser pulses to ablate a carbon target containing 0.5 atomic percent of nickel and cobalt. The target is placed in a tube furnace heated to 1200°C in Fig. 2.5(b). During laser ablation, a flow of inert gas is passed through the growth chamber to carry the grown nanotubes downstream to be collected on a cold finger.

### **Chemical Vapor Deposition (CVD)**

A schematic experimental setup for CVD growth is depicted in Fig. 2.5(c). The growth process involves heating a catalyst material to high temperatures in a tube furnace and flowing a hydrocarbon gas through the tube reactor for a period of time. Materials grown over the catalyst are collected upon cooling the system to room temperature. The key parameters in nanotube CVD growth are the hydrocarbons, catalysts and growth temperature. The active catalytic species are typically transition-metal nanoparticles formed on a support material such as silicon.

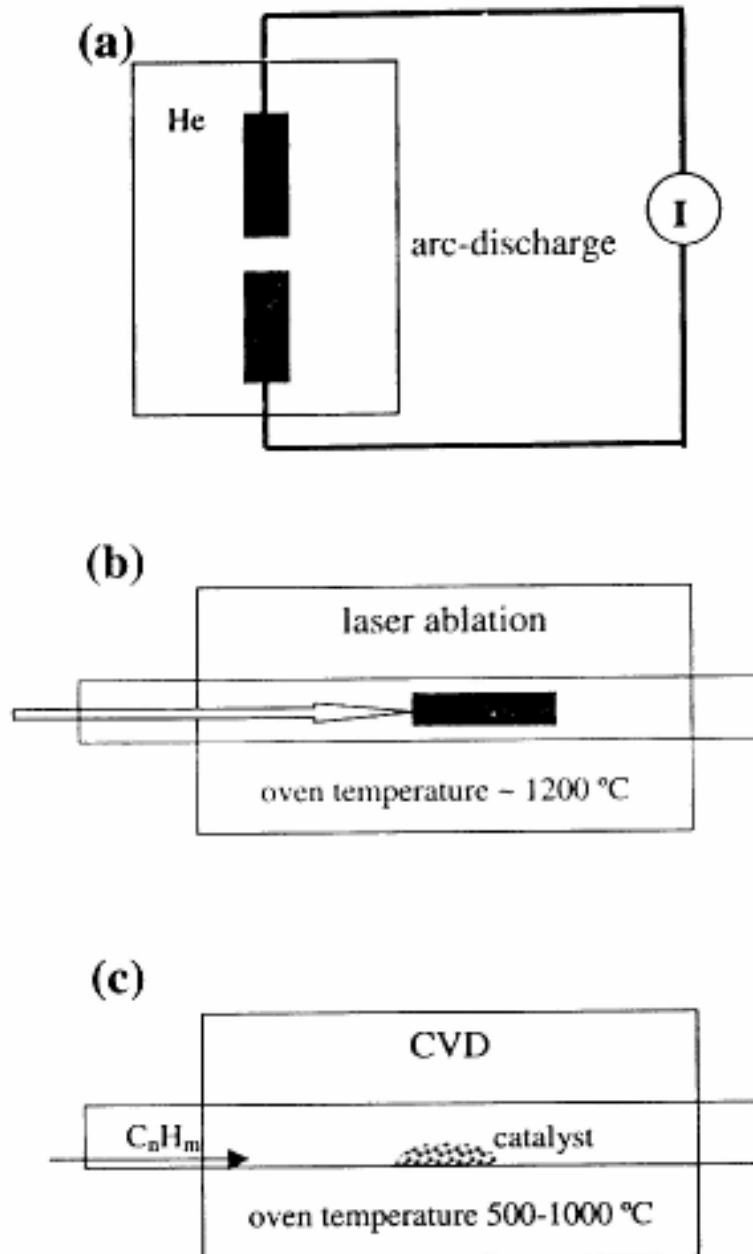


**Fig. 2.5 (a)-(c) Schematic experimental setups for nanotube growth methods**

### 2.3.2 The growth mechanism of Carbon nanotubes

The general nanotube growth mechanism in a CVD process involves the dissociation of hydrocarbon molecules catalyzed by the transition metal, and dissolution and saturation of carbon atoms in the metal nanoparticle in Fig. 2.6. The precipitation of carbon from the saturated metal particle leads to the formation of tubular carbon solids in  $sp^2$  structure. Tube formation is favored over other forms of carbon such as graphitic sheets with open edges. This is because a tube contains no dangling bonds and therefore is in a low energy form. For MWNTs growth, most of the CVD methods employ ethylene or acetylene as the carbon feedstock and the growth temperature is typically in the range of 550-750°C. Iron, nickel or cobalt nanoparticles are often used as catalyst. The rationale for choosing these metals as catalyst for CVD growth of nanotubes lies in the phase diagrams for the metals and carbon. At high temperatures, carbon has finite solubility in these metals, which leads to the formation of metal-carbon solutions and therefore the aforementioned growth mechanism. Noticeably, iron, cobalt and nickel are also the favored catalytic metals used in laser ablation and arc-discharge. This simple fact may hint that the laser, discharge and CVD growth methods may share a common nanotube growth mechanism, although very different approaches are used to provide carbon feedstock.

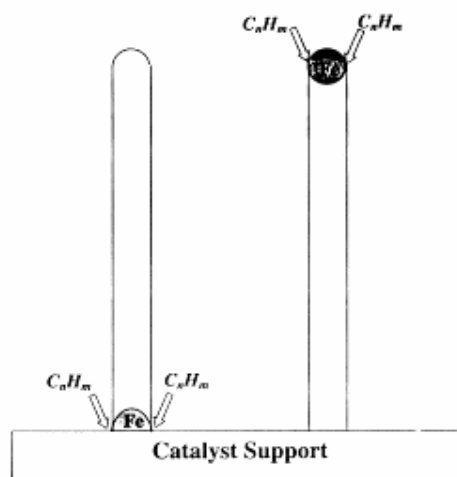


**Fig. 2.6 Two general growth modes of nanotube in chemical vapor deposition**

## 2.4 Modification of Carbon Nanotube

The components of the produced gas were identified as CO, CO<sub>2</sub> and NO by the gas chromatograph (GC) and gas chromatography-mass spectrometry (GCMS) analyses. This implies that the carbon atoms constituting the MWNTs were partly removed by HNO<sub>3</sub> oxidation [32].



The reaction pathways for the functional group formation most probably involve the following two reactions in Fig. 2.7: (i) hydration of the olefinic C=C moieties released from the conjugation network by the decarbonization due to HNO<sub>3</sub> oxidation. The nanotube sidewalls and more active top of the nanotube form the COOH and C–OH bonds) (ii) A hydration–dehydration equilibrium between adjoining C–OH groups and C=O ether groups.

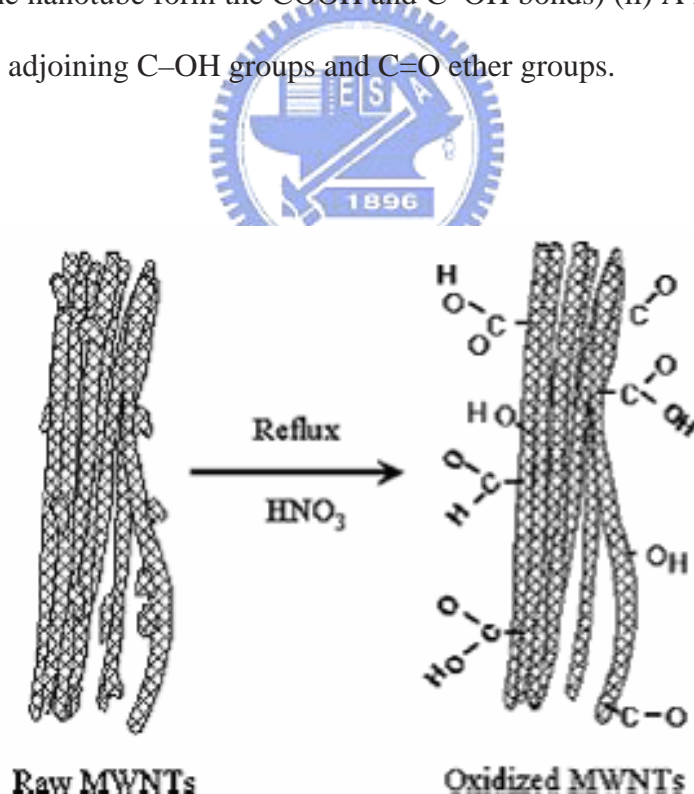
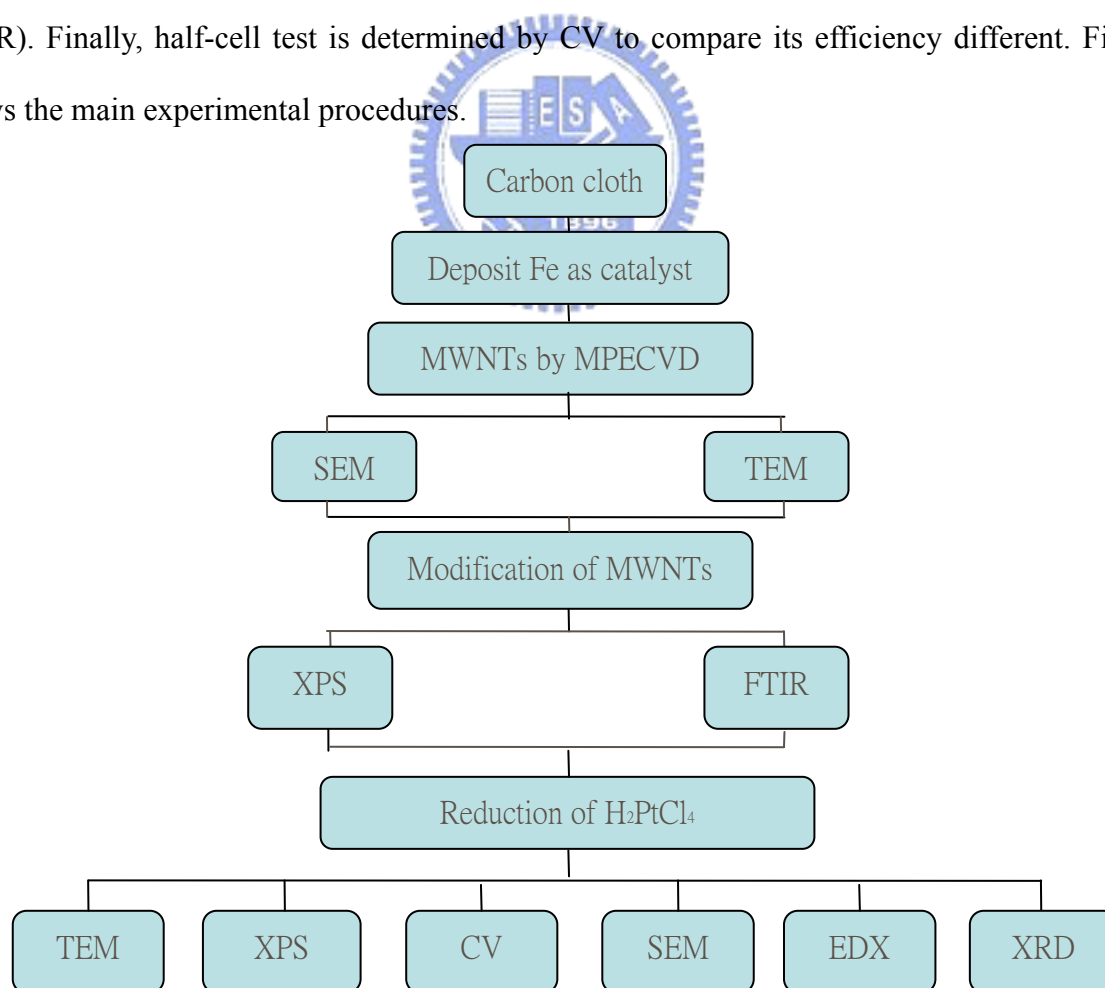


Fig. 2.7 MWNTs are modified by HNO<sub>3</sub>



## Chapter 3 Experimental procedures

New cathode material for direct Methanol Fuel Cells (DMFC) based on multi-wall carbon nanotubes (MWNTs), aiming to improve the performance of the cell is analyzed. In this study, MWNTs are fabricated directly on carbon cloth by Microwave plasma enhanced chemical vapor deposition (MPECVD) and then functionalized by several chemical solutions. Therefore MWNTs can be functionalized with groups such as hydroxyl (-OH), carboxyl (-COOH), and carbonyl (>C=O) that are necessary to anchor metal ions to the tube. Pt catalyst is electroless deposited on MWNTs using a chloroplatinic acid solution, based on  $\text{H}_2(\text{PtCl}_6) \cdot 6\text{H}_2\text{O}$ . The morphology of MWNTs and Pt nanoparticles are analyzed by SEM, TEM, and XRD. Surface-to-depth analysis of functionalized multi-wall carbon nanotubes is achieved by high resolution x-ray photoelectron spectroscopy (XPS) and Fourier Transform Infrared Spectroscopy (FTIR). Finally, half-cell test is determined by CV to compare its efficiency different. Fig. 3.1 shows the main experimental procedures.



**Fig.3.1 Flow chart of experimental procedures**

### 3.1 Fabrication of carbon nanotube on carbon cloth

MWNTs on carbon cloth are fabricated by MPECVD without bias. The 20nm of Fe film is deposited on carbon cloth as catalyst for growth of carbon nanotubes by using ion-beam sputter. Its sample size is 0.5\*0.5 cm<sup>2</sup> and six samples are fabricated in the chamber together in order to keep the same condition.

The chamber is evacuated at pressure of  $\sim 10^{-2}$  Torr with a mechanical pump. The reactive gases are mixture of H<sub>2</sub> and CH<sub>4</sub>, which held a ratio of 90/30 sccm to a pressure set at 10 Torr. The microwave power of 300W is applied to light the plasma which let the temperature reaches up to 500°C ~ 600°C for 20 min without bias-assisted. Fig. 3.2 shows schematic diagram of the MPECVD system. Table 3.1 reports the parameters of the growth of MWNTs.

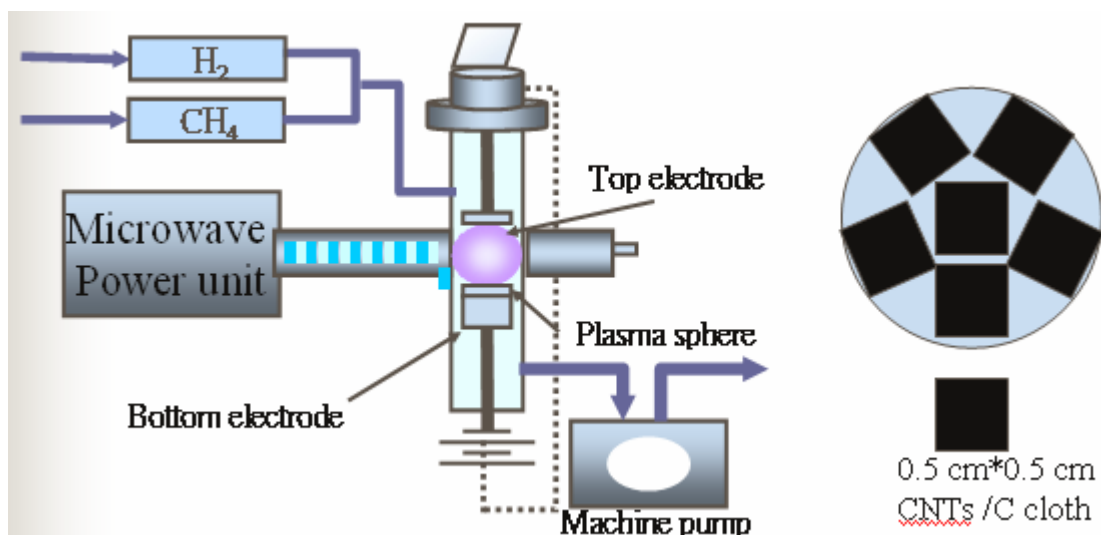


Fig. 3.2 Schematic diagram of the MPECVD system

Table 3.1 The parameters of the growth of MWNTs

Metallic catalyst	Reactive gases	Power	Pressure	Reaction time	Bias
Fe: ~20nm	CH <sub>4</sub> : 30 sccm H <sub>2</sub> : 90 sccm	300 W	10 Torr	20 min	0 V

### 3.2 Modification of carbon nanotube on carbon cloth

MWNTs on carbon cloth are functionalized by several chemical solutions in the sample tube with sand bath. The parameters of chemical modification are chemical solutions ( $\text{HNO}_3$ ,  $\text{H}_2\text{SO}_4$ , and  $\text{KOH}$ ), temperature ( $80^\circ\text{C}$ ,  $90^\circ\text{C}$ , and  $100^\circ\text{C}$ ), concentration (2M and 14M), and time (0 hr, 6 hr, 12 hr, 18 hr, 24 hr, and 48 hr). Then, the sample is collected after immersing with deionized water until the filtrate pH became nearly the pristine pH. Fig. 3.3 shows schematic diagram of the chemical modification

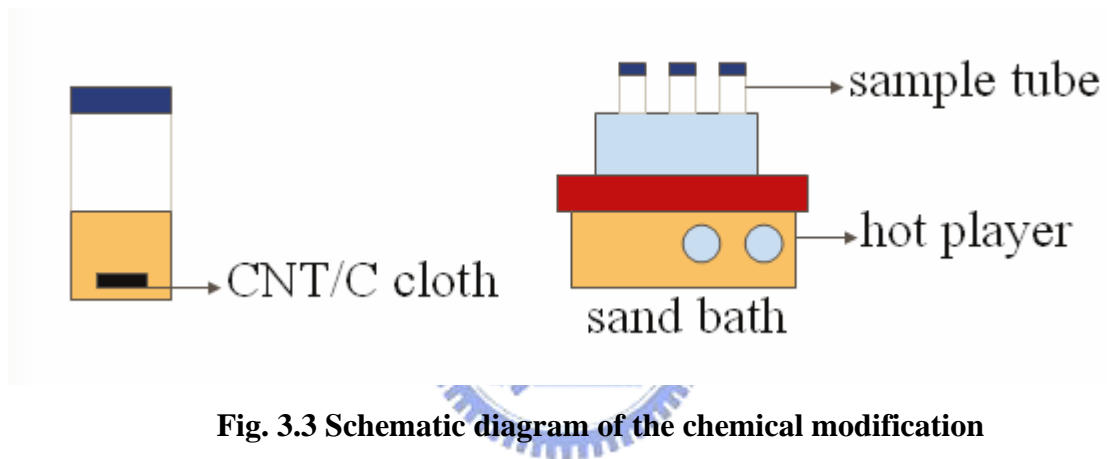
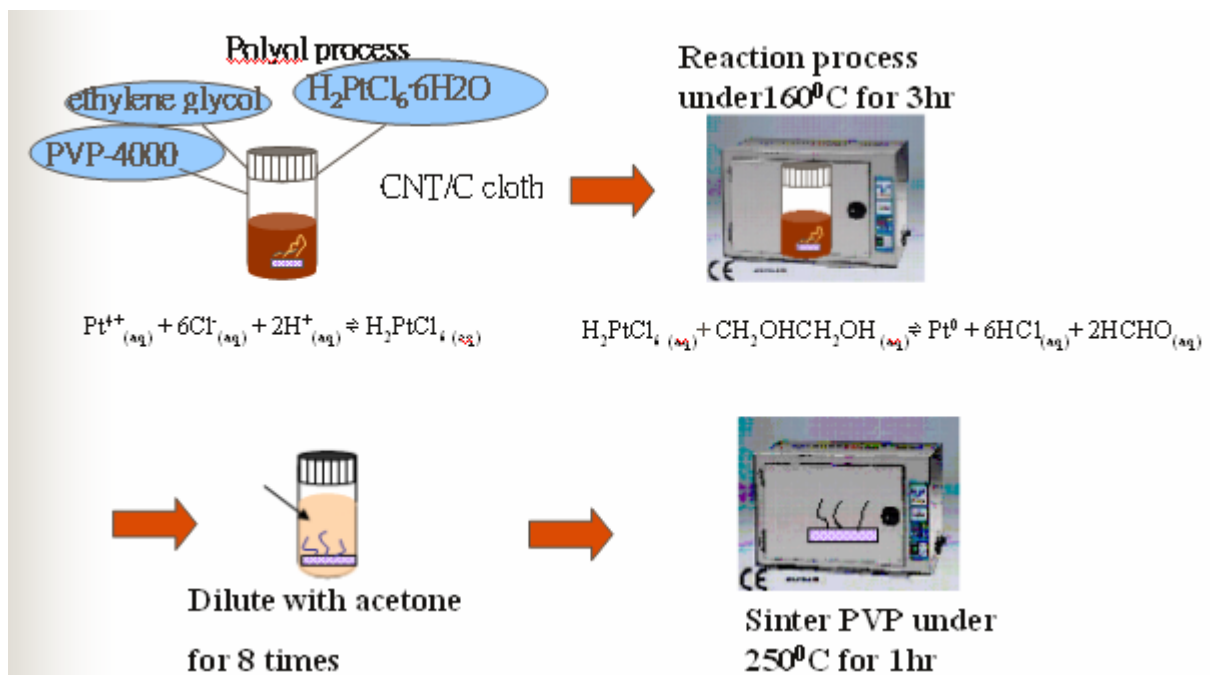


Fig. 3.3 Schematic diagram of the chemical modification

### 3.3 Dispersion of Pt on prepared carbon cloth

The prepared carbon cloth is immersed in a chemical solution containing  $\text{H}_2\text{PtCl}_6 \cdot 6\text{H}_2\text{O}$ , PVP-4000, and ethylene glycol mixture diluted with acetone. Polymer (PVP) is the protection agent to limit metal particle growth spacing. Pt is deposited by synthesis from  $\text{H}_2\text{PtCl}_6 \cdot 6\text{H}_2\text{O}$  in ethylene glycol solution under  $160^\circ\text{C}$  for 3 hr, followed by filtration with acetone for 8 times and sintered for 1 hr at  $250^\circ\text{C}$ . This method, polyol process, is expected a uniformly homogeneous nucleation and growth mechanism of nanoparticle. The reaction dominates by temperature control and solvent plays as reductant as well. Fig 3.4 shows the experimental procedures of polyol process.



**Fig. 3.4 The experimental procedures of polyol process**

## 3.4 Analysis Instruments

### 3.4.1 Scanning Electron Microscopy (SEM)

Scanning electron microscopy (SEM) is used to observe the surface morphology of wide range kinds of objects. There are many advantages including of easy sample preparation, high image resolution, large depth of field, and high magnification. [33]

The SEM image is that signals (secondary electrons and backscattered electrons) emit from the sample surface as the sample is bombarded by the high energy incident electrons. The fabricating CNT morphology and the dispersing Pt on CNT morphology could be observed by JEOL JSM6500F in NCTU with field emission electron source and 15kV accelerate voltage.



**Fig.3.5 Diagram of a Scanning Electron Microscopy**

[<http://www.le.imm.cnr.it/sito/laboratories/jsm6500f.html>]

### 3.4.2 Transmission Electron Microscopy (TEM)

In a typical TEM a static beam of electrons at 100-400kV accelerating voltage illuminate a region of an electron transparent specimen which is immersed in the objective lens of the microscope. The transmitted and diffracted electrons are recombined by the objective lens to form a diffraction pattern in the back focal plane of that lens and a magnified image of the sample in its image plane. [33]

The raw MWNTs and the modified MWNTs morphology could be compared by TEM using

a JEOL JEM 4000 system in NCTU operating at 200kV. And the particle morphology, size and size distribution of Pt nanoparticles dispersed on the surface of MWNTs are also characterized by TEM.

### 3.4.3 X-ray Photoelectron Spectroscopy (XPS)

The phenomenon is based on the photoelectric effect. The concept of the photon was used to describe the ejection of electrons from a surface when photons impinge upon it. The XPS technique is highly surface specific (< 5nm) due to the short range of the photoelectrons that are excited from the solid. The energy of the photoelectrons leaving the sample is determined using a Spherical Capacitor Analyzer (SCA) this gives a spectrum with a series of photoelectron peaks. The binding energy of the peaks is characteristic of each element. The peak areas can be used (with appropriate sensitivity factors) to determine the composition of the materials surface. [33]

XPS could determine the difference of the raw CNT and the modified CNT due to the element C chemical shifts. Furthermore, it may ensure if Pt is reductive by the same way. In this study, XPS analysis is carried out on a ESCA PHI 1600 using an Mg K $\alpha$  X-ray source in NTHU.

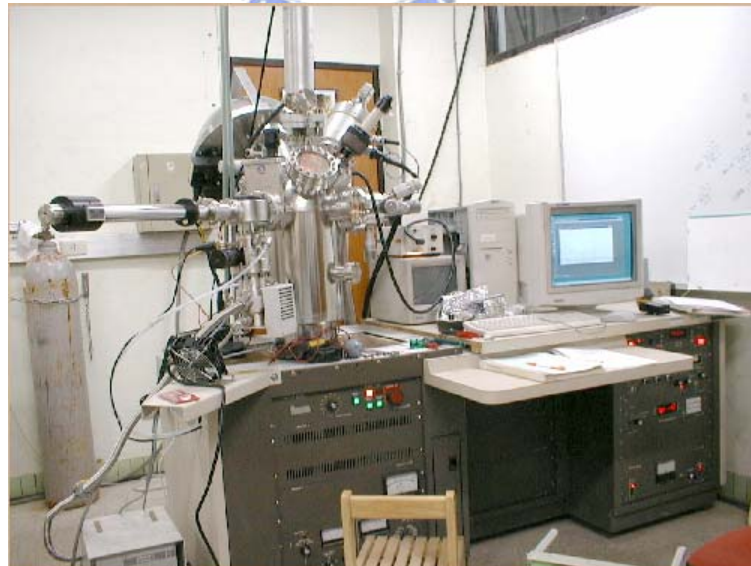


**Fig.3.6 Diagram of a X-ray Photoelectron Spectroscopy**

[<http://www.nscric.nthu.edu.tw/Other/augeresca/auesca.html>]

### 3.4.4 Fourier Transform Infrared Spectrometer (FTIR)

Fourier Transform Infrared Spectroscopy (FTIR) is an analytical technique used to identify organic and inorganic materials. This technique measures the absorption of various infrared light wavelengths by the material of interest. These infrared absorption bands identify specific molecular components and structures. [33]

The functional groups on the surface of MWNTs modified by chemical solution could be determined by FTIR. The FTIR measurements are performed on a PROTEGE 460 series FTIR apparatus by transmission spectroscopy in NCTU.

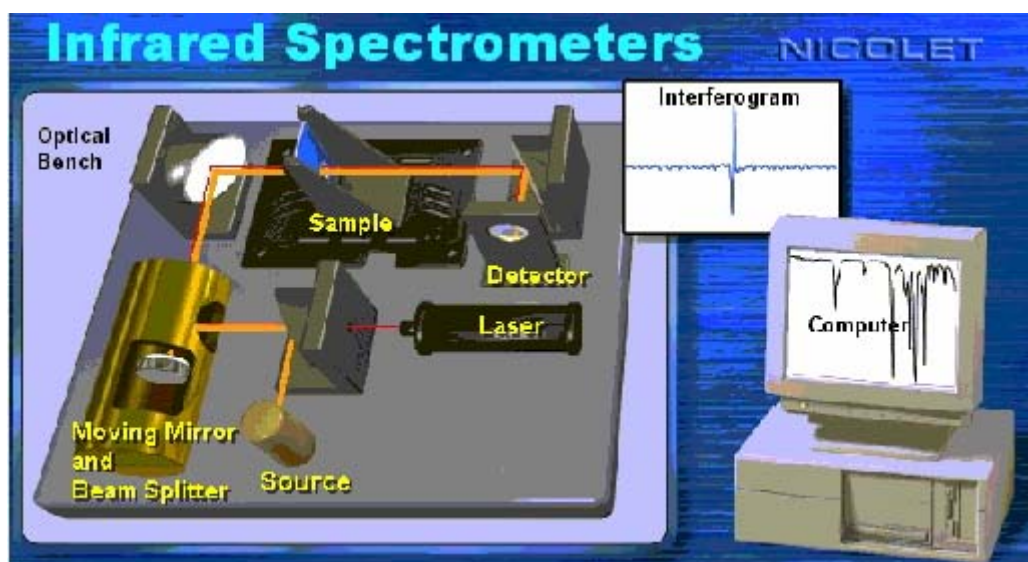


**Fig.3.7 Diagram of a Fourier Transform Infrared Spectrometer**

[[http://www.forumsci.co.il/HPLC/FTIR\\_page.html](http://www.forumsci.co.il/HPLC/FTIR_page.html)]

### 3.4.5 Cyclic Voltammetry (CV) Potentiostat

A potentiostat is an electronic device that controls the voltage difference between a working electrode and a reference electrode. Both electrodes are contained in an electrochemical cell. The potentiostat implements this control by injecting current into the cell through an auxiliary, or counter, electrode. In almost all applications, the potentiostat measures the current flow between the working and auxiliary electrodes. The controlled variable in a potentiostat is the cell potential

and the measured variable is the cell current.

The CHI Version 5.01 system in the potentiostat in NCTU is used to measure the electrochemical specific surface area of the dispersive Pt on the surface of MWNTs for the fuel-cell electrodes. From the CV, the charge equivalent to the area under the hydrogen desorption region is evaluated and the electrochemical specific surface area is calculated assuming that the charge is required for the adsorption-desorption of a monolayer of atomic hydrogen on the surface.

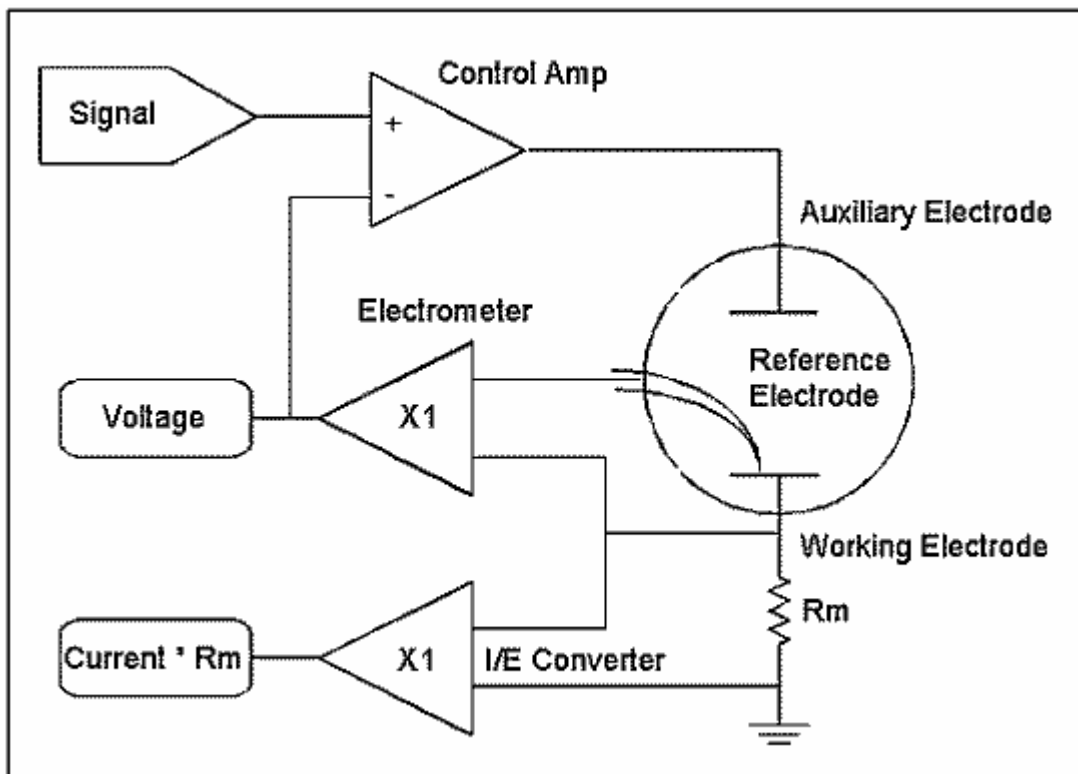


**Fig.3.8 Schematic of a Cyclic Voltammetry (CV) Potentiostat**

[[http://www.gamry.com/App\\_Notes/Potentiostat\\_Primer.htm#Workking](http://www.gamry.com/App_Notes/Potentiostat_Primer.htm#Workking)]

### 3.4.6 Energy Dispersive X-ray (EDX)

It is a technique used for identifying the elemental composition of the specimen, or an area of interest thereof. The EDX analysis system works as an integrated feature of SEM (JEOL JSM6500F) in NCTU. An EDX spectrum plot not only identifies the element corresponding to each of its peaks, but the type of X-ray to which it corresponds as well. For example, a peak



corresponding to the amount of energy possessed by X-rays emitted by an electron in the L-shell going down to the K-shell is identified as a K-Alpha peak. The peak corresponding to X-rays emitted by M-shell electrons going to the K-shell is identified as a K-Beta peak. [33]

EDX measurements show the element on the MWNTs and the content of Pt/MWNTs. It appears that the difference content of Pt is on the raw MWNTs and the modified MWNTs.

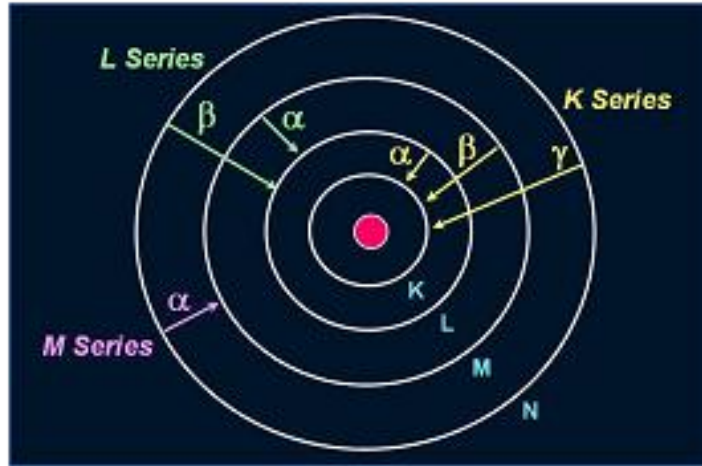


Fig.3.9 Elements in an EDX spectrum are identified based on the energy content of the X-rays

[<http://www.semiconfareast.com/edxwdx.htm>]

### 3.4.7 X-Ray Diffraction (XRD)

X-ray Diffraction (XRD) is one of the primary techniques used by solid state chemists to characterize materials. XRD can provide information about crystalline structure and particle size in a sample even when the crystallite size is too small for single crystal x-ray diffraction. [33]

An X-ray beam hits a sample and is diffracted. We can observe the diffraction peaks when the distances between the planes of the atoms apply to Bragg's Law. Bragg's Law is:

$$n\lambda = 2d \sin \theta \quad (1)$$

Where the integer  $n$  is the order of the diffracted beam,  $\lambda$  is the wavelength of the incident X-ray beam,  $d$  is the distance between adjacent planes of atoms (the  $d$ -spacings), and  $\theta$  is the angle of incidence of the X-ray beam.

The broader diffraction peaks for the catalyst led to smaller average particle size as calculated by the Scherrer equation.

$$L = \frac{K \lambda_{K\alpha 1}}{B_{2\theta} \cos \theta_B} \quad (2)$$

Where L is the average particle size, K is the constant,  $\lambda_{K\alpha 1}$  is the X-ray wavelength (1.54056 Å for Cu  $K_{\alpha 1}$  radiation),  $B_{2\theta}$  is the peak broadening, and  $\theta_B$  is the angle corresponding to the peak maximum.

In this study, the particle size calculated by XRD is compared with the data measured by TEM. It is determined how the functional group (COOH) on the MWNTs affects the Pt particle size forming.

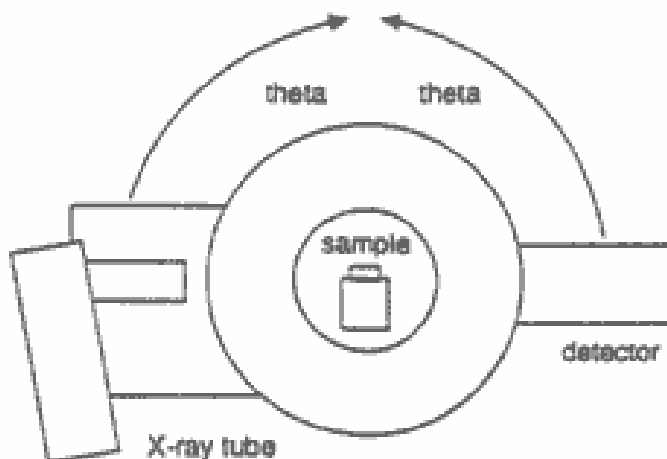


Fig.3.10 Schematic of X-Ray Diffraction

[<http://pubs.usgs.gov/info/diffraction/html/index.html>]

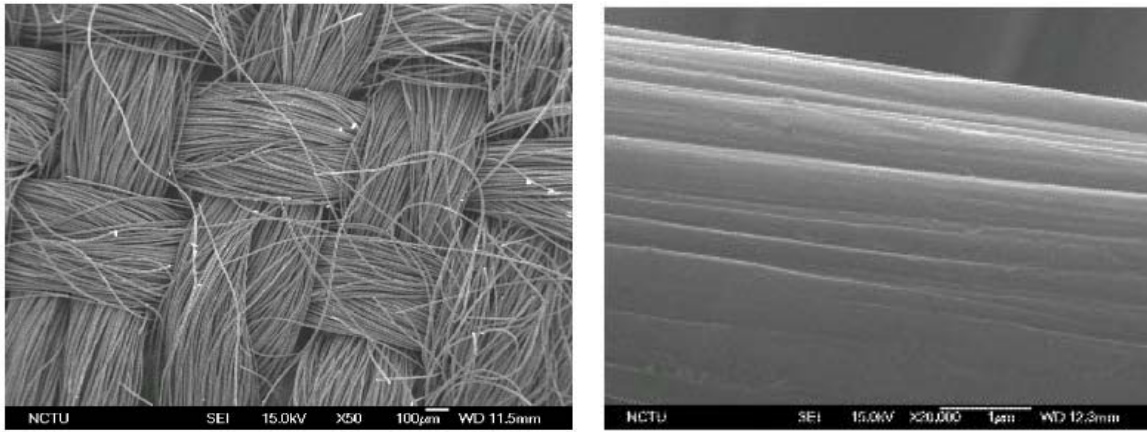
## Chapter 4 Results and Discussion

### 4.1 Morphology of carbon nanotube on carbon cloth

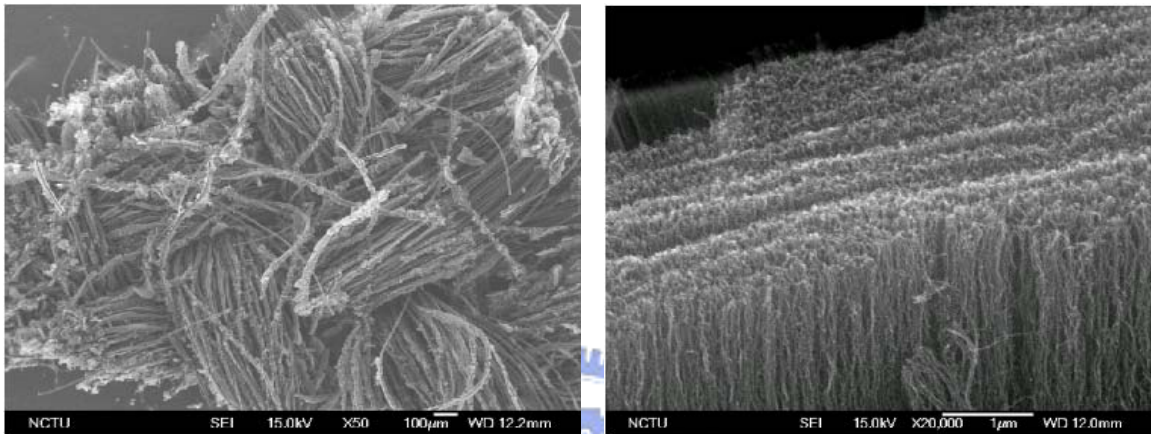
In this study, the purpose is that the longer MWNTs are fabricated vertically by MPECVD. The use of a support, well-aligned MWNTs, for catalyst has many advantages including more the anchoring sites of available catalyst, producing a lot of functional groups to attract catalyst at the caps and the sidewalls of MWNTs easily by modified the surface structure, using inner specific surface area of tube by opening end of MWNTs.

Fig 4.1 shows that a piece of carbon cloth without any treatment. It is composed of textured carbon fibers which have a smooth surface. Fig 4.2 shows that the images of long MWNTs fabricated on carbon cloth densely and vertically. Then, MWNTs are analyzed in the higher magnification. The length of MWNTs is about 20  $\mu\text{m}$  and its diameter is about 20 nm in Fig 4.3. As shown in Fig. 4.4, the TEM images show that MWNTs display hollow tubes with amorphous and crystalline layers. On the other hand, the growth model of MWNTs could be found including tip growth model and base growth model.

The density of the vertical MWNTs may not be controlled dispersedly so the spraying of Pt particle may just stop on the top surface. Therefore, even the high specific surface area of MWNTs still can not be utilized totally until Pt is deposited uniformly by using polyol process. However, the raw surface of MWNTs is relatively inert and difficult to support particles homogeneously, which often results in the agglomeration of nanoparticles. Thus, it is important to improve the adhesion through the following surface chemical modification techniques.



**Fig. 4.1 SEM images of pristine carbon cloth with different magnification**



**Fig 4.2 SEM images of MWNTs on carbon cloth with different magnification**

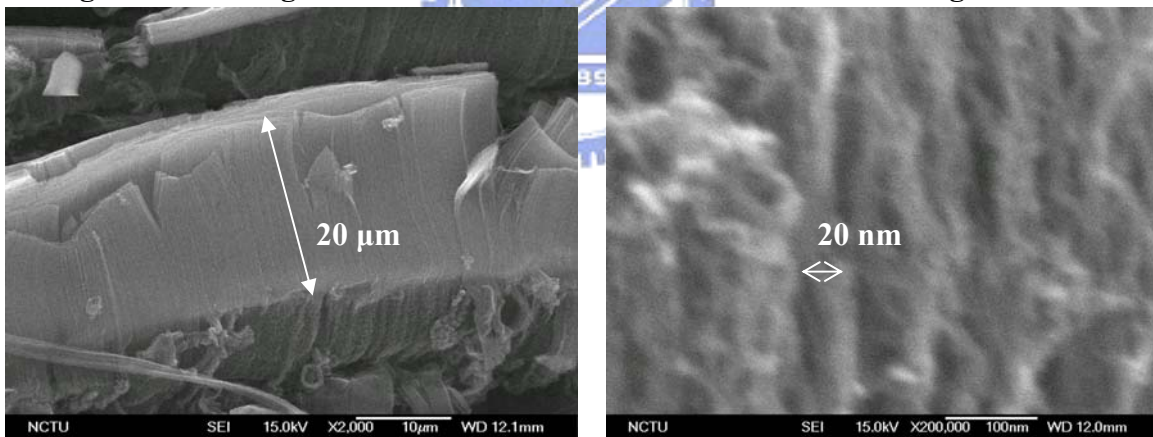


**Fig 4.3 The length of MWNTs is about 20 μm and its diameter is about 20 nm.**

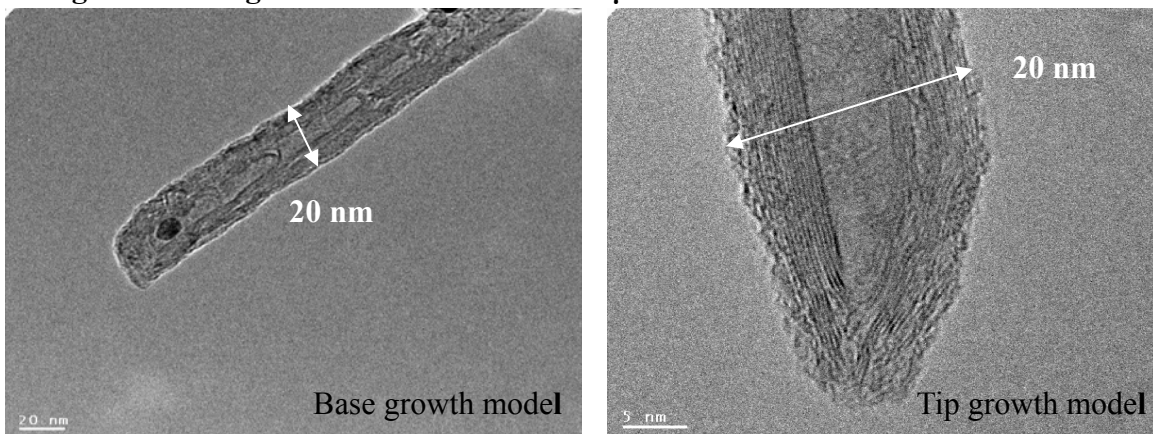


**Fig. 4.4 MWNTs display hollow tubes with amorphous and crystalline layer**

## 4.2. Multi-wall carbon nanotubes are modified by HNO<sub>3</sub>, H<sub>2</sub>SO<sub>4</sub>, and KOH

Surface chemical modification is a common method and is essential for the deposition of catalysts and other species onto carbon nanotube surfaces for nanocatalytic applications [34]. Oxidation, with popular oxidants including HNO<sub>3</sub>, KMnO<sub>4</sub>, HNO<sub>3</sub>/ H<sub>2</sub>SO<sub>4</sub>, is an often attempted approach to activate the surface of CNTs [35, 36]. However, there is little analysis about functional groups after surface chemical modification of CNTs. In this study, MWNTs are modified by HNO<sub>3</sub>, H<sub>2</sub>SO<sub>4</sub>, and KOH at 80°C in Table 4.1 and may produce different functional groups to attract more Pt ions nucleating uniformly and densely. Thus, after the following experiments, it would be found that which chemical solution is better for surface chemical modification of MWNTs.



**Table 4.1 MWNTs are modified by HNO<sub>3</sub>, H<sub>2</sub>SO<sub>4</sub>, and KOH**

<b>Solution</b>	<b>HNO<sub>3</sub></b>	<b>H<sub>2</sub>SO<sub>4</sub></b>	<b>KOH</b>
<b>Concentration</b>	16M	18M	6M
<b>Temperature</b>	80°C	80°C	80°C
<b>Time</b>	6 hr	6 hr	6 hr
<b>Hypothetical functional groups</b>	-COOH -OH	-SO <sub>3</sub> H	-OH

## 4.2.1 Analysis of functional groups

The information on the surface chemistry of the modified nanotubes has been provided by the FTIR. Table 4.2 indicates the absorption spectra ranges of several functional groups. Fig 4.5 shows the absorption spectra of MWNTs modified by HNO<sub>3</sub>, H<sub>2</sub>SO<sub>4</sub>, and KOH at 80<sup>0</sup>C for 6 hr. In fact, one broad intensive band observing at 1375 cm<sup>-1</sup> is assigned to the alcoholic hydroxyl groups (-OH) or the carboxylic acids (-COOH) and the other observing at 1574 cm<sup>-1</sup> is assigned to the carboxylic acids (-COOH). However, the functional group, sulfonic acid (-SO<sub>3</sub>H), can not be observed. Therefore, the reaction pathways for forming the functional group most probably involve the following reaction. Hydration of the olefinic C=C moieties is released from the conjugation network by decarbonization of the nanotube sidewalls due to HNO<sub>3</sub>, H<sub>2</sub>SO<sub>4</sub>, and KOH oxidation so the alcoholic hydroxyl groups (-OH) and carboxylic acids (-COOH) could be formed [32].

Indeed, we try to assay sulfonic acid (-SO<sub>3</sub>H) groups with FTIR. However, the detection is too difficult because of their weak response in the IR mode. For the reason, we used XPS to directly detect the sulfur atom [37]. No S spectra of various MWNTs, given in Fig. 4.6, show that there is no sulfonic acid (-SO<sub>3</sub>H). On the other hand, the carboxyl groups would be detected in Fig. 4.7(a) (b) (c). The C 1s spectrum appears to be composed of C=C (~284.6 eV), C-C (~285.85 eV), CO (287.46 eV), COO-(289.24 eV), OCOO- (~291.5 eV) functional groups [38]. The observed chemical shift following the chemical treatment is about 1 eV. Therefore, the result from the FTIR and XPS analysis indicates that MWNTs merely forms the alcoholic hydroxyl groups (-OH) and the carboxylic acids (-COOH) with chemical modification of HNO<sub>3</sub>, H<sub>2</sub>SO<sub>4</sub>, and KOH at 80<sup>0</sup>C for 6 hr.

Table 4.2 The absorption spectra ranges of several functional groups

Functional group		Wave number (cm <sup>-1</sup> )
-OH	alcoholic hydroxyl groups	1410-1260
-SO <sub>3</sub> H	sulfonic acid	1150-1250
-COOH	carboxylic acids	1610-1550    1420-1300
-C=O	carboxyl groups	1690-1760

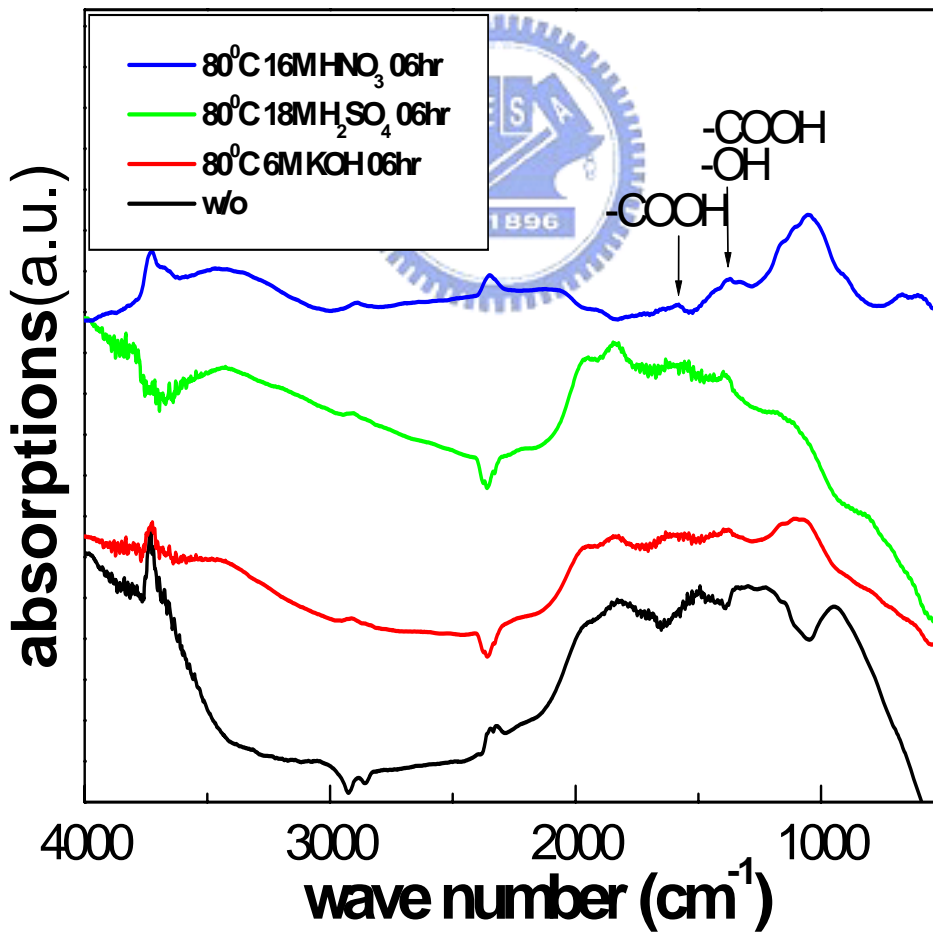


Fig 4.5 The absorption spectra of MWNTs modified by HNO<sub>3</sub>, H<sub>2</sub>SO<sub>4</sub>, and KOH

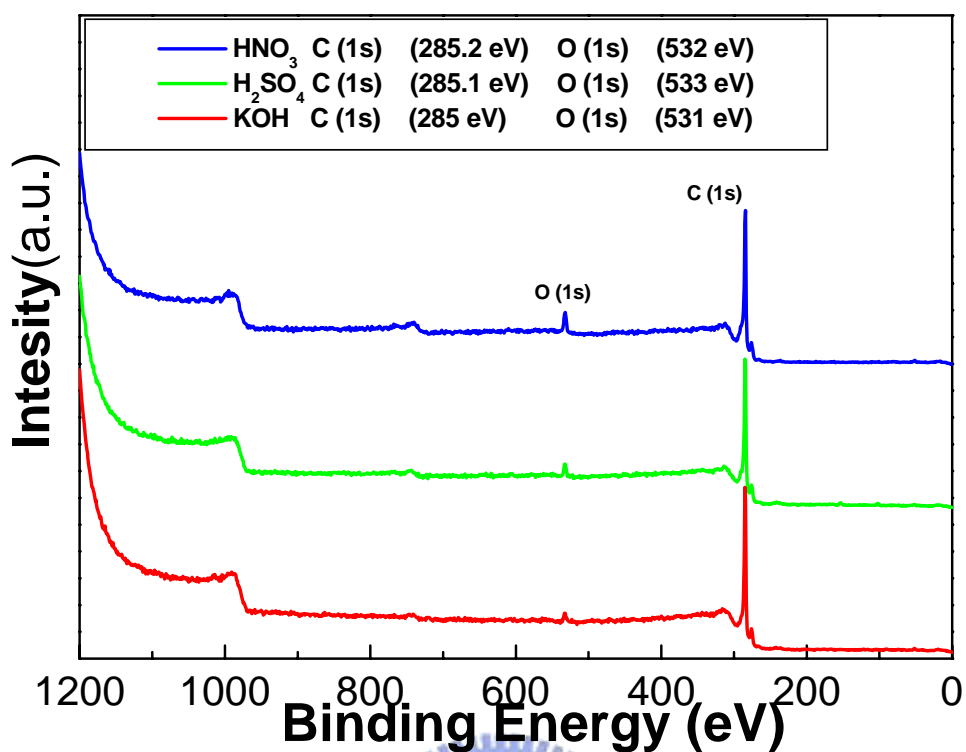


Fig. 4.6 XPS survey spectra of MWNTs modified by HNO<sub>3</sub>, H<sub>2</sub>SO<sub>4</sub>, and KOH

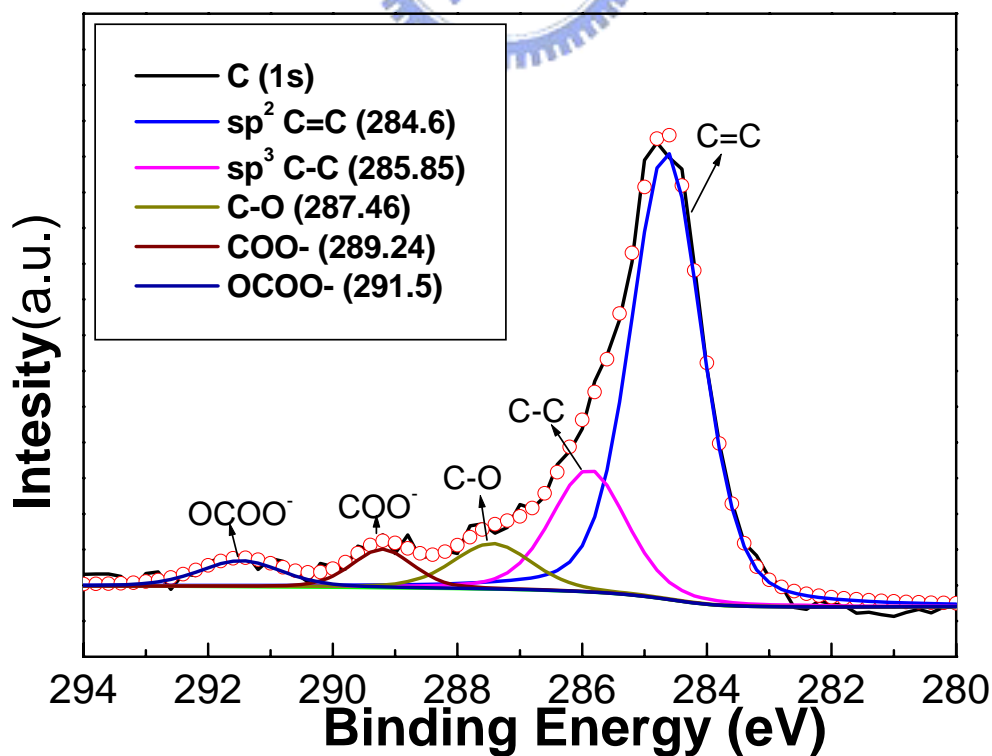


Fig.4.7 (a) The C 1s spectrum of HNO<sub>3</sub>-MWNTs



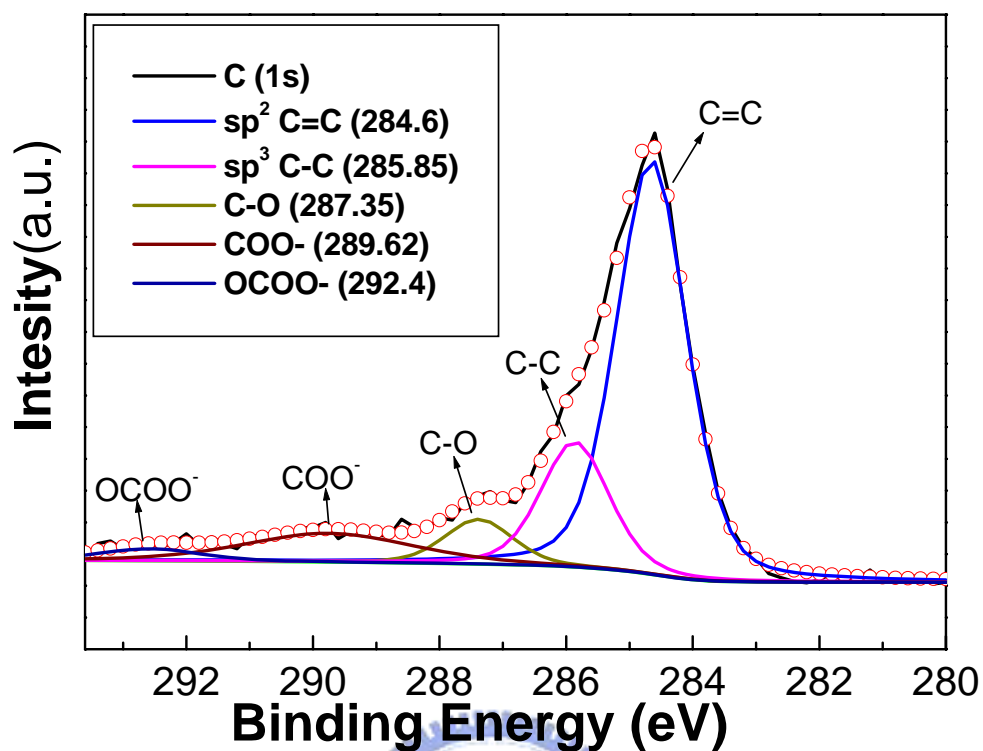


Fig.4.7 (b) The C 1s spectrum of H<sub>2</sub>SO<sub>4</sub>-MWNTs

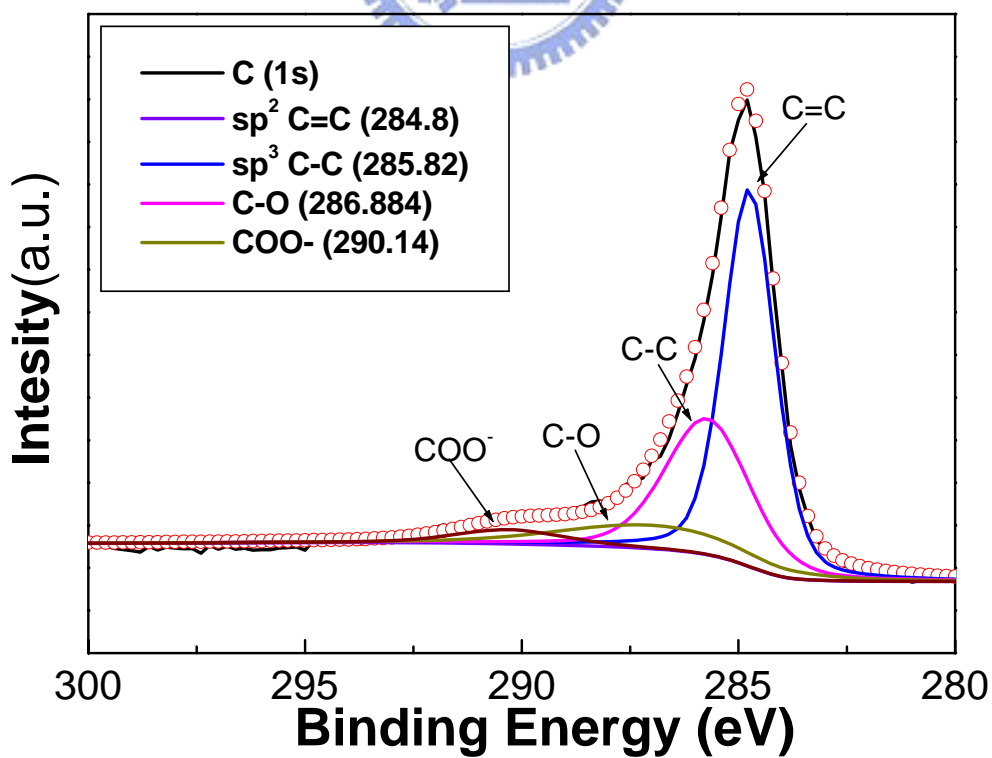
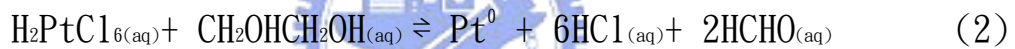


Fig.4.7 (c) The C 1s spectrum of KOH-MWNTs

## 4.2.2 Qualitative analysis of Pt on MWNTs

Pt particles are deposited on MWNTs by using polyol process after samples are modified chemically. Then, we take EDX and XPS of qualitative analysis for samples in order to be sure that polyol process is successful. Fig. 4.8 shows the mapping of EDX for HNO<sub>3</sub>-MWNTs. It indicates that the dispersive nanoparticles on MWNTs are Pt. On the other hand, Fig. 4.9 also shows the XPS survey spectrum of HNO<sub>3</sub>-MWNTs after the Pt reduction. Notably, a very strong Pt4f peak indicates that there are Pt nanoparticles on MWNTs because XPS is a surface-sensitive tool.

The formation process of PVP-protected Pt nanoparticles synthesized in ethylene glycol is presented that the H<sub>2</sub>PtCl<sub>6</sub> may be completely reduced according to the eq (1) and the eq (2).



As mentioned above, the Pt precursors are reduced to Pt<sup>0</sup> atoms at 160<sup>0</sup>C for 3hr [39]. Fig. 4.10 shows that the dispersive Pt nanoparticles on MWNTs are Pt<sup>0</sup> because there is no significant chemical shift of binding energy in Pt4f<sub>7/2</sub> and Pt4f<sub>5/2</sub> with Ar<sup>+</sup> etching [40]. Table 4.3 shows that the binding energy of Pt4f<sub>7/2</sub> and Pt4f<sub>5/2</sub> are developed by Ar<sup>+</sup> etching (25mA and 3kV) with time. Finally, the Pt<sup>0</sup> nanoparticles are stabilized on MWNTs by using ethylene glycol.

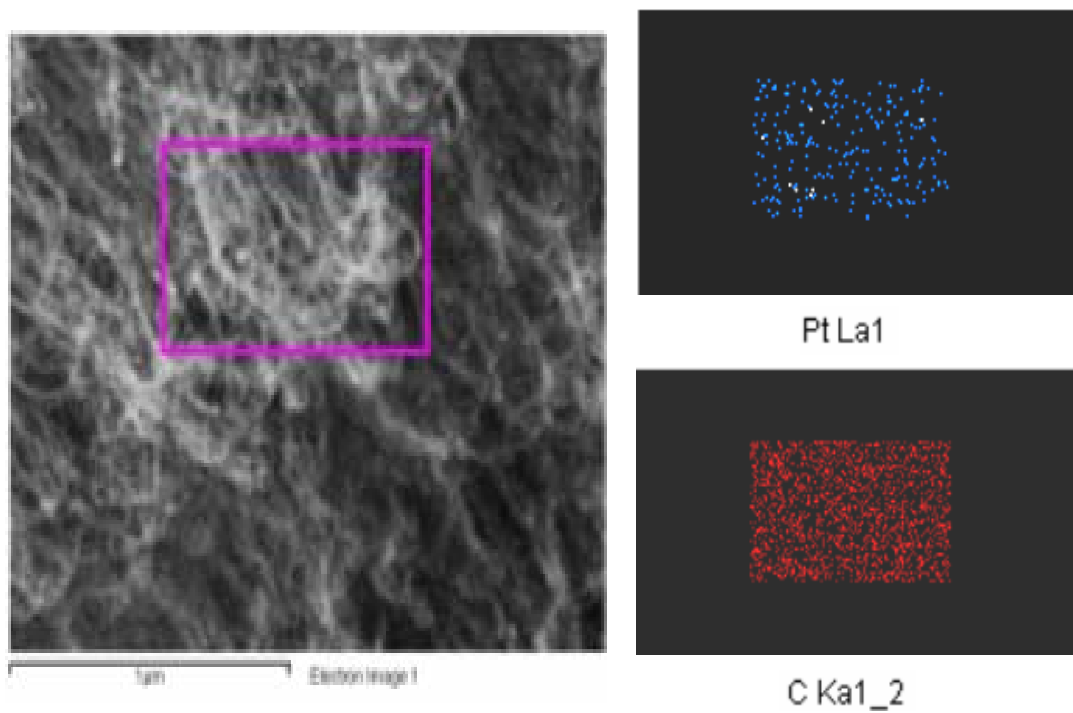


Fig. 4.8 The mapping of EDX for HNO<sub>3</sub>-MWNTs

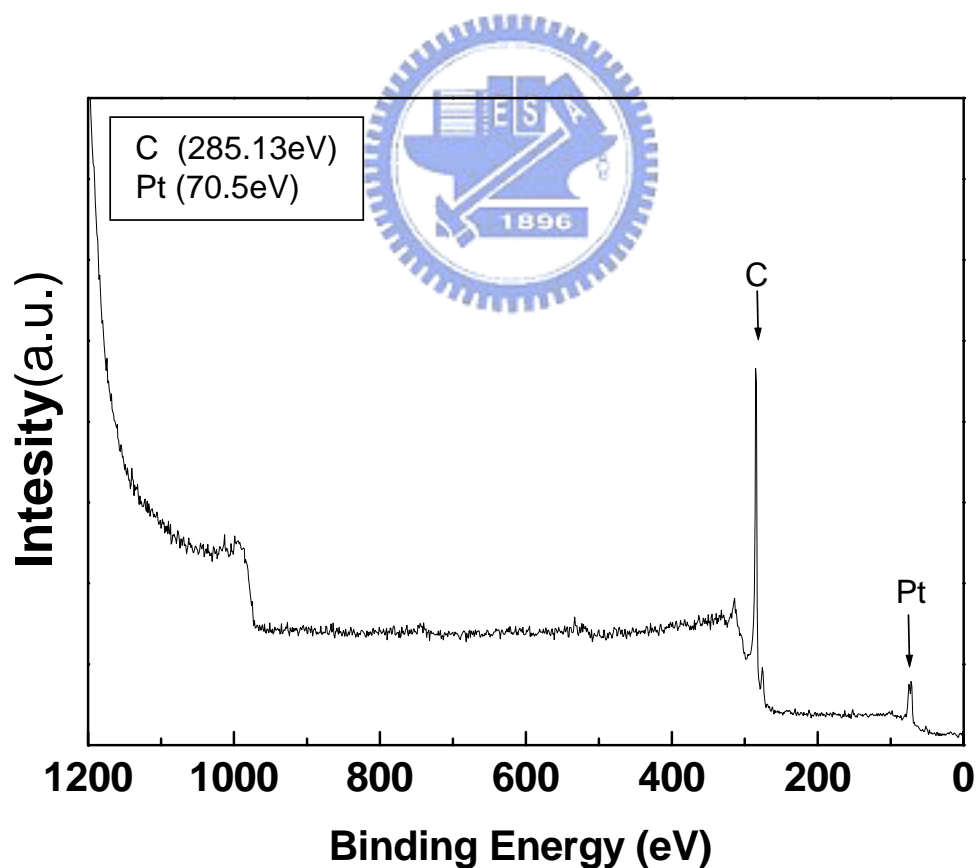


Fig. 4.9 The XPS survey spectrum of HNO<sub>3</sub>-MWNTs after reduction of Pt

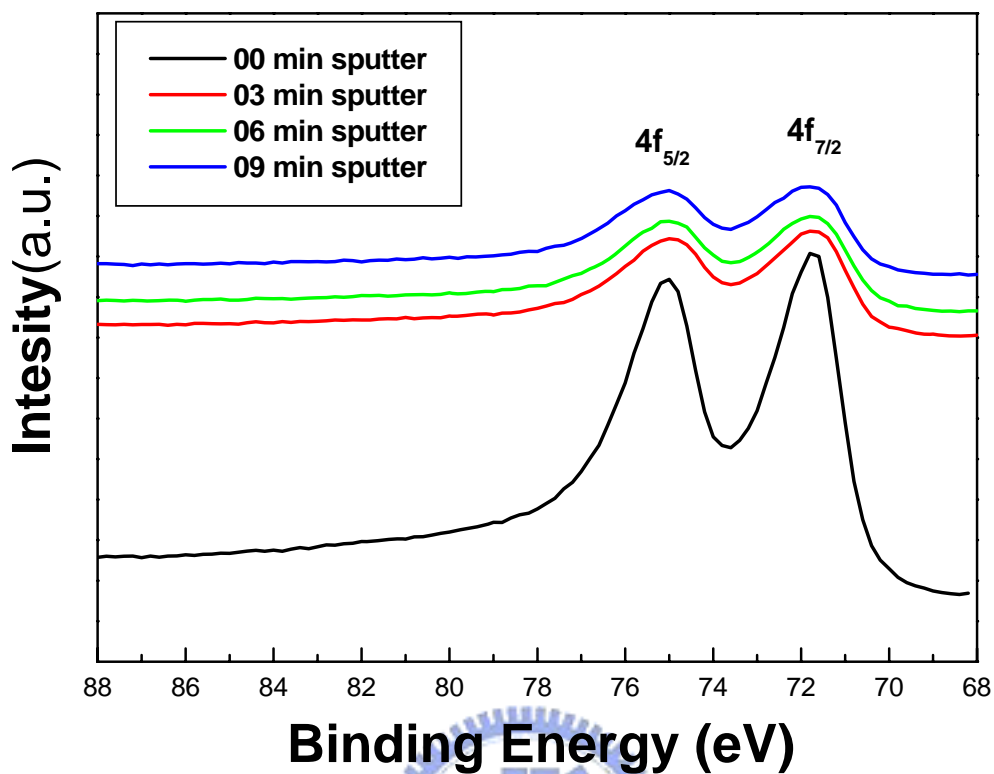


Fig. 4.10 Chemical shift of binding energy in Pt $4f_{7/2}$  and Pt $4f_{5/2}$  with Ar<sup>+</sup> etching

Table 4.3 The development of the binding energy of Pt $4f_{7/2}$  and Pt $4f_{5/2}$  with time

Ar <sup>+</sup> (25mA, 3kV)	$4f_{5/2}$	$4f_{7/2}$
0 min	75.04 eV	71.77 eV
3 min	74.99 eV	71.76 eV
6 min	75.03 eV	71.77 eV
9 min	75.07 eV	71.80 eV

### 4.2.3 Analysis of dispersive Pt on MWNTs

Pt nanoparticles are actually deposited onto the surface of MWNTs from the last section. Then, by comparing Pt on the raw and modified MWNTs, we would like to understand the influence of the functional groups on Pt dispersion on MWNTs. Fig. 4.11 illustrates many Pt nanoparticles are agglomerated on some areas like a larger nanoparticle. Fig. 4.12 illustrates many Pt nanoparticles disperse uniformly on HNO<sub>3</sub>-MWNTs due to presence of the carboxylic acids (-COOH). If Pt nanoparticles were agglomerated, the total effective activating catalyst area would decrease due to the clustered shelter of Pt nanoparticles. Therefore, MWNTs have to be modified chemically in order to disperse Pt nanoparticles on MWNTs uniformly.

### 4.2.4 EDX analysis of Pt on MWNTs

Pt loading on carbon nanotube would be increased because more functional groups, the carboxylic acids (-COOH), act nucleation sites and make active catalyst areas large. The energy dispersive analysis in Fig. 4.13, Fig. 4.14, Fig. 4.15, and Fig. 4.16 show that the amount of Pt loaded on MWNTs with reference to carbon can be evaluated qualitatively as 16.88 wt%, 21.23 wt%, 22.84 wt%, and 26.08 wt% after the different chemical modification. The most Pt loading on MWNTs modified by HNO<sub>3</sub> (strong oxidizing agent) in Fig. 4.17 may be suggested that the most functional groups would be formed on the surface of MWNTs at the same time with different chemical solutions.

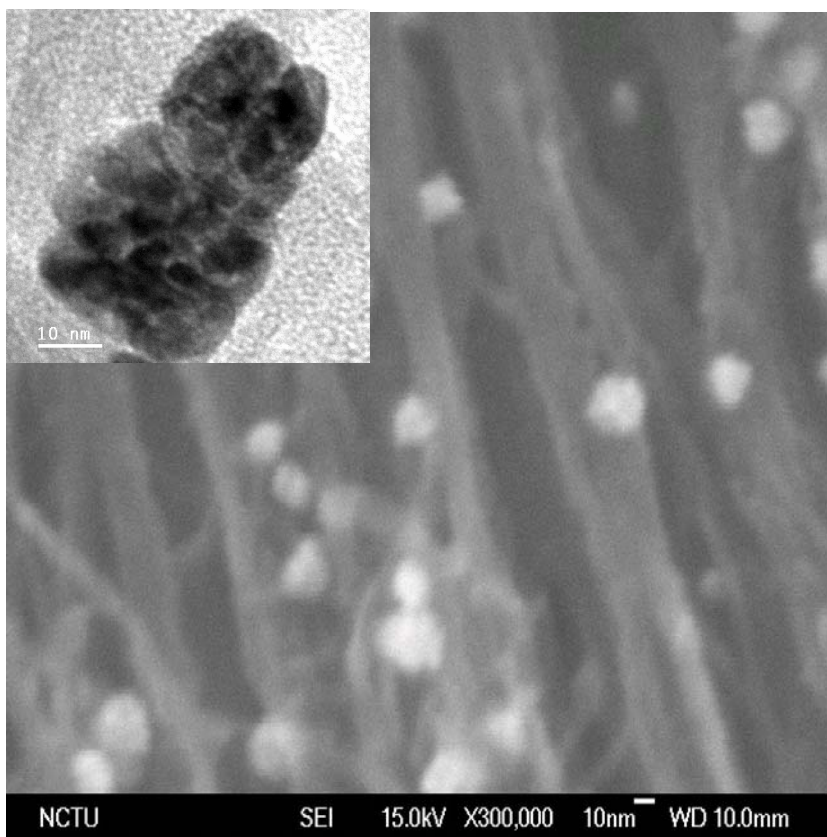


**Fig. 4.11 Pt nanoparticles are agglomerated like a larger nanoparticle**

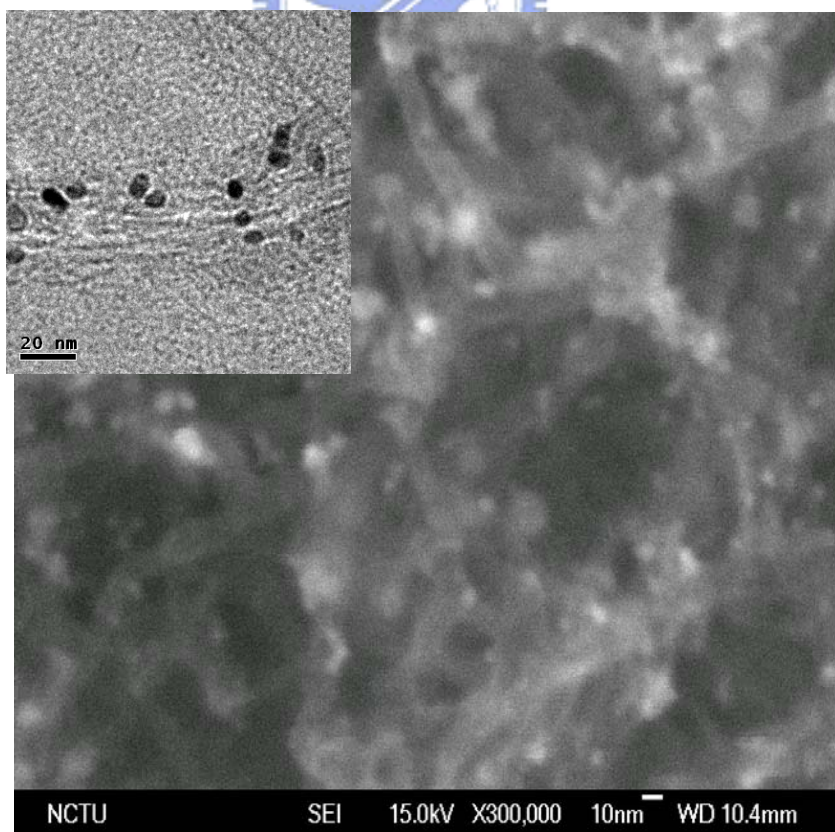


**Fig. 4.12 Pt nanoparticles disperse uniformly on HNO<sub>3</sub>-MWNTs**

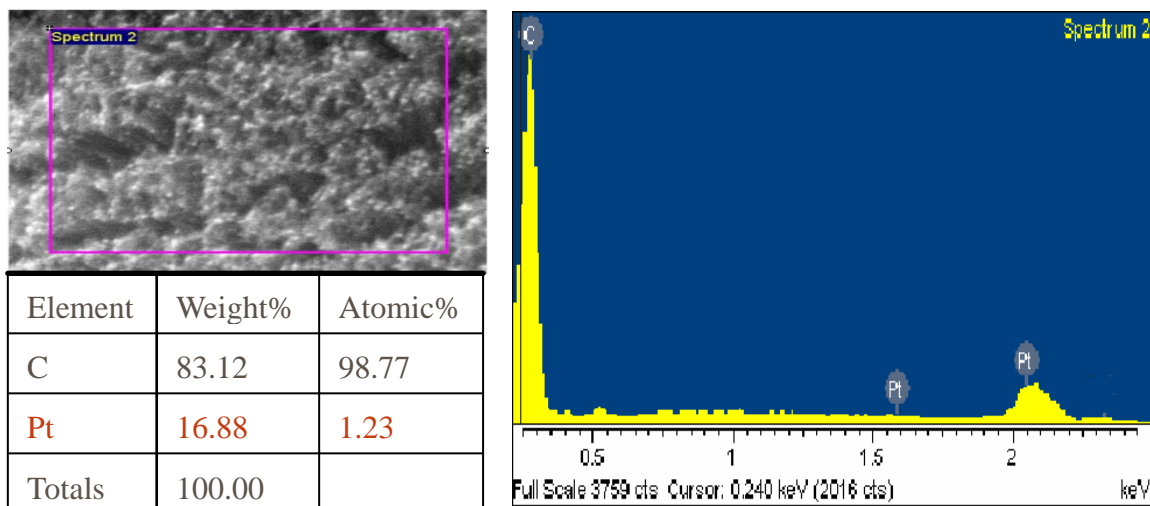


**Fig. 4.13** The amount of Pt loading on raw MWNTs is 16.88 wt%.

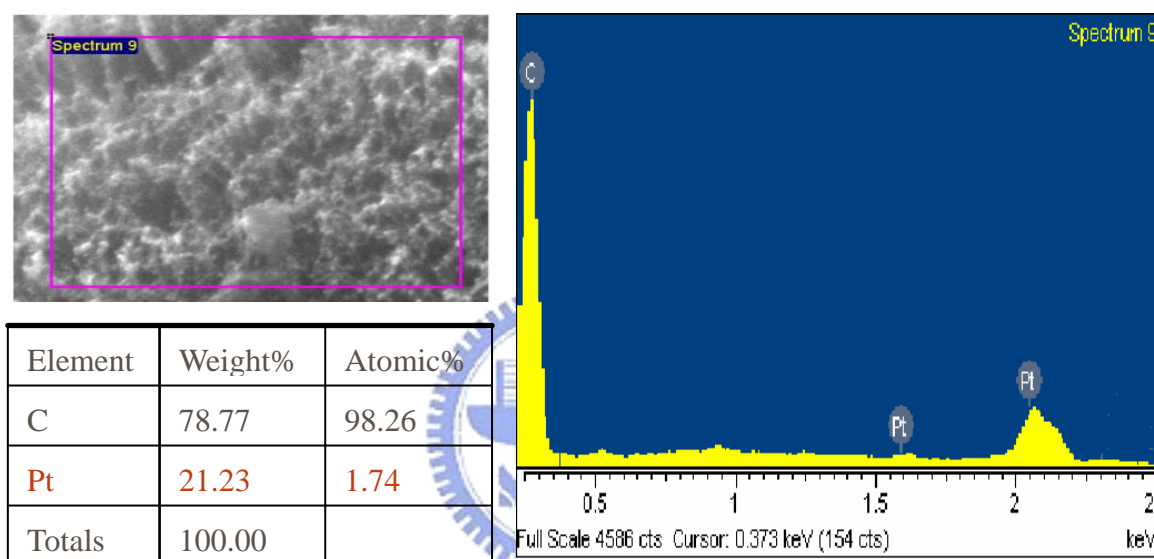


**Fig. 4.14** The amount of Pt loading on KOH -MWNTs is 21.23 wt%.

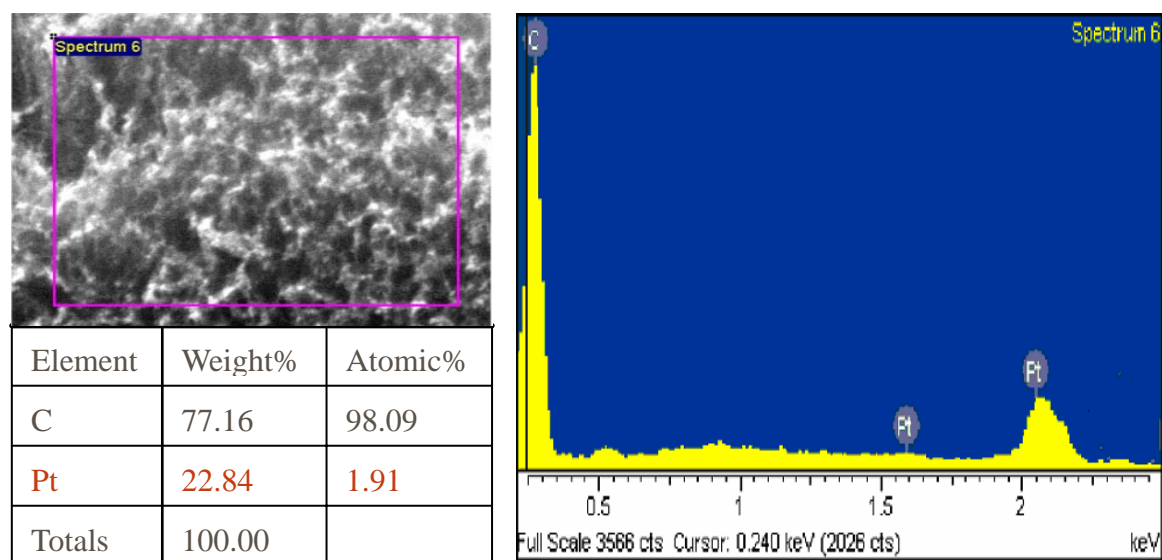


**Fig. 4.15** The amount of Pt loading on H<sub>2</sub>SO<sub>4</sub> -MWNTs is 22.84 wt%.

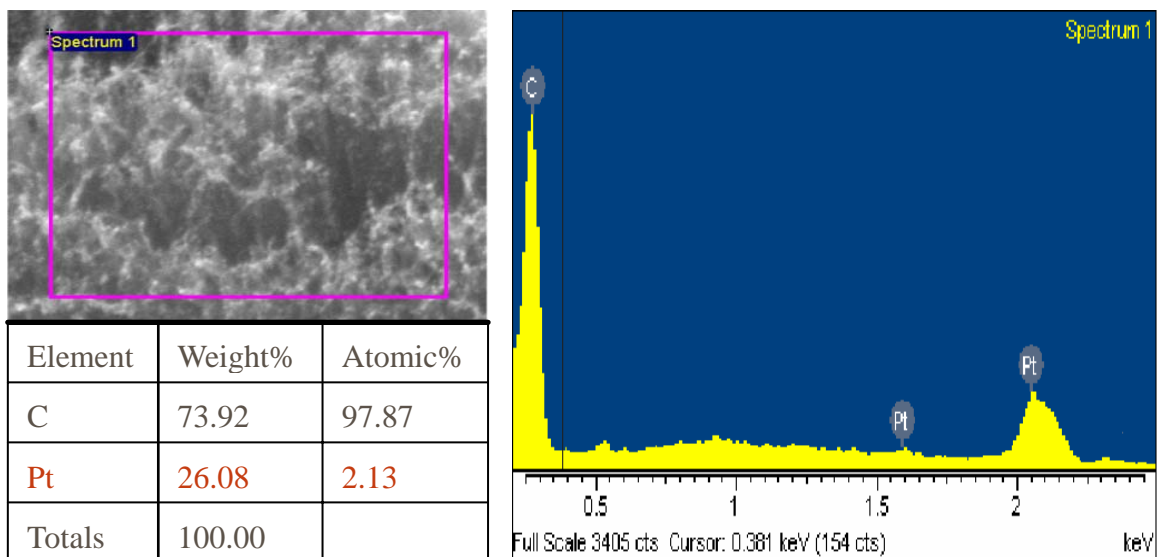


Fig. 4.16 The amount of Pt loading on HNO<sub>3</sub>-MWNTs is 26.08 wt%.

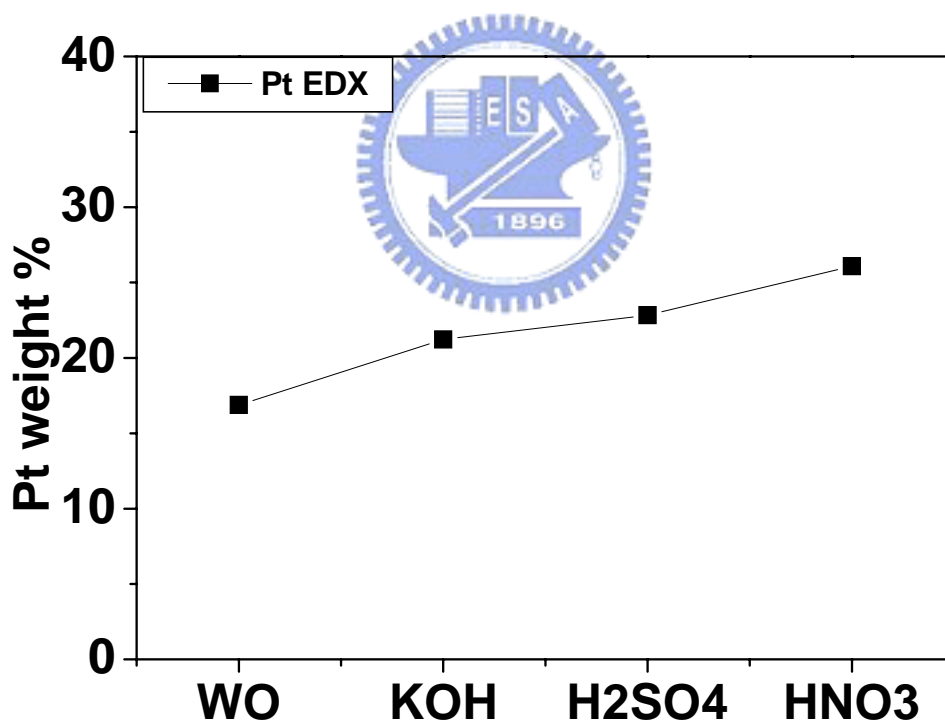
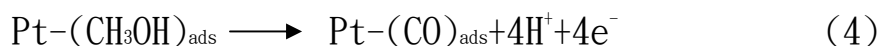


Fig. 4.17 Pt loading on MWNTs with different chemical modification



## 4.2.5 Half-cell test

The activity of catalyst is practically important in the study on fuel cell, which is usually evaluated by the current peaks with the dispersion and the amount of catalyst. The electrocatalytic activity of Pt nanoparticles is obtained from the CV measurements performed in 1M methanol and 1M sulfuric acid electrolyte. Fig. 4.18 shows that the electrocatalytic activity of Pt nanoparticles is evaluated by the current peaks of methanol oxidation in eq. (3) and eq. (4)



As well known, it can be observed that the electrocatalytic activity of Pt nanoparticles on HNO<sub>3</sub>-MWNTs is higher than the others due to more amounts of dispersive Pt nanoparticles.



## 4.2.6 Summary

1. Various solvents, eg. HNO<sub>3</sub>, H<sub>2</sub>SO<sub>4</sub>, and KOH (80<sup>0</sup>C, 6 hr), modified MWNTs can form the same functional group -COOH and -OH.
2. Well-dispersed functional groups on MWNTs could improve the efficiency of half-cell test.
3. The functional groups on MWNTs increase anchoring sites of Pt precursor to increase the efficiency of half-cell test.
4. The amount of functional groups in order to attract Pt on HNO<sub>3</sub>-MWNTs is more than on H<sub>2</sub>SO<sub>4</sub>-MWNTs and on KOH-MWNTs due to a strong oxidizing agent HNO<sub>3</sub>.

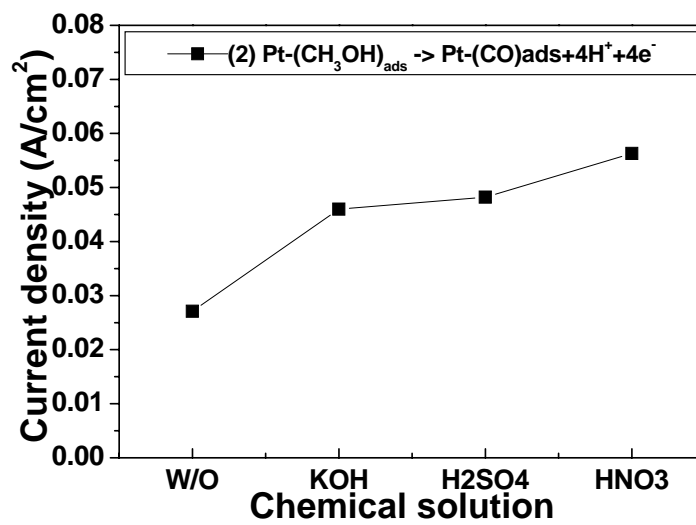
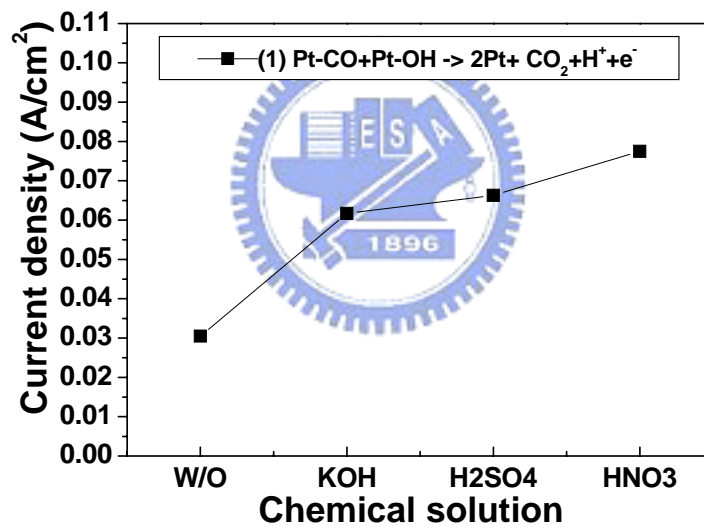
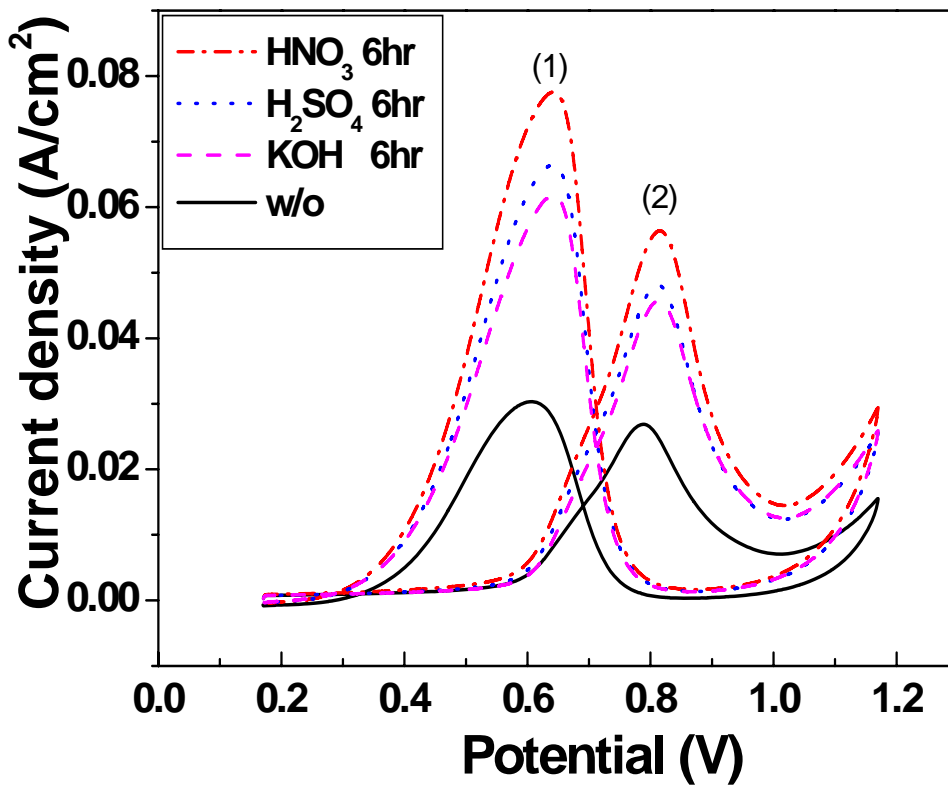


Fig. 4.18 Electrocatalytic activity is evaluated by the current peaks

### 4.3. Multi-wall carbon nanotubes are modified by HNO<sub>3</sub> with Temperature (T), time (t), and concentration (conc.).

MWNTs are modified by HNO<sub>3</sub>, H<sub>2</sub>SO<sub>4</sub>, and KOH at high temperature in Section 4.2 and may produce the same functional groups, the alcoholic hydroxyl groups (-OH) and carboxylic acids (-COOH), to attract more Pt ions nucleating uniformly and densely. Moreover, the amount of functional groups in order to attract Pt on HNO<sub>3</sub>-MWNTs is more than on H<sub>2</sub>SO<sub>4</sub>-MWNTs and on KOH-MWNTs due to a strong oxidizing agent HNO<sub>3</sub>. However, there are the other parameters, temperature, time, and concentration, in the function of chemical modification for MWNTs. In this work, we would find the best temperature (T) for HNO<sub>3</sub>-MWNTs may produce a lot of functional groups to increase Pt anchoring sites in Table. 4.4. Furthermore, for 2M HNO<sub>3</sub>, the highest temperature would be lower 100<sup>0</sup>C to maintain the concentration.



**Table 4.4 HNO<sub>3</sub>-MWNTs with different T**

<b>Temperature (T)</b>	<b>80<sup>0</sup>C</b>	<b>90<sup>0</sup>C</b>	<b>100<sup>0</sup>C</b>
<b>2M HNO<sub>3</sub></b> <b>(b.p. ~105<sup>0</sup>C)</b>	24 hr	24 hr	24 hr
<b>14M HNO<sub>3</sub></b> <b>(b.p. ~122<sup>0</sup>C)</b>	24 hr	24 hr	24 hr

### 4.3.1.1 Analysis of MWNTs morphology with T

Fig. 4.19 and Fig. 4.20 show that there is little damage for 14 M HNO<sub>3</sub>-MWNTs at 80<sup>0</sup>C and 90<sup>0</sup>C for 24 hr. On the contrary, Fig. 4.21 shows that there is a serious damage for 14 M HNO<sub>3</sub>-MWNTs at 100<sup>0</sup>C for 24 hr. The total loading amount of Pt would decrease if the amount of MWCNT as support were broken. Therefore, the temperature of chemical modification would be lower than 100<sup>0</sup>C.

### 4.3.1.2 Analysis of functional groups with T

We try to assay the functional groups with FTIR after MWNTs are modified by 2 M or by 14 M HNO<sub>3</sub> with temperature. Fig. 4.22(a) (b) show that oxidization with HNO<sub>3</sub> at 90<sup>0</sup>C and 100<sup>0</sup>C successfully introduced carboxylic acids (-COOH), carboxyl groups (-C=O), and alcoholic hydroxyl groups (-OH) on MWNTs surfaces. However, the functional groups of 2M and 14M HNO<sub>3</sub>-MWNTs at 80<sup>0</sup>C would be difficult to be detected because of their weak response in the IR mode. It is suggested that temperature is a main factor if the oxidization of chemical reaction could proceed. Finally, 90<sup>0</sup>C is the optimum temperature for 2M and 14M HNO<sub>3</sub>-MWNTs to form a lot of functional groups.

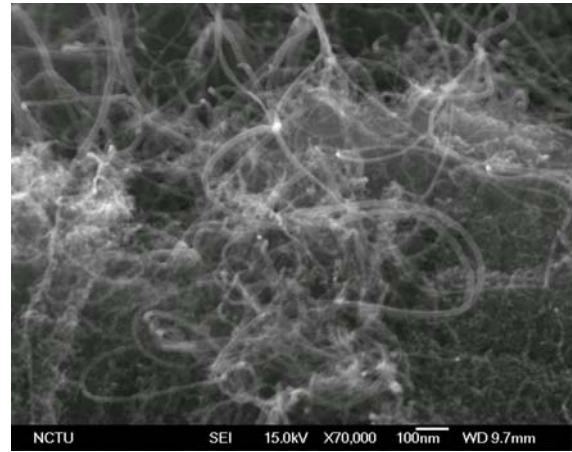
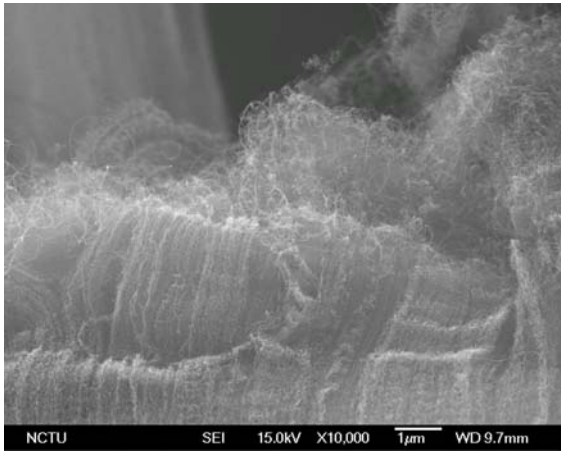


**Fig. 4.19** Little damage for 14M HNO<sub>3</sub>-MWNTs at 80<sup>0</sup>C

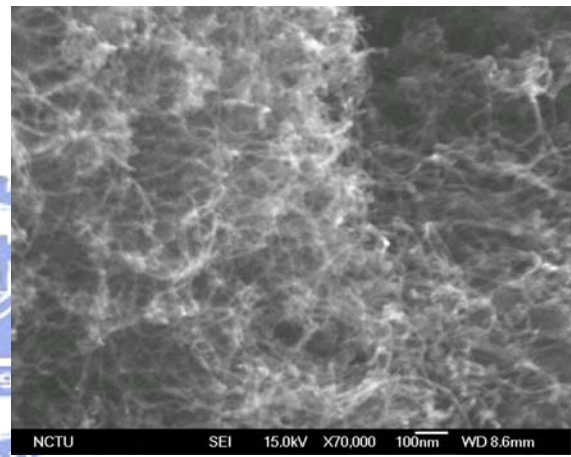
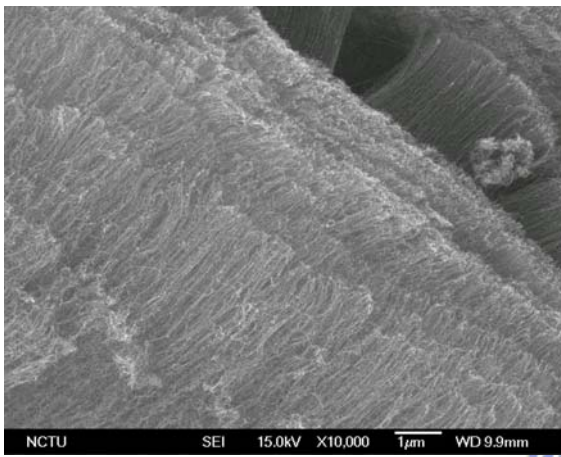


**Fig. 4.20** Little damage for 14M HNO<sub>3</sub>-MWNTs at 90<sup>0</sup>C

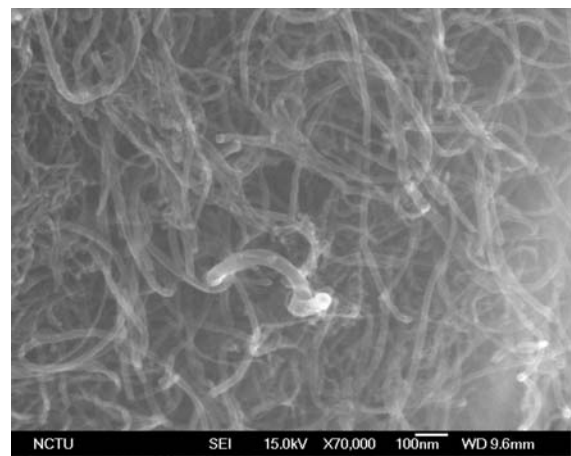
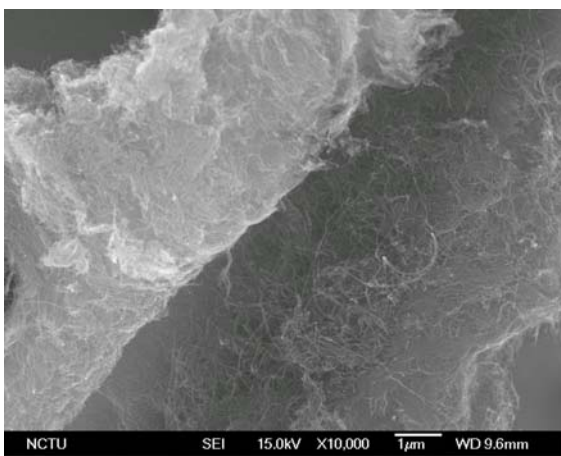


**Fig. 4.21** A serious damage for 14M HNO<sub>3</sub>-MWNTs at 100<sup>0</sup>C

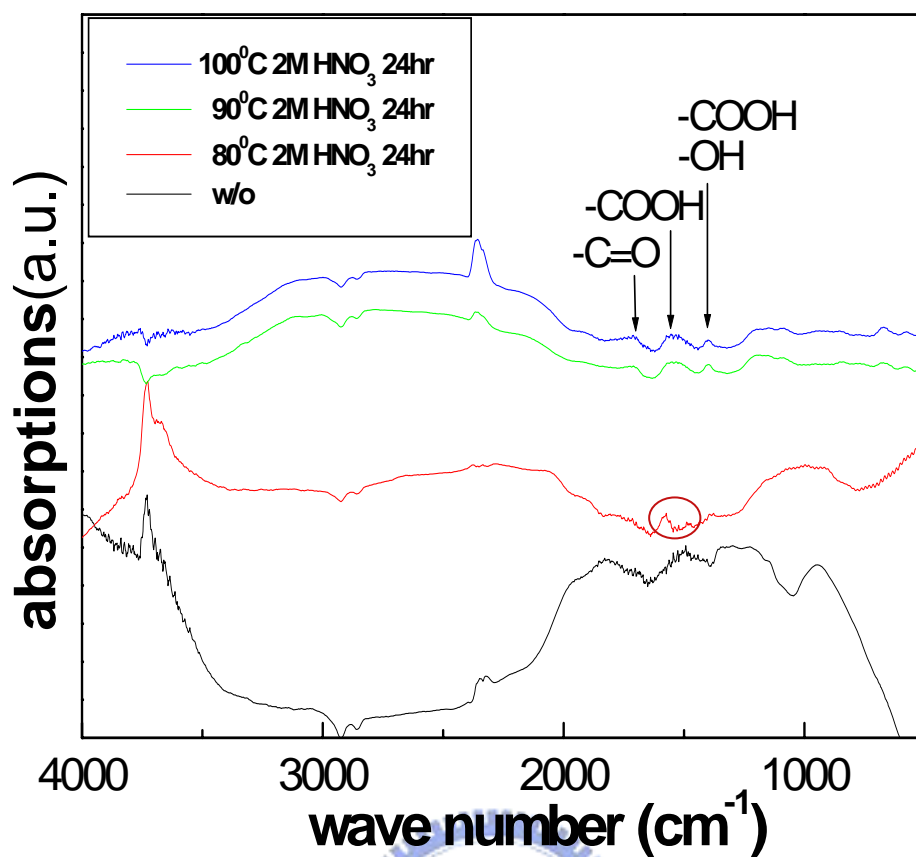


Fig. 4.22 (a) FTIR of 2M HNO<sub>3</sub>-MWNTs with different T

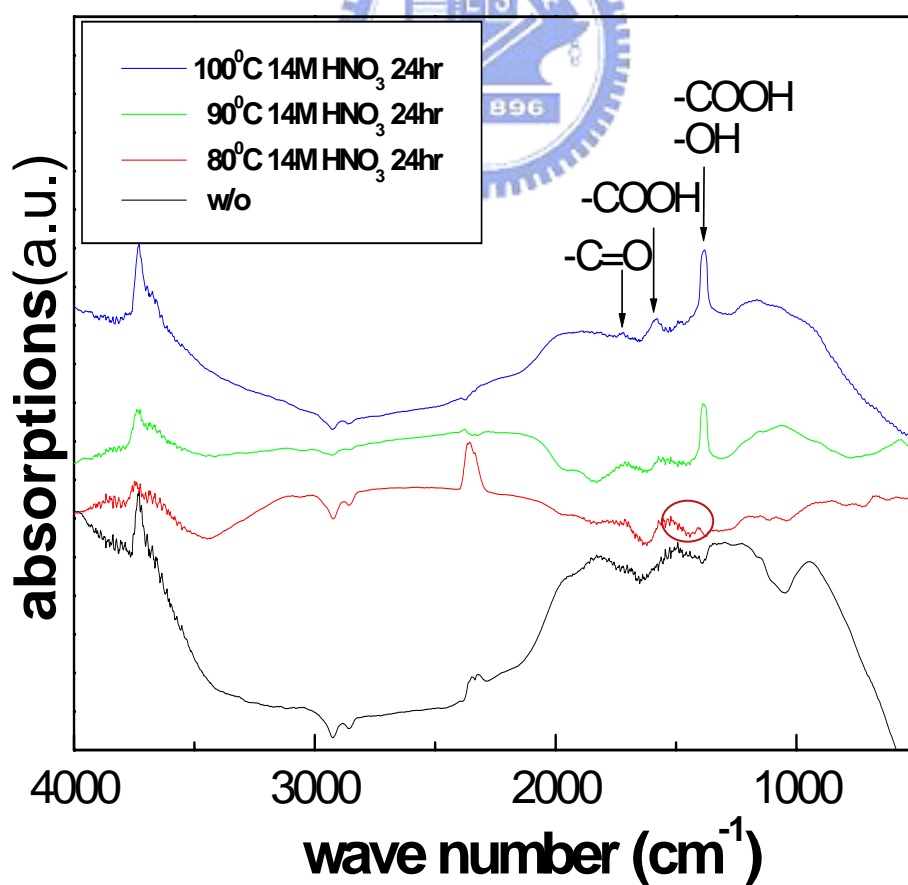


Fig. 4.22 (b) FTIR of 14M HNO<sub>3</sub>-MWNTs with different T

From Section 4.3.1, the modified MWNTs at 90<sup>0</sup>C form a lot of functional groups for 2 M HNO<sub>3</sub> and 14 M HNO<sub>3</sub>. In the followed Section 4.3.2 and Section 4.3.3, we would find the other best parameters time (t) with high (14M) and low (2M) concentration (conc.) for HNO<sub>3</sub>-MWNTs may produce the most functional groups to increase Pt anchoring sites in Table. 4.5

**Table 4.5 MWNTs are modified by HNO<sub>3</sub> at 90<sup>0</sup>C for 2M and 14M with t**

90 <sup>0</sup> C	Time (hr)					
2M HNO <sub>3</sub>	00	06	12	18	24	48
14M HNO <sub>3</sub>	00	06	12	18	24	48



#### **4.3.2.1 FTIR of 2M HNO<sub>3</sub>-MWNTs with t**

The number of carboxylic acids (-COOH) would be expected by its intensity in the FTIR spectrum as MWNTs (0.01g) are diluted with a potassium bromide (KBr) dispersedly [32]. Fig. 4.23 shows that the number of carboxylic acids (-COOH) would increase with time gradually so more Pt could be anchored on MWNTs by more carboxylic acids (-COOH).

#### **4.3.2.2 EDX analysis of Pt/2M HNO<sub>3</sub>-MWNTs**

Pt loading on carbon nanotube would be increased because more functional groups, the carboxylic acids (-COOH), act nucleation sites and make active catalyst areas large.

The energy dispersive analysis in Fig. 4.24, Fig. 4.25, Fig. 4.26, Fig. 4.27 and Fig. 4.28 show that the amount of Pt loaded on MWNTs with reference to carbon can be evaluated qualitatively as 14.37 wt%, 16.72 wt%, 24.38 wt%, 28.21 wt%, and 26.99 wt% after the chemical modification of 2M HNO<sub>3</sub> with time. As mentioned above, 2M HNO<sub>3</sub>-MWNTs from 12 hr to 24 hr may anchor the most amount of Pt in Fig. 4.29. Therefore, it is called stable state for the most loading of Pt.

### 4.3.2.3 Half-cell test

The activity of catalyst is practically important in the study on fuel cell, which is usually evaluated by the current peaks with the dispersion and the amount of catalyst. The electrocatalytic activity of Pt nanoparticles is obtained from the CV measurements performed in 1M methanol and 1M sulfuric acid electrolyte. Fig. 4.30 shows that the electrocatalytic activity of Pt nanoparticles is evaluated gradually by the current peaks of methanol oxidation. As a whole, it can be observed that the highest electrocatalytic activity of Pt nanoparticles for 2M HNO<sub>3</sub>-MWNTs range from 12 hr to 24 hr (stable state) due to the most amounts of dispersive Pt nanoparticles. However, the electrocatalytic activity of Pt nanoparticles for 2M HNO<sub>3</sub>-MWNTs decreases much significantly from 24 hr to 48 hr because MWNTs may be destroyed very much at 48 hr.

### 4.3.2.4 Effective activating area

The electrochemically active surface areas of the Pt nanoparticles are obtained from the CV measurements performed in 1M sulfuric acid electrolyte. A typical voltammogram is shown in Fig. 4.31, in which the potential is expressed versus that of a



reference platinum electrode. The hydrogen absorption and desorption peaks are clearly seen in the voltammogram at potentials between -0.1 and 0.2 V, which is consistent with those observed for platinized Pt. In detail, a redox peak at 0.5-0.7 V in all voltammograms can be attributed to the quinone and hydroquinone groups. Furthermore, there is a couple of redox peak at about 0.4 V, which may be associated with the C-O and C=O groups [41].

The electrochemically active surface area,  $S_{act}$ , in units of  $\text{cm}^2/\text{mg Pt}$ , is calculated from the CV curves for Pt [42] by eq. (5)

$$S_{act} = \frac{Q_H}{210} \quad (5)$$

In which  $Q_H$ , in units of  $(\text{mA}/\text{mg Pt}) \text{ V}$ , is the integrated area of the hydrogen adsorption region in the voltammogram and the charge for monolayer hydrogen adsorption on Pt equal to  $210 \mu\text{C}/\text{cm}^2$ . To obtain the integrated area for the hydrogen adsorption peaks in Fig. 4.31, a horizontal line is drawn to correct the double-layer charging, and a vertical line is drawn to separate the molecular hydrogen region [42]. Thus, in Table 4.6, the electrochemically active surface areas of the Pt nanoparticles are evaluated gradually with the time of 2M  $\text{HNO}_3$ -MWNTs due to the trend of the electrocatalytic activity of Pt nanoparticles.

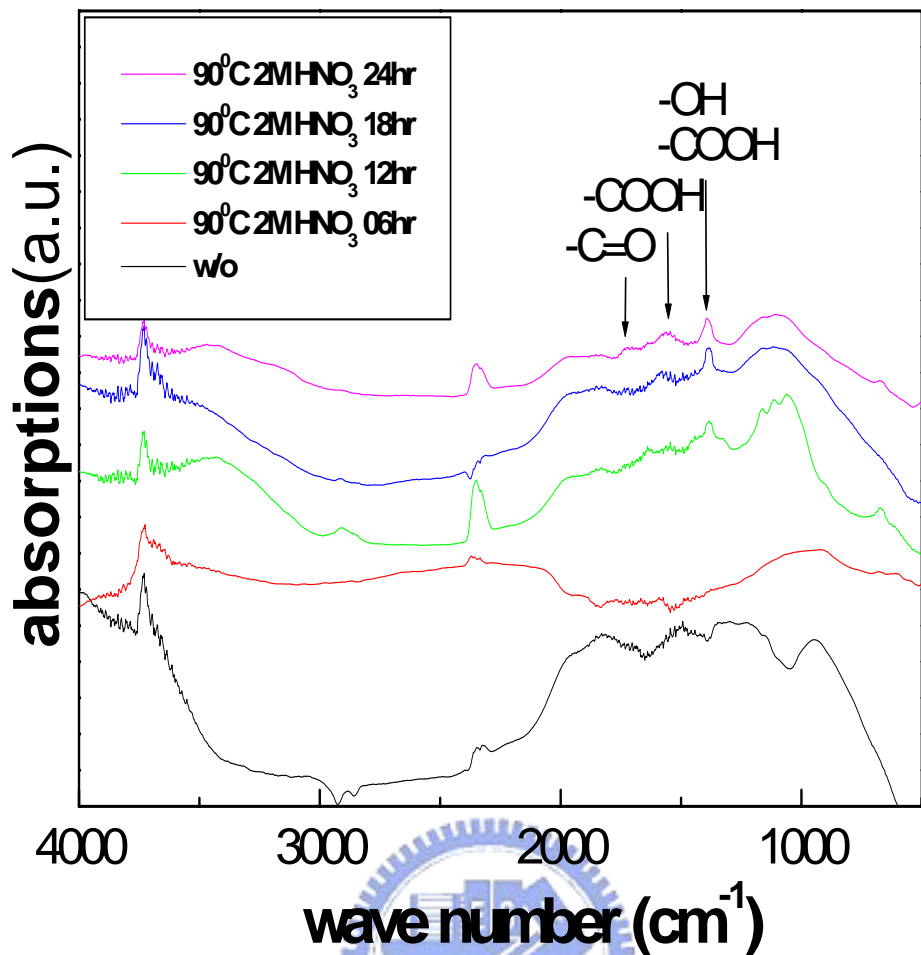


Fig. 4.23 The number of -COOH would increase with t gradually

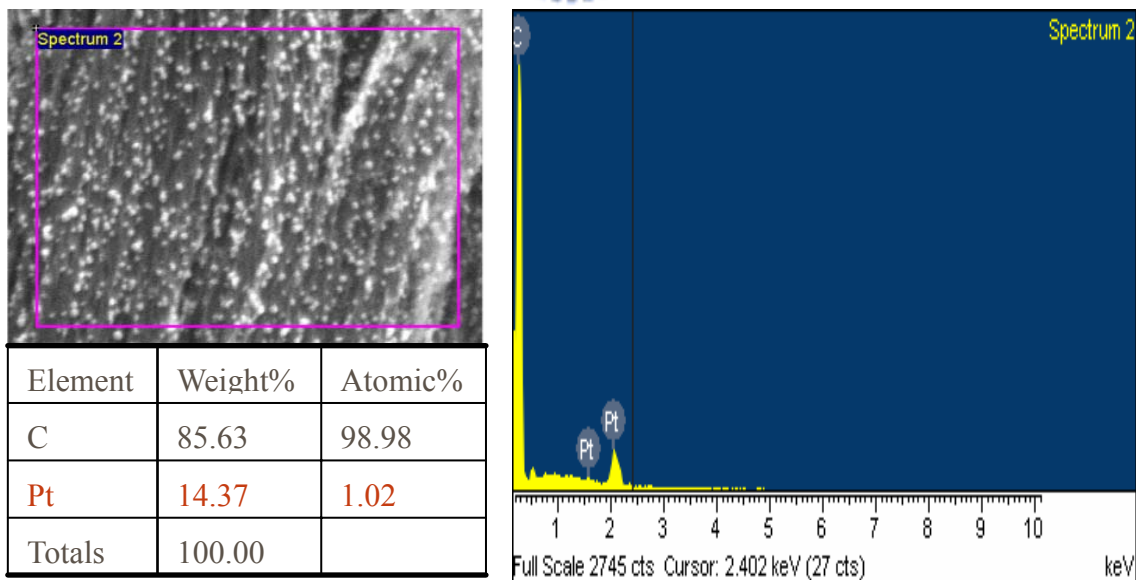
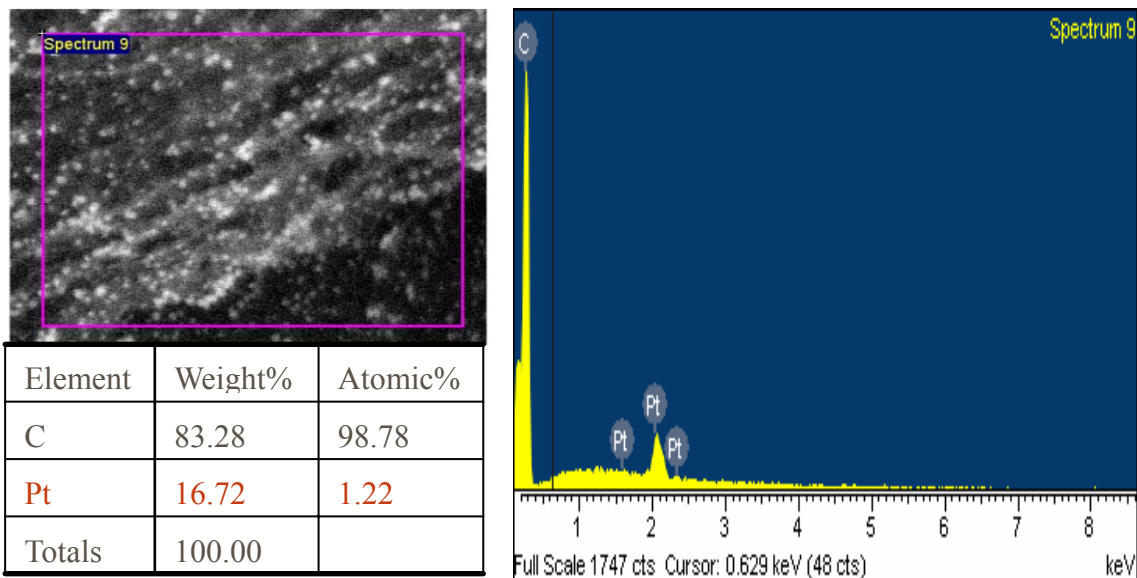
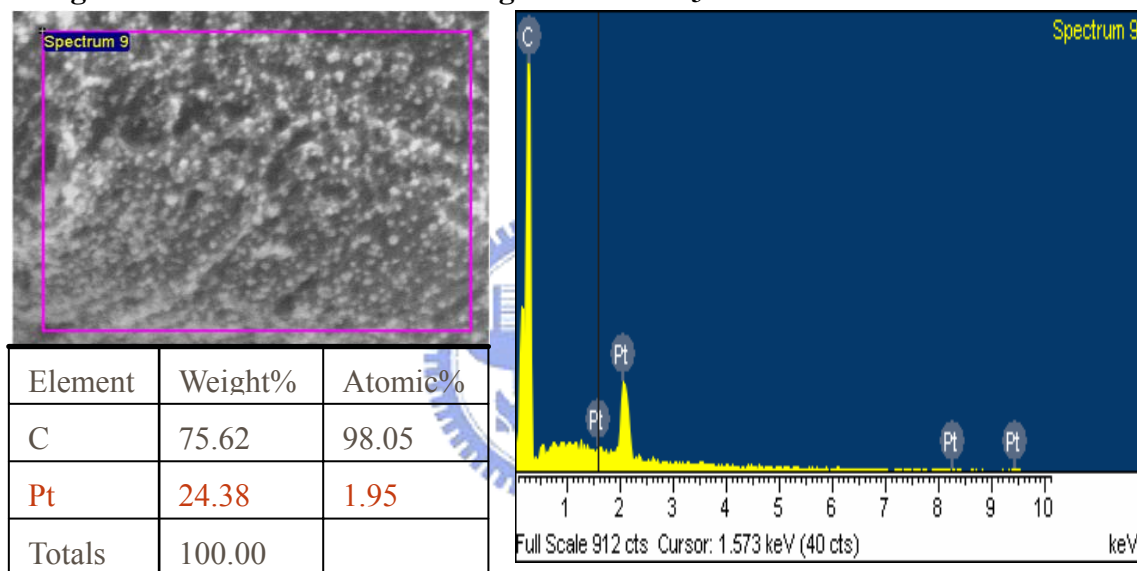


Fig. 4.24 The amount of Pt loading on raw MWNTs is 14.37 wt%



**Fig. 4.25** The amount of Pt loading on 2M HNO<sub>3</sub>-MWNTs at 6 hr is 16.72 wt%



**Fig. 4.26** The amount of Pt loading on 2M HNO<sub>3</sub>-MWNTs at 12 hr is 24.38 wt%

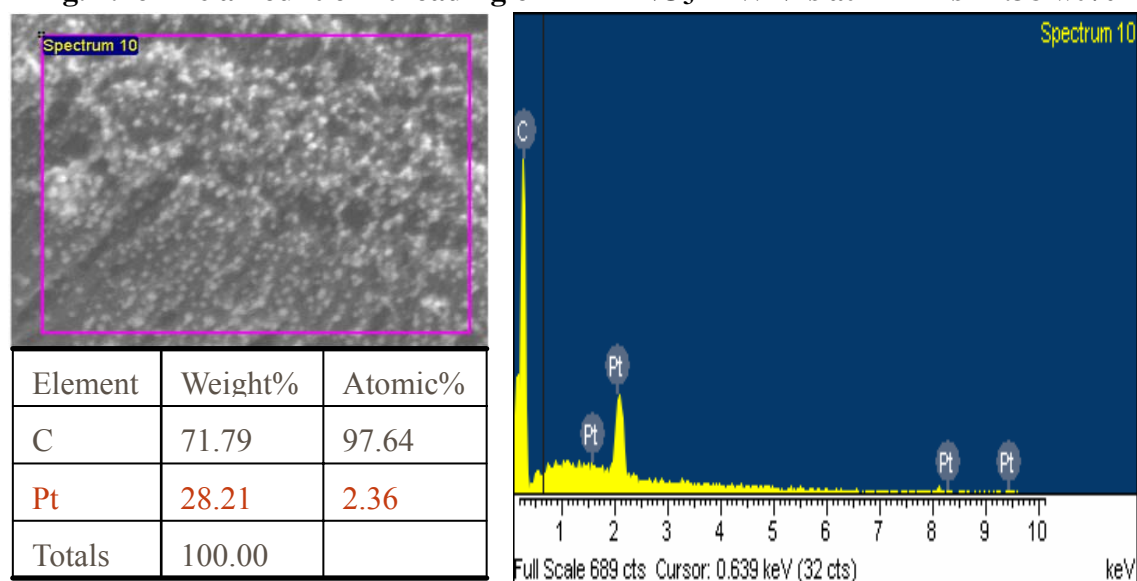


**Fig. 4.27** The amount of Pt loading on 2M HNO<sub>3</sub>-MWNTs at 18 hr is 28.21 wt%

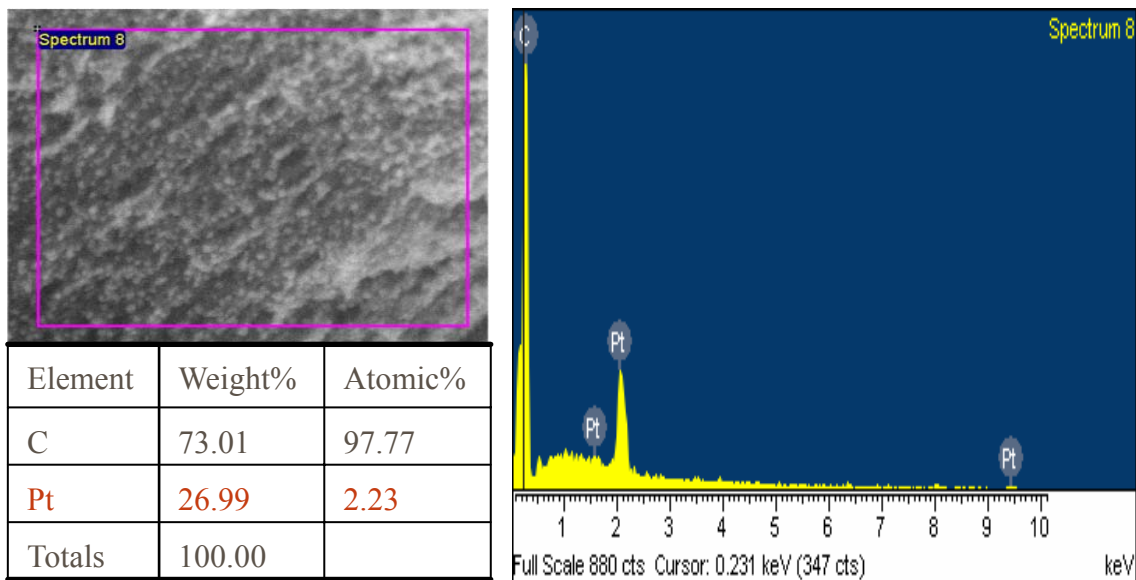


Fig. 4.28 The amount of Pt loading on 2M HNO<sub>3</sub>-MWNTs at 24 hr is 26.99 wt%

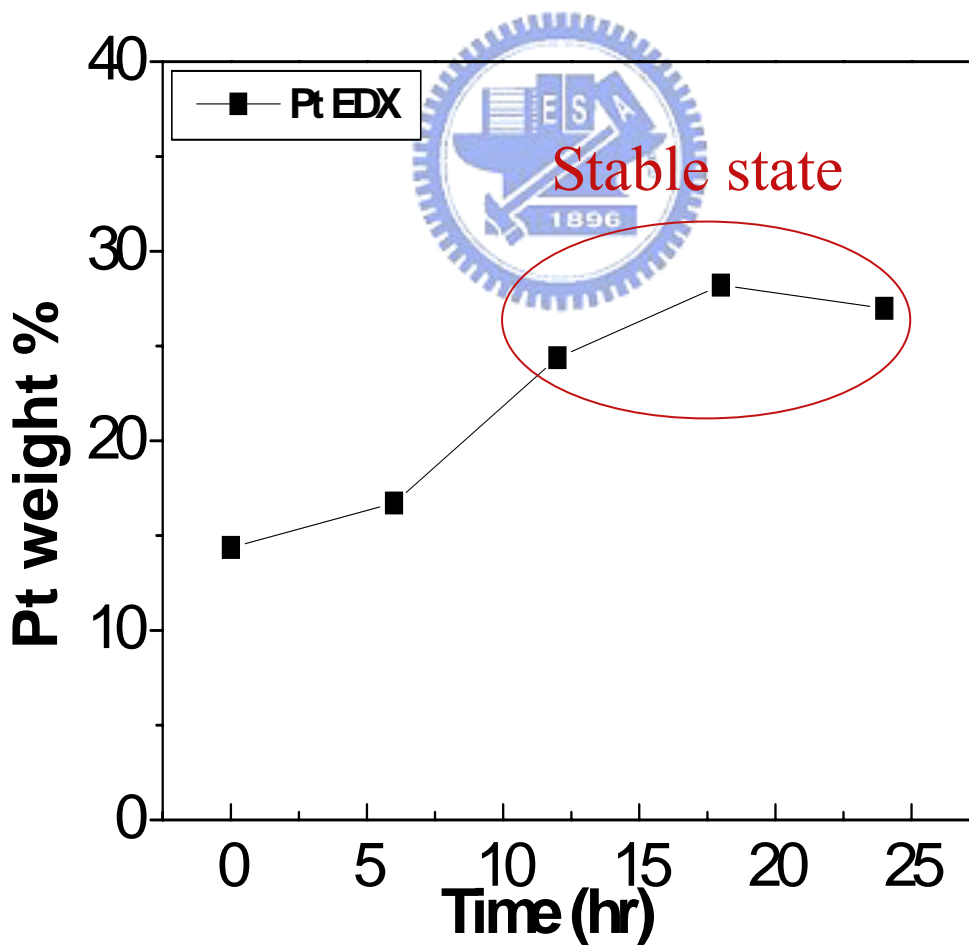


Fig. 4.29 2M HNO<sub>3</sub>-MWNTs from 12 hr to 24 hr may anchor the most Pt

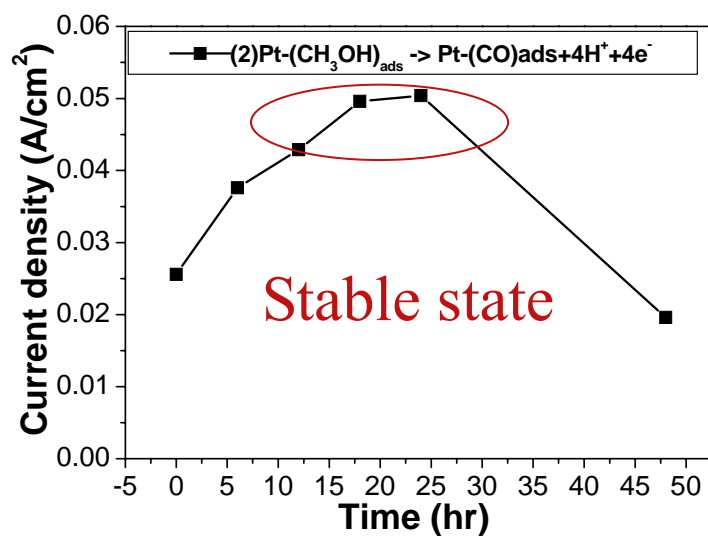
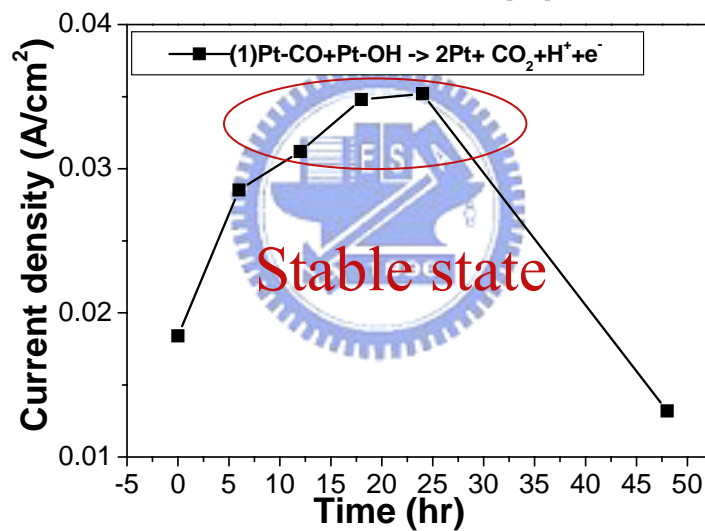
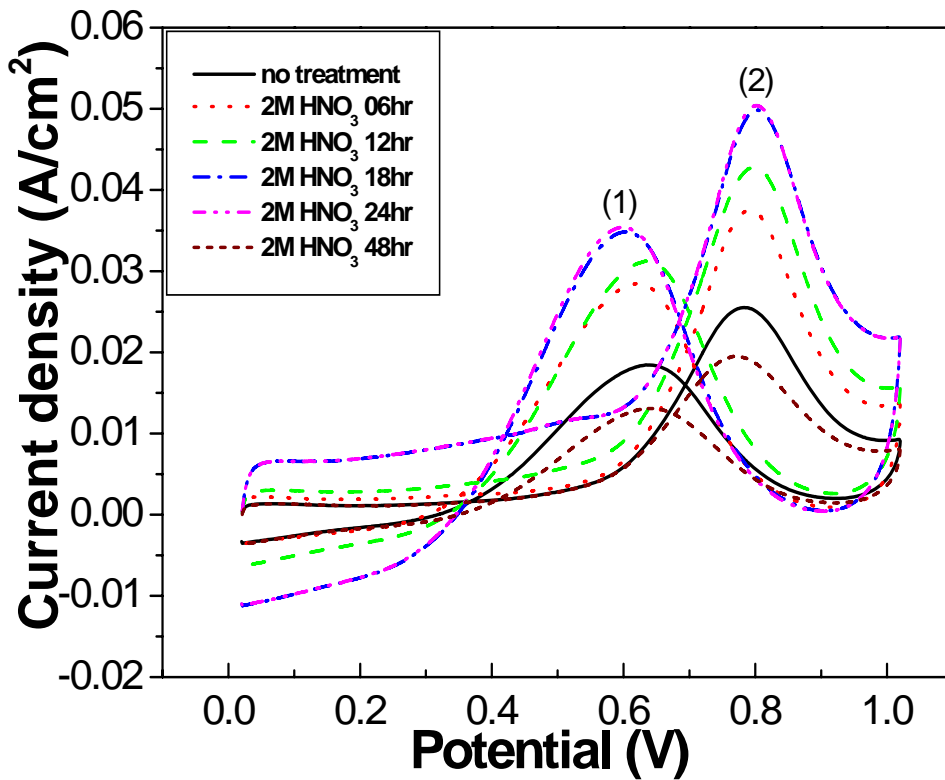


Fig. 4.30 The currents peaks represent the activity of Pt with t

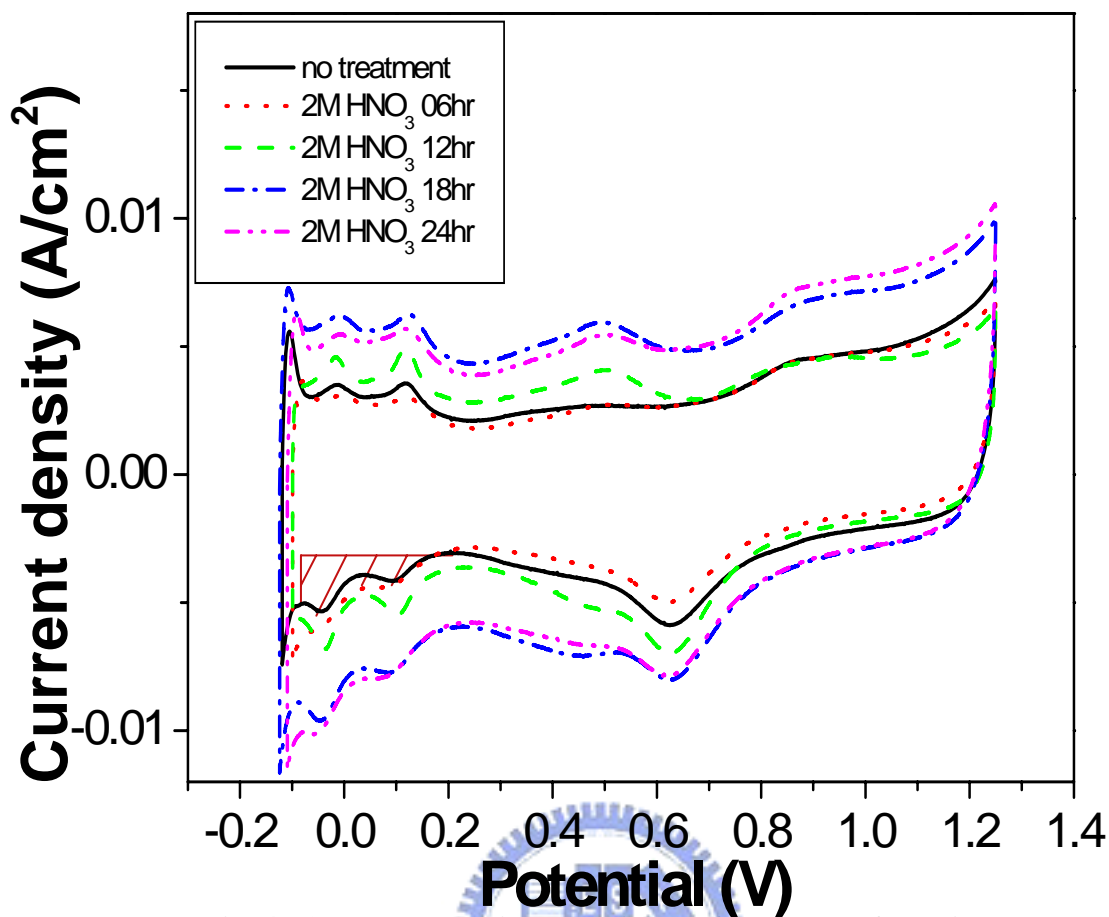


Fig. 4.31 Electrochemically active surface areas of Pt with t

Table 4.6 The value of electrochemically active surface areas of the Pt with the t

Time of 2M HNO <sub>3</sub>	Q <sub>H</sub> (mC)	S <sub>pt</sub> (cm <sup>2</sup> )
00hr	0.28363	1.35064
06hr	0.43399	2.0666
12hr	0.44241	2.10672
18hr	0.52727	2.51081
24hr	0.6042	2.877

### 4.3.3.1 FTIR of 14M HNO<sub>3</sub>-MWNTs with t

The number of carboxylic acids (-COOH) would be expected by its intensity in the FTIR spectrum as MWNTs (0.01g) are diluted with a potassium bromide (KBr) dispersedly [32]. Fig. 4.32 shows that the number of carboxylic acids (-COOH) for 14M HNO<sub>3</sub>-MWNTs would increase with time more fast than for 2M HNO<sub>3</sub>-MWNTs so more Pt nanoparticles could be anchored on MWNTs in the short time.

### 4.3.3.2 EDX analysis of Pt/14M HNO<sub>3</sub>-MWNTs

Pt loading on carbon nanotube would be increased because more functional groups, the carboxylic acids (-COOH), act nucleation sites and make active catalyst areas large. The energy dispersive analysis in Fig. 4.33, Fig. 4.34, Fig. 4.35, Fig. 4.36 and Fig. 4.37 show that the amount of Pt loaded on MWNTs with reference to carbon can be evaluated qualitatively as 15.38 wt%, 26.52 wt%, 27.94 wt%, 25.79 wt%, and 25.95 wt% after the chemical modification of 14M HNO<sub>3</sub> with time. As mentioned above, 14M HNO<sub>3</sub>-MWNTs from 6 hr to 24 hr may anchor the most amount of Pt in Fig. 4.38. Thus, it is called stable state for the most loading of Pt.

### 4.3.3.3 Half-cell test

The activity of catalyst is practically important in the study on fuel cell, which is usually evaluated by the current peaks with the dispersion and the amount of catalyst. The electrocatalytic activity of Pt nanoparticles is obtained from the CV measurements performed in 1M methanol and 1M sulfuric acid electrolyte. Fig. 4.39 shows that the electrocatalytic activity of Pt nanoparticles is evaluated gradually by the current peaks

of methanol oxidation. As a whole, it can be observed that the highest electrocatalytic activity of Pt nanoparticles for 14M HNO<sub>3</sub>-MWNTs range from 6 hr to 24 hr (stable state) due to the most amounts of dispersive Pt nanoparticles. However, like the decay of the electrocatalytic activity for 2M HNO<sub>3</sub>-MWNTs, the electrocatalytic activity of Pt nanoparticles for 14M HNO<sub>3</sub>-MWNTs decreases much significantly from 24 hr to 48 hr because MWNTs may be destroyed very much at 48 hr.

#### **4.3.3.4 Effective activating area**

The electrochemically active surface areas of the Pt nanoparticles are obtained from the CV measurements performed in 1M sulfuric acid electrolyte. A typical voltammogram is shown in Fig. 4.40, in which the potential is expressed versus that of a reference platinum electrode. It is the same as 2M HNO<sub>3</sub>-MWNTs to obtain the integrated area for the hydrogen adsorption peaks in Fig. 4.40. Thus, a horizontal line is drawn to correct the double-layer charging, and a vertical line is drawn to separate the molecular hydrogen region [42]. Moreover, in Table 4.7, the electrochemically active surface areas of the Pt nanoparticles for 14M HNO<sub>3</sub>-MWNTs from 6 hr to 24 hr are in the stable state due to the trend of the electrocatalytic activity of Pt nanoparticles.

#### **4.3.4 Summary**

1. Temperature is one of the main factors if MWNTs modified by HNO<sub>3</sub> form functional groups -COOH and -OH.
2. 2M and 14M HNO<sub>3</sub>-MWNTs at 80<sup>0</sup>C are unfavorable to form functional groups.



3. The modified MWNTs at 100<sup>0</sup>C could oxidize and destroy the surface of MWNTs very much.
4. 90<sup>0</sup>C is the optimum temperature for 2M and 14M HNO<sub>3</sub>-MWNTs to form functional groups.
5. 2M HNO<sub>3</sub>-MWNTs form a lot of functional groups (stable state) from 12hr to 24hr.
6. 14M HNO<sub>3</sub>-MWNTs form a lot of functional groups (stable state) from 6hr to 24hr.
2. Higher concentration of HNO<sub>3</sub> allows the surface of MWNTs to form functional groups quickly.



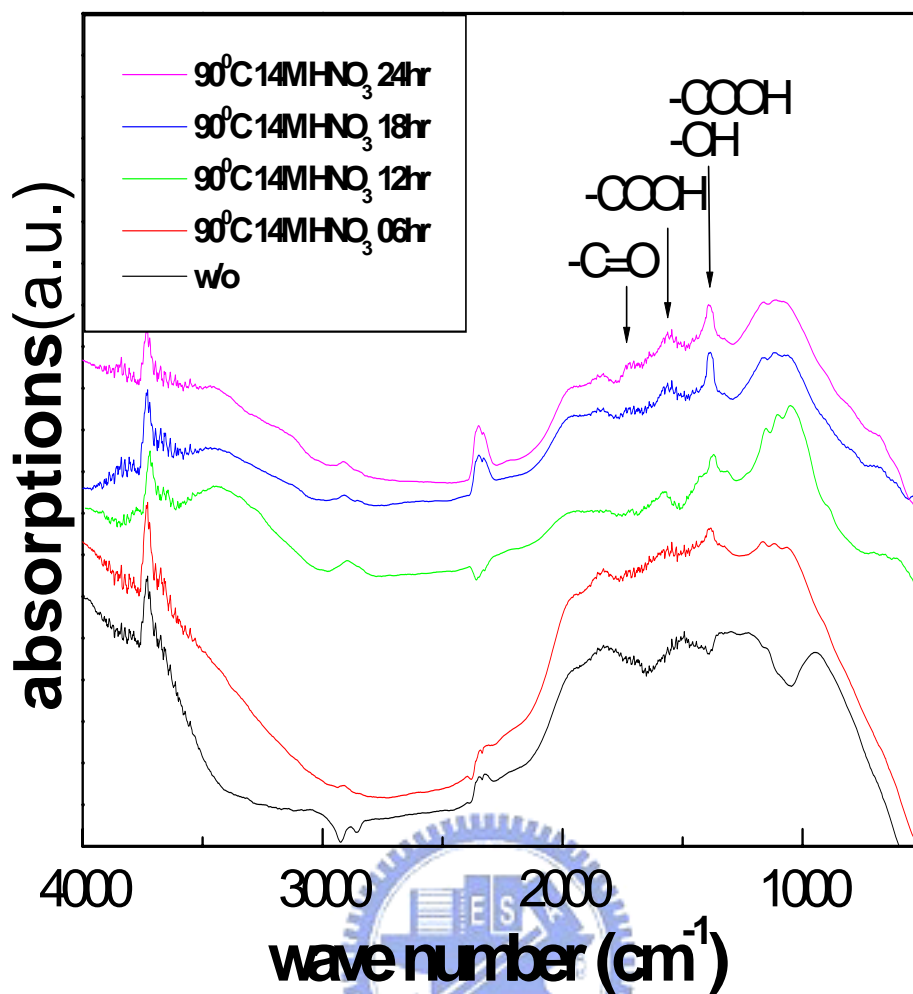


Fig. 4.32 The number of -COOH would increase with t gradually

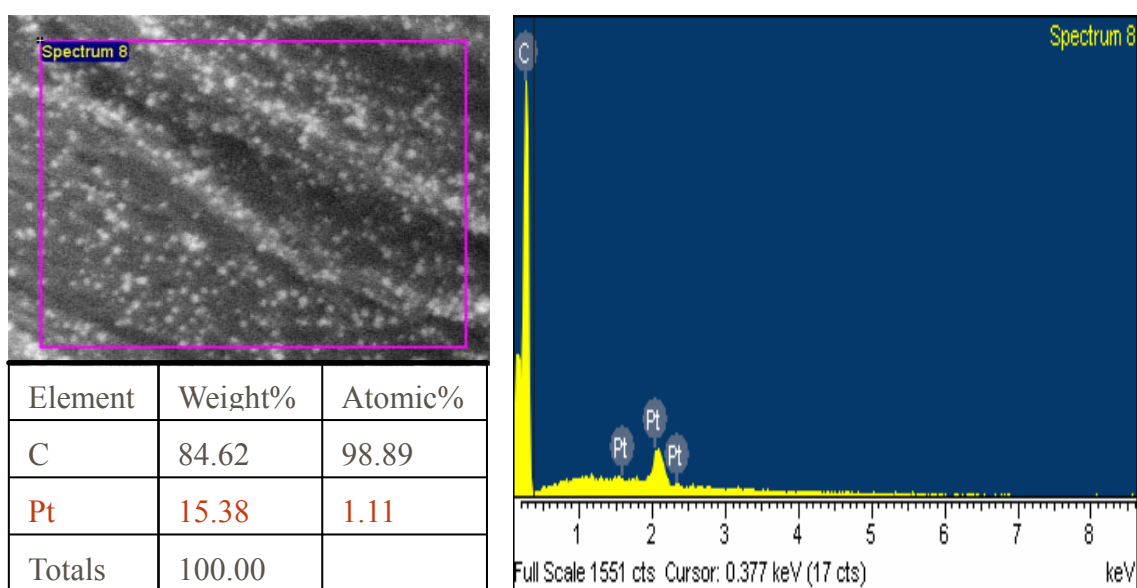
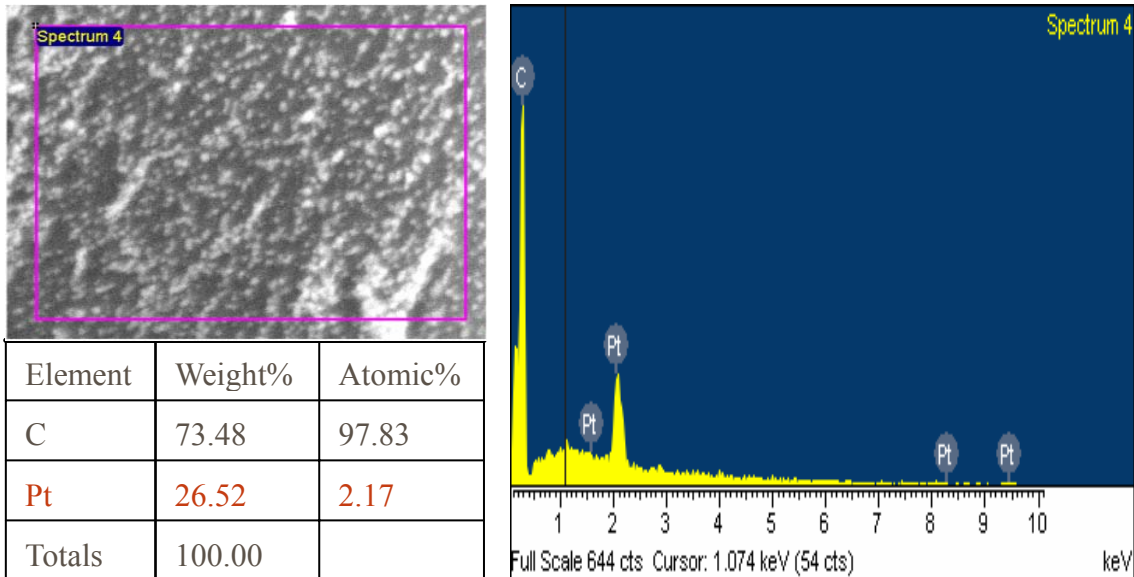
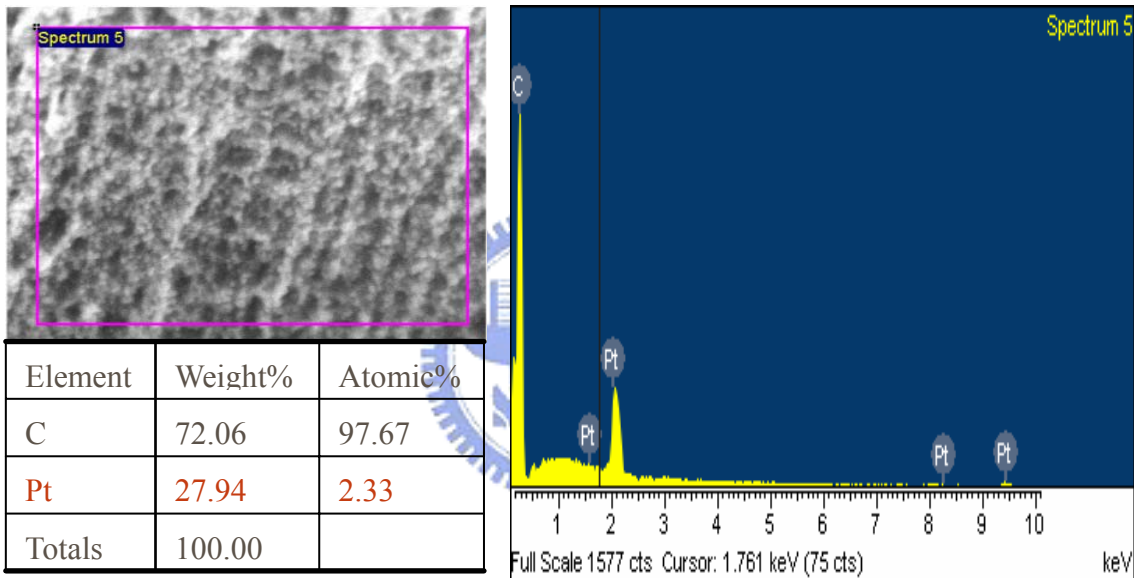


Fig. 4.33 The amount of Pt loading on raw MWNTs is 15.38 wt%



**Fig. 4.34** The amount of Pt loading on 14M HNO<sub>3</sub>-MWNTs at 6 hr is 26.52 wt%



**Fig. 4.35** The amount of Pt loading on 14M HNO<sub>3</sub>-MWNTs at 12 hr is 27.94 wt%

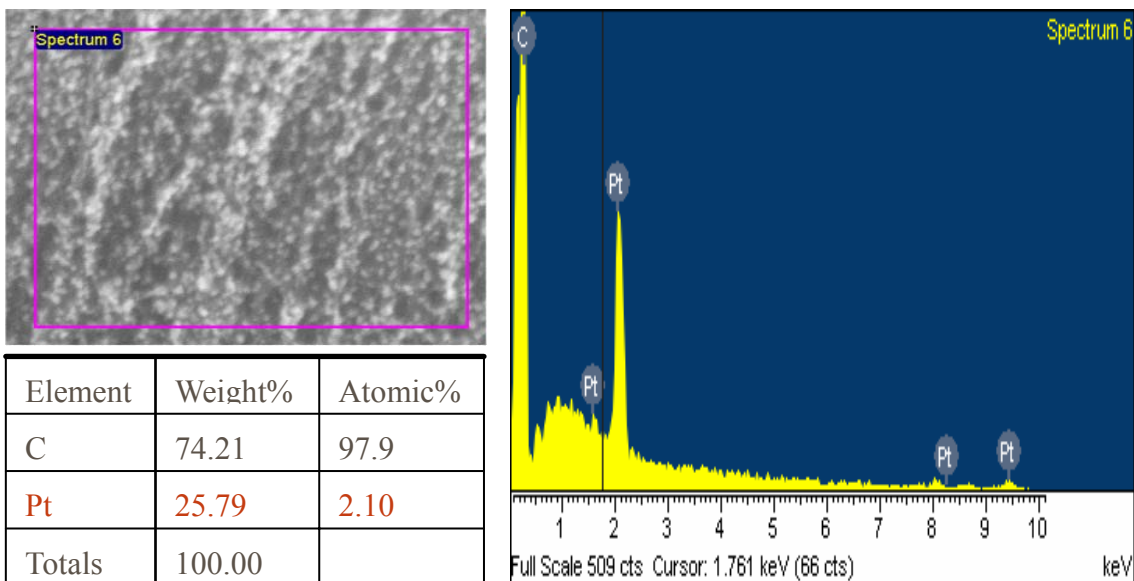


**Fig. 4.36** The amount of Pt loading on 14M HNO<sub>3</sub>-MWNTs at 18 hr is 25.79 wt%

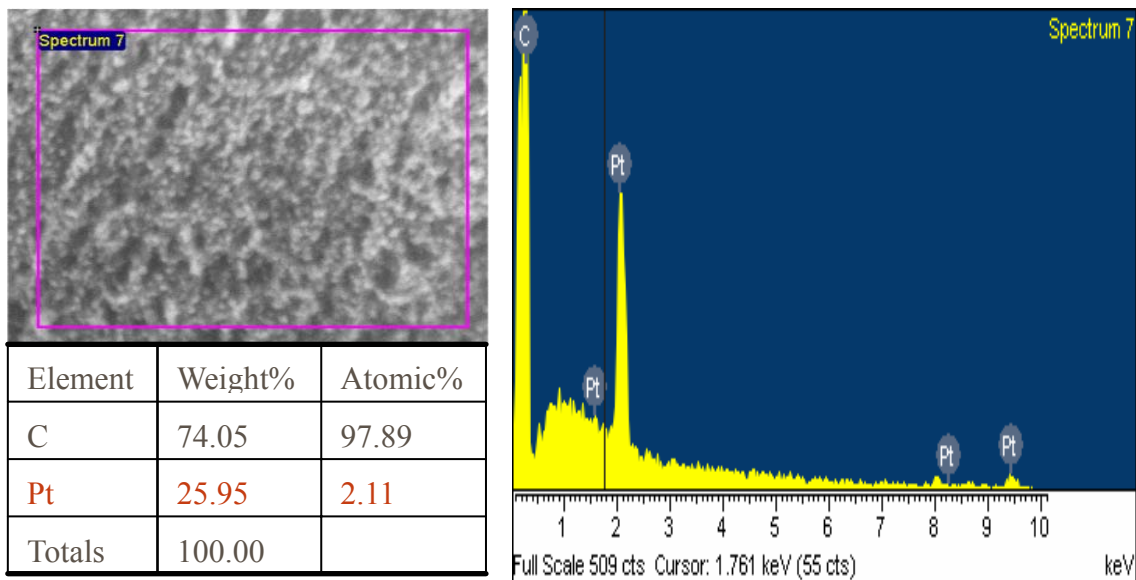


Fig. 4.37 The amount of Pt loading on 14M HNO<sub>3</sub>-MWNTs at 24 hr is 25.95 wt%

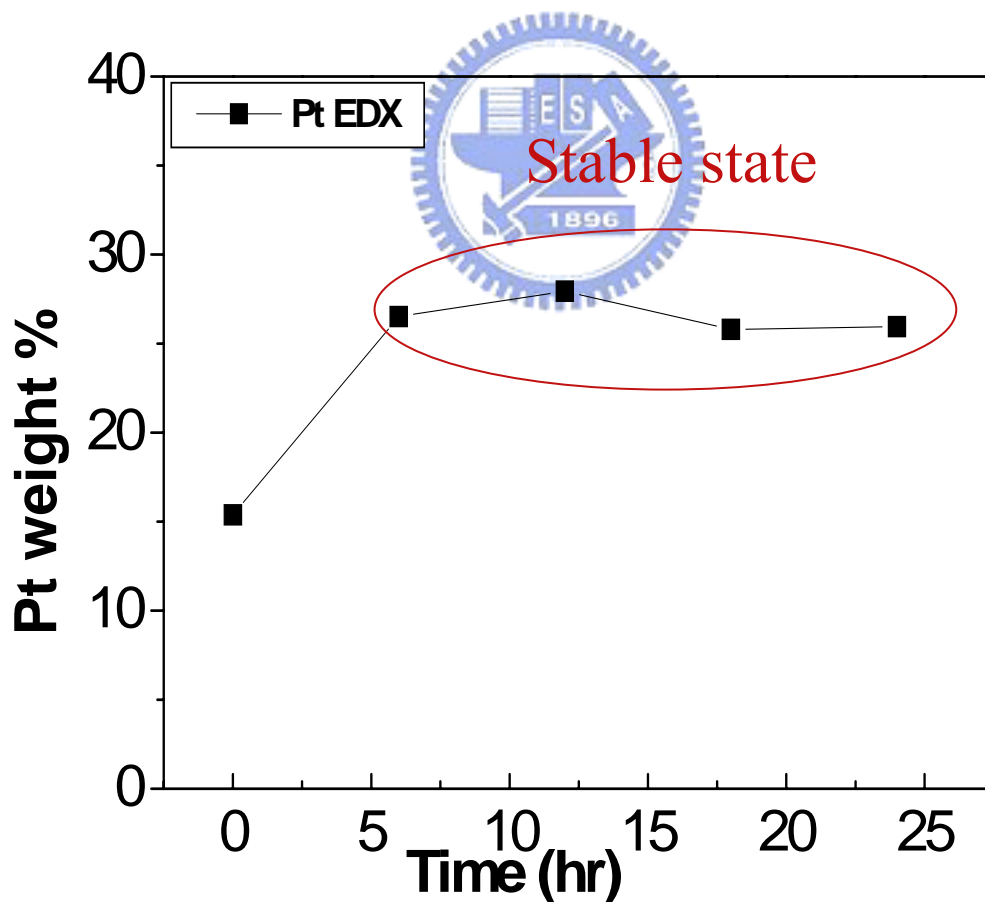


Fig. 4.38 14M HNO<sub>3</sub>-MWNTs from 6 hr to 24 hr may anchor the most Pt

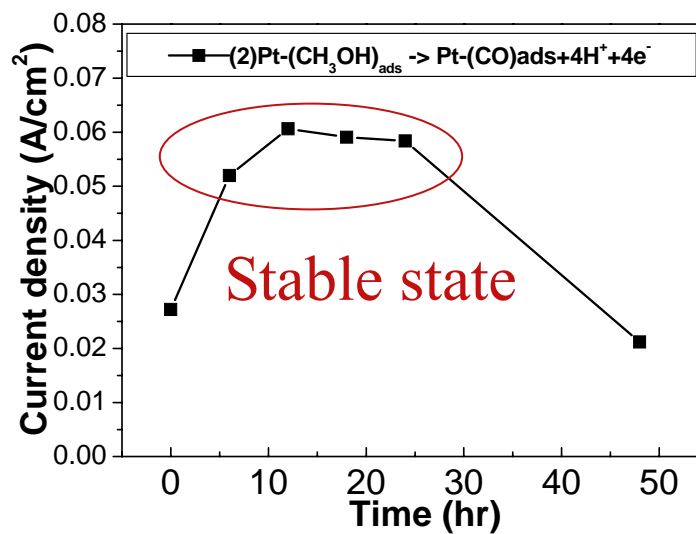
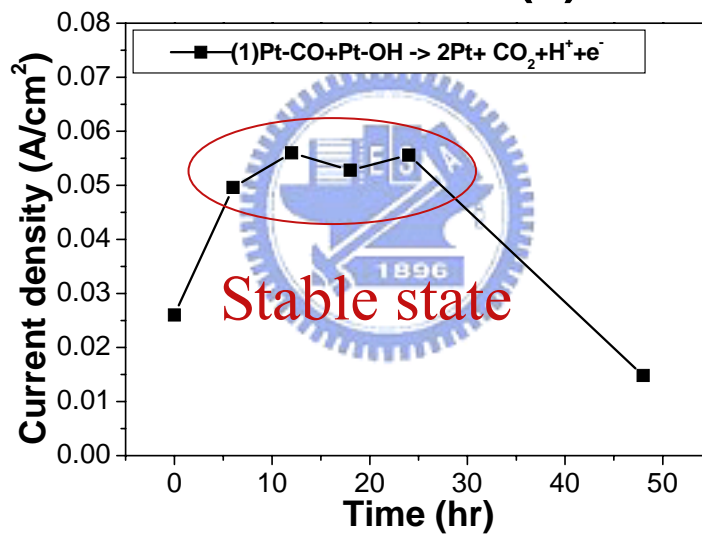
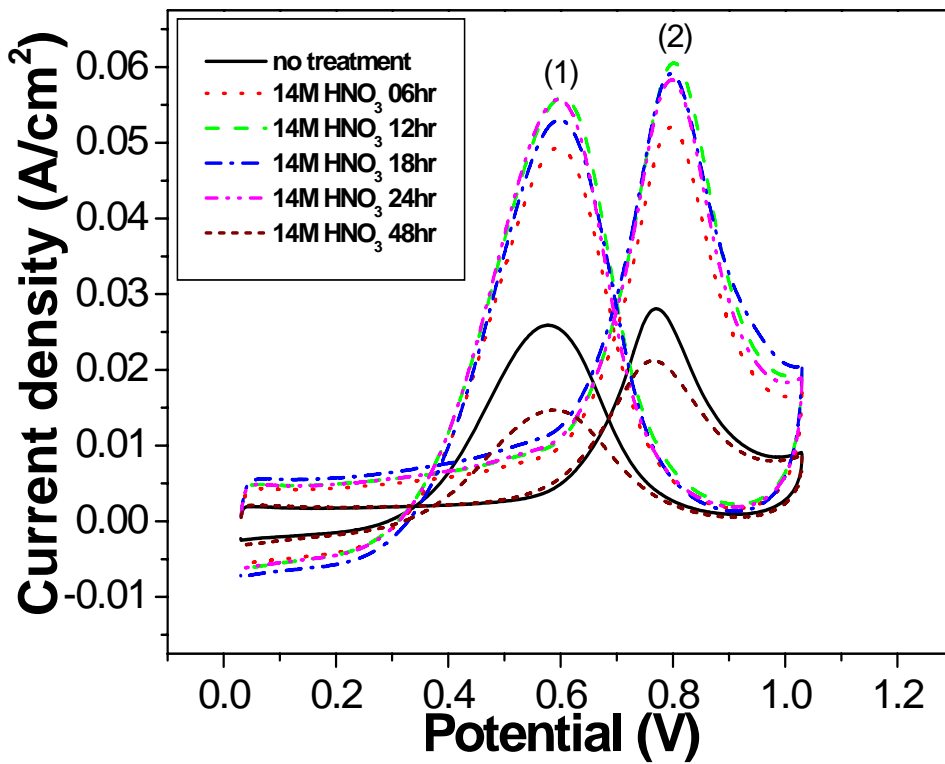


Fig. 4.39 The currents peaks represent the activity of Pt with t

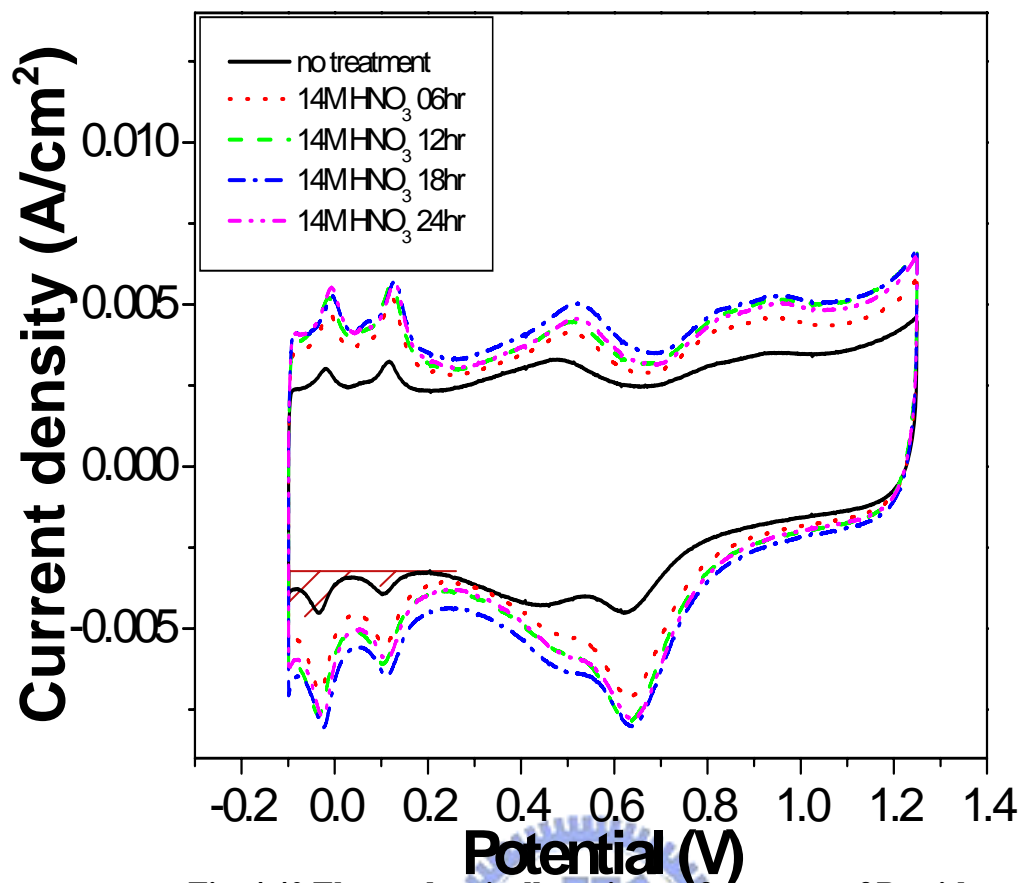


Fig. 4.40 Electrochemically active surface areas of Pt with t



Table 4.7 The value of electrochemically active surface areas of the Pt with the t

Time of 14M HNO <sub>3</sub>	Q <sub>H</sub> (mC)	S <sub>pt</sub> (cm <sup>2</sup> )
00hr	0.1304	0.621
06hr	0.42083	2.004
12hr	0.5032	2.3962
18hr	0.48	2.286
24hr	0.49685	2.366

## 4.4 Analysis of 14M HNO<sub>3</sub>-MWNTs

This chemical modification of MWNTs enabled us to obtain a high dispersion of Pt nanoparticles, even when a large metal load is required on the supports with small surface areas, as in the case of electrocatalysts for fuel cells. Hence, there are two positive factors to rise the electrocatalytic activity and the effective activating surface areas very much. However, there is no significant rise for Pt nanoparticles on MWNTs modified by HNO<sub>3</sub>. For the reason, there may be some negative factors to reduce its electrocatalytic activity. In the other hand, we try to explain the stable state with analyzing 14M HNO<sub>3</sub>-MWNTs. Moreover, TEM images as evidences to support the hypothetical model.

### 4.4.1 Analysis of mean Pt nanoparticle size

The size of Pt nanoparticle is also a factor for electrocatalytic activity in the same weight. Furthermore, the smaller Pt nanoparticles in the same weight represent the more effective activating surface areas. Then, the mean Pt nanoparticle size is analyzed by XRD and TEM.

The Pt nanoparticles on raw-MWNTs and on 14M HNO<sub>3</sub>-MWNTs are shown in Fig. 4.41. Both Pt on raw-MWNTs and on 14M HNO<sub>3</sub>-MWNTs displays the characteristic patterns of Pt fcc diffraction. The 2θ values of the (111) peak is about 39.8° and the Pt (200) diffraction is about 46.4°. The broader diffraction peaks for the catalysts also led to smaller average metal particle size as calculated by the Scherrer equation (1) [43].

$$L = \frac{K \lambda_{K\alpha 1}}{B_{2\theta} \cos \theta_B} \quad (1)$$

where L is the average particle size, K is the constant,  $\lambda_{K\alpha 1}$  is the X-ray

wavelength ( $1.54056 \text{ \AA}$  for  $\text{Cu K}\alpha_1$  radiation),  $B_{2\theta}$  is the peak broadening, and  $\theta_B$  is the angle corresponding to the peak maximum. The calculation results are estimated the average size of about 5.3226 nm for Pt/raw-MWNTs and about 6.76 nm for Pt/14M  $\text{HNO}_3$ -MWNTs in Table. 4.8.

In the other approach, the mean size of Pt nanoparticles on raw-MWNTs and 14M  $\text{HNO}_3$ -MWNTs are analyzed by TEM. The particle size distributions of the metal on MWNTs are obtained by directly measuring the sized of 60 randomly chosen particles in the magnified TEM images. Fig.4.42 and Fig.4.43 show that the average diameters of 5.8802 nm for Pt/raw-MWNTs and 7.29 nm for Pt/14M  $\text{HNO}_3$ -MWNTs are accompanied by relatively narrow particle size distributions (4~10 nm). The estimated average size of Pt nanoparticles is in good agreement with the XRD measurements.

Finally, from XRD and TEM measurements, it is observed that, for 14M  $\text{HNO}_3$ -MWNTs, the diameter of the metal particles deposited is larger than that of raw-MWNTs. By the way, the particle size of Pt may be correlated with the oxidation of MWNTs, which indicates that the efficient deposition of Pt nanoparticles is due to a strong interaction between the metal salt precursor and the functional groups of the MWNTs. Chemical functional groups, namely  $-\text{COOH}$  and  $-\text{OH}$  derived from chemical oxidation processes, act as anchoring sites for metal nanoparticles. These  $-\text{COOH}$  sites may induce the impregnation of larger particles which is a negative factor to rise the electrocatalytic activity and the effective activating surface areas. Hence, there is no significant rise for Pt nanoparticles on MWNTs modified by  $\text{HNO}_3$ .



## 4.4.2 Analysis of MWNTs morphology

Fig. 4.44 (a) shows that raw MWNTs display hollow tubes with amorphous and crystalline layers. It is known that 14M HNO<sub>3</sub>-MWNTs not only opens the closed tips of the tubes, but creates functional groups, -COOH, on the surface to attract metal ions to nucleate. Fig. 4.44 (b) shows that the amorphous surface layers and the cap of MWNTs are removed first with 14M HNO<sub>3</sub> due to its non-crystalline structure. The open cap of MWNTs may allow Pt to get into the inner surface of tubes by the other method in Fig. 4.45. Then, even crystalline layer may be broken for a longer time. In other words, the functional groups on the surface layer of 14M HNO<sub>3</sub>-MWNTs may be removed for a longer time. However, the total number of functional groups may keep a balance on 14M HNO<sub>3</sub>-MWNTs after a certain time. In this work, we take a hypothetical model for stable state in Fig. 4.46 to explain it with TEM image. Although functional groups on the surface layer of 14M HNO<sub>3</sub>-MWNTs may be removed, new functional groups would be formed on the new surface layer which is inner the removed surface layer. Therefore, the total number of functional groups may keep a balance after some time.

## 4.4.3 Summary

1. The amount of functional groups is in the equilibrium during the stable state.
2. COO<sup>-</sup>H<sup>+</sup> attract more Pt precursors to nucleate Pt particle so it produce the larger particle against its efficiency.

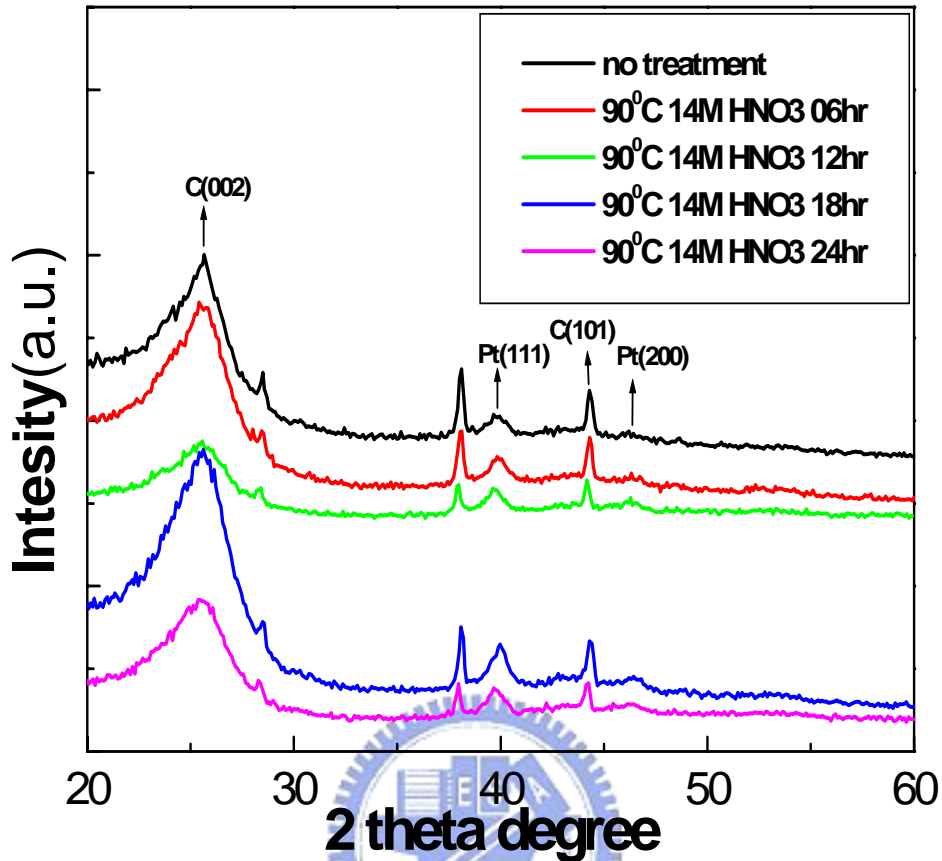


Fig. 4.41 XRD patterns of Pt on raw-MWNTs and 14M HNO<sub>3</sub>-MWNTs

Table 4.8 The average size of Pt/raw-MWNTs and Pt/14M HNO<sub>3</sub>-MWNTs

time	K	$\lambda_{K\alpha 1}$	$B_{2\theta}$	$\theta_B$	size ( $\text{\AA}$ )
0	29.74	1.54	1.08	39.8	53.226
6	29.74	1.54	0.88	39.8	67.74
12	29.74	1.54	0.884	39.7	67.34
18	29.74	1.54	0.8832	39.93	67.6
24	29.74	1.54	0.882	39.7	67.5

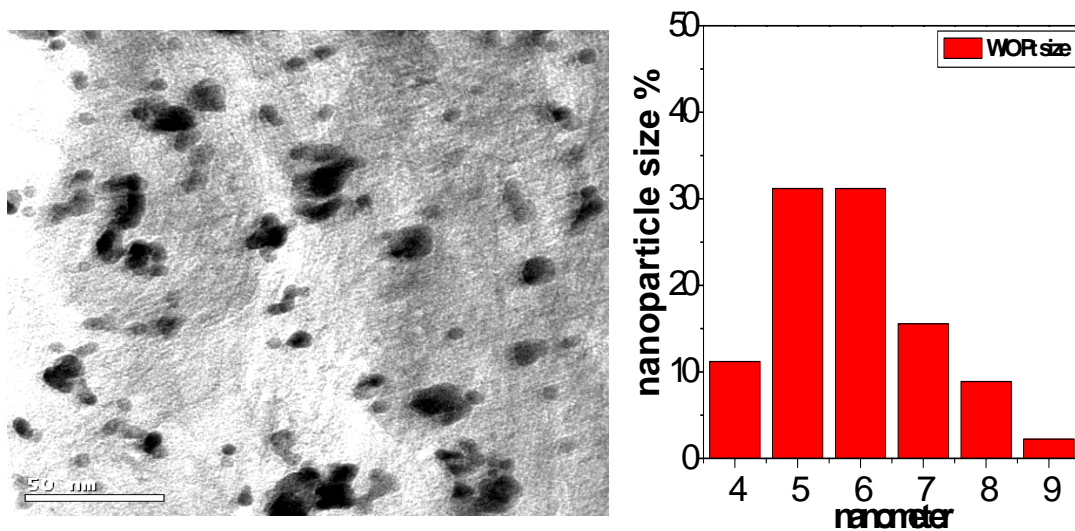


Fig. 4.42 The average diameters for Pt/raw-MWNTs is 5.8802 nm

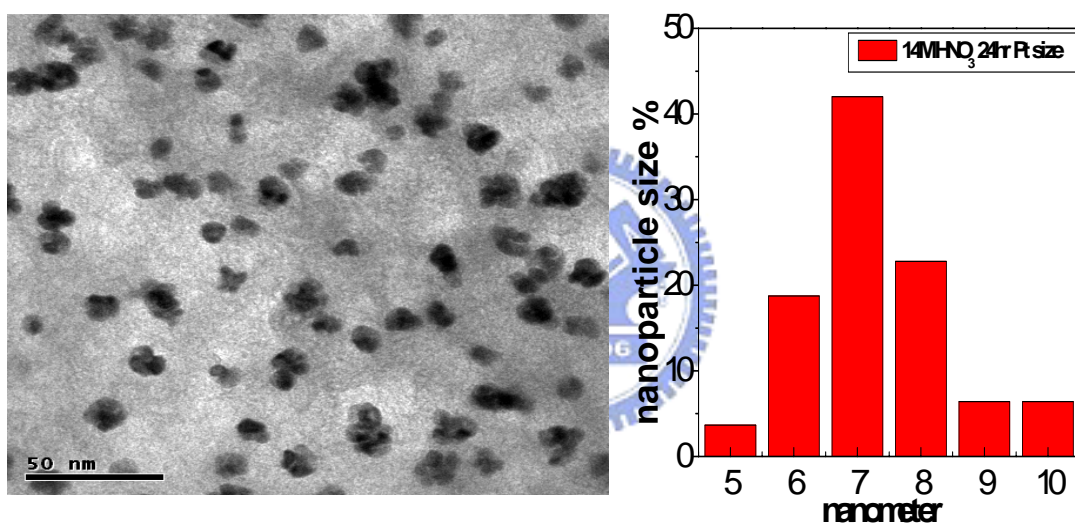


Fig. 4.43 The average diameters for Pt/14M HNO<sub>3</sub>-MWNTs is 7.29 nm

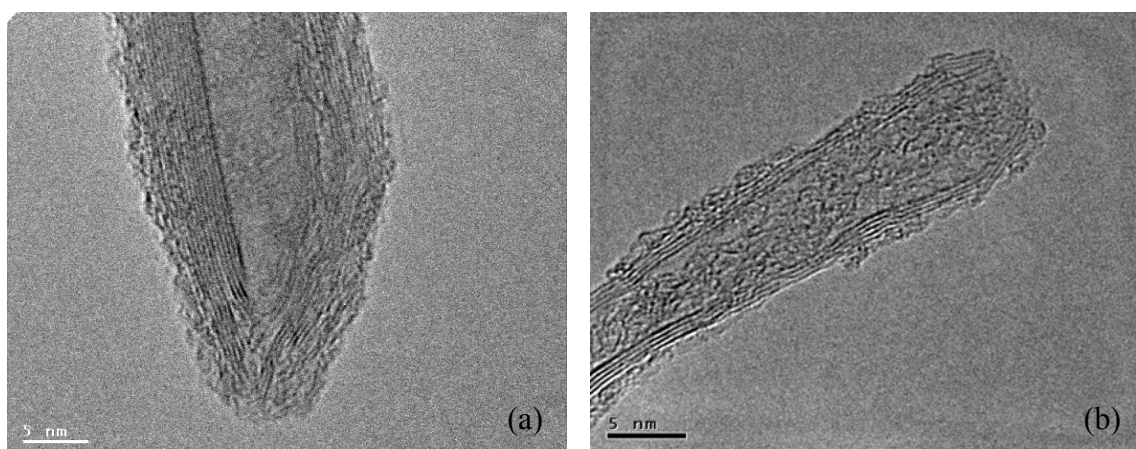


Fig. 4.44 (a) raw MWNTs (b) 14M HNO<sub>3</sub>-MWNTs

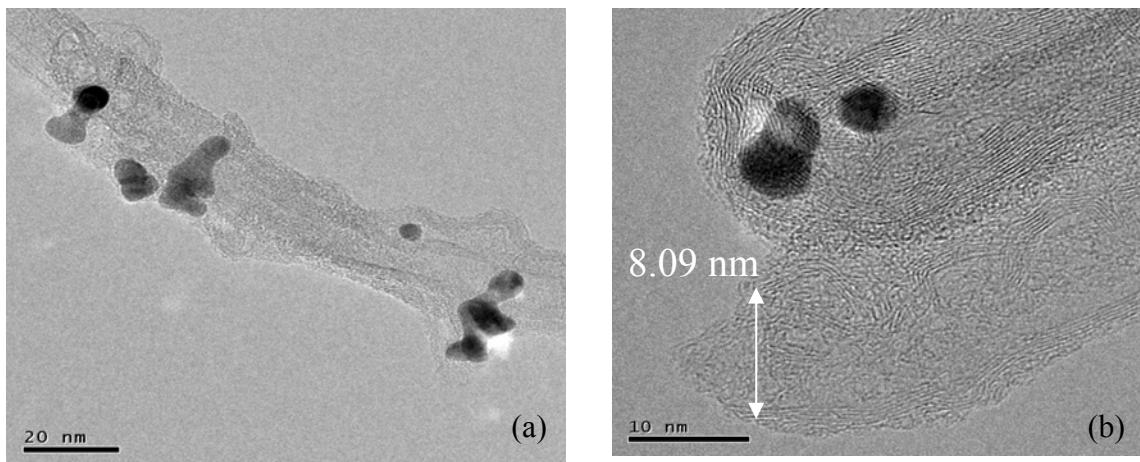


Fig. 4.45 (a) raw MWNTs with Pt (b) 14M HNO<sub>3</sub>-MWNTs with Pt

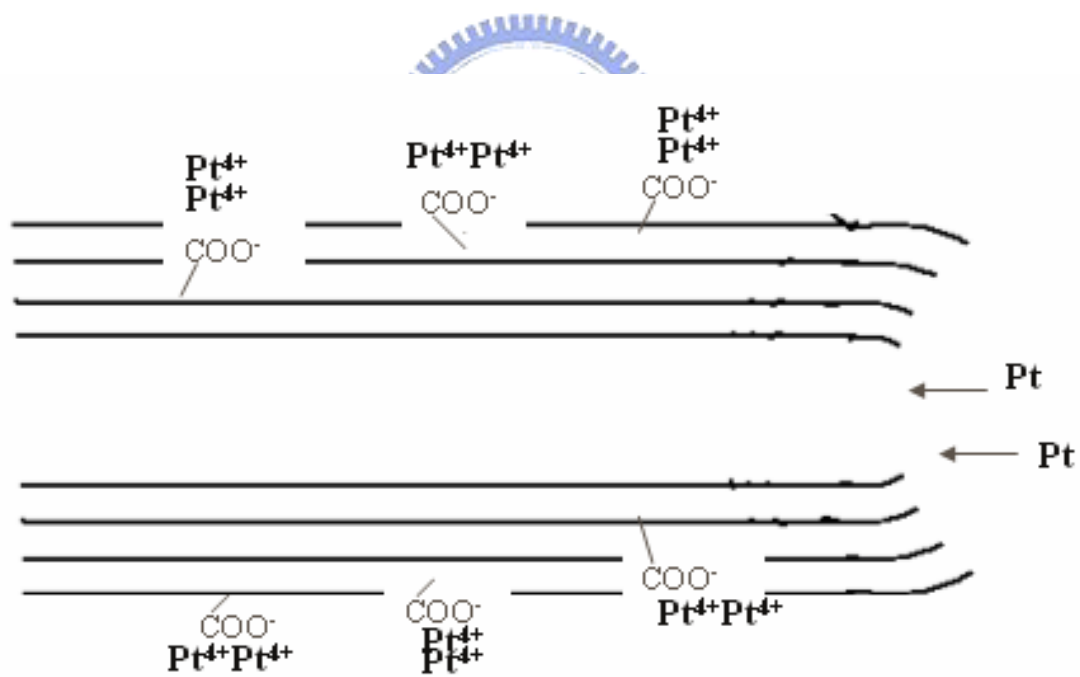


Fig. 4.46 Hypothetical model for stable state of 14M HNO<sub>3</sub>-MWNTs

## Chapter 5 Conclusions

1. Various solvents, eg.  $\text{HNO}_3$ ,  $\text{H}_2\text{SO}_4$ , and  $\text{KOH}$  ( $80^\circ\text{C}$ , 6 hr), modified MWNTs can form the same functional group  $-\text{COOH}$  and  $-\text{OH}$ .
2. Well-dispersed functional groups on MWNTs could improve the efficiency of half-cell test.
3. The functional groups on MWNTs increase anchoring sites of Pt precursors to increase the efficiency of half-cell test.
4. The amount of functional groups in order to attract Pt on  $\text{HNO}_3$ -MWNTs is more than on  $\text{H}_2\text{SO}_4$ -MWNTs and on  $\text{KOH}$ -MWNTs due to a strong oxidizing agent  $\text{HNO}_3$ .
5. Temperature is one of the main factors if MWNTs modified by  $\text{HNO}_3$  form functional groups  $-\text{COOH}$  and  $-\text{OH}$ .
6. 2M and 14M  $\text{HNO}_3$ -MWNTs at  $80^\circ\text{C}$  are unfavorable to form functional groups.
7. The modified MWNTs at  $100^\circ\text{C}$  could oxidize and destroy the surface of MWNTs very much.
8.  $90^\circ\text{C}$  is the optimum temperature for 2M and 14M  $\text{HNO}_3$ -MWNTs to form functional groups.
9. 2M  $\text{HNO}_3$ -MWNTs form a lot of functional groups (stable state) from 12hr to 24hr.
10. 14M  $\text{HNO}_3$ -MWNTs form a lot of functional groups (stable state) from 6hr to 24hr.
11. Higher concentration of  $\text{HNO}_3$  allows the surface of MWNTs to form functional groups quickly.
12. The amount of functional groups is in the equilibrium during the stable state.
13.  $\text{COO}^-\text{H}^+$  attract more Pt precursors to nucleate Pt particle so it produce the larger particle against its efficiency.

## Reference:

1. M.S. Wilson, Membrane catalyst layer for fuel cells, U.S. Pat. No.5,234,777 (1993).
2. Y.-G. Chun, C.-S. Kim, D.-H. Peck, D.-R. Shin, *J. Power Sources* **71** (1998) 174.
3. S.J. Lee, S. Mukerjee, J. McBreen, Y.W. Rho, Y.T. Kho, T.H. Lee, *Electrochim. Acta* **43** (1998) 3693.
4. O.J. Murphy, G.D. Hitchens, D.J. Manko, *J. Power Sources* **47** (1994) 353.
5. E.A. Ticianelli, C.R. Derouin, A. Redondo, S. Srinivasan, *J. Electrochem. Soc.* **135** (1988) 2209.
6. X. Cheng, B. Yi, M. Han, J. Zhang, Y. Qiao, J. Yu, *J. Power Sources* **79** (1999) 75.
7. M.S. Wilson, S. Gottesfeld, *J. Appl. Electrochem.* **22** (1992) 1.
8. M. Uchida, Y. Fukuoka, Y. Sugawara, N. Eda, A. Ohta, *J. Electrochem. Soc.* **143** (1996) 2245.
9. S.H. Joo, S.J. Choi, I. Oh, J. Kwak, Z. Liu, O. Terasaki, R. Ryoo, *Nature* **412** (2001) 169.
10. C.A. Bessel, K. Laubernds, N.M. Rodriguez, R. Terry, K. Baker, *J. Phys. Chem. B* **105** (2001) 1115.
11. N.M. Rodriguez, M.-S. Kim, R. Terry, K. Baker, *J. Phys. Chem.* **98** (1994) 13108.
12. Y.-C. Liu, X.-P. Qiu, Y.-Q. Huang, W.-T. Zhu, *J. Power Sources* **111** (2002) 160.
13. B.C. Satishkumar, E.M. Vogl, A. Govindaraj, C.N.R. Rao, *J. Phys. D* **29** (1996) 3173.
14. B.C. Satishkumar, A. Govindaraj, J. Mofokeng, G.N. Subbanna, C.N.R. Rao, *J. Phys. B* **29** (1996) 4925.
15. W. Li, C. Liang, J. Qiu, W. Zhou, H. Han, Z. Wei, G. Sun, Q. Xin, *Carbon* **40** (2002) 791.
16. G. Che, B.B. Lakshmi, C.R. Martin, E.R. Fisher, *Langmuir* **15** (1999) 750.
17. V. Lordi, N. Yao, J. Wei, *Chem. Mater.* **13** (2001) 733.
18. G. Che, B.B. Lakshmi, C.R. Martin, E.R. Fisher, *Langmuir* **15** (1999) 346.
19. G. Girishkumar, K. Vinodgopal, P.V. Kamat, *J. Phys. Chem. B* **108** (2004) 19960.
20. Z. Liu, J.Y. Lee, W. Chen, M. Han, L.M. Gan, *Langmuir* **20** (2004) 181.

21. Elzbieta Frackowiak, Grzegorz Lota, Thomas Cacciaguerra, Francois Beguin, *Electrochem. Commun.* **8** (2002) 129.
22. B. Rajesh, K.R. Thampi, J.M. Bonard, N. Xanthopoulos, H.J. Mathieu, B. Viswanathan, *J. Phys. Chem. B* **107** (2003) 2701.
23. Z. He, J. Chen, D. Liu, H. Tang, W. Deng, Y. Kuang, *Mater. Chem. Phys.* **85** (2004) 396.
24. Z. He, J. Chen, D. Liu, H. Zhou, Y. Kuang, *Diam. Relat. Mater.* **13** (2004) 1764.
25. D.J. Guo, H.L. Li, *J. Electroanal. Chem.* **573** (2004) 197.
26. Z. Liu, X. Lin, J.Y. Lee, W. Zhang, M. Han, L.M. Gan, *Langmuir* **18** (2002) 4054.
27. B. Rajesh, V. Karthik, S. Karthikeyan, K.R. Thampi, J.M. Bonard, B. Viswanathan, *Fuel* **81** (2002) 2177.
28. C. Wang, M. Waje, X. Wang, J.M. Tang, R.C. Haddon, Y. Yan, *Nano Lett.* **4** (2004) 345.
29. B. Xue, P. Chen, Q. Hong, J.Y. Lin, K.L. Tan, *J. Mater. Chem.* **11** (2001) 2378.
30. R.Q. Yu, L.W. Chen, Q.P. Liu, J.Y. Lin, K.L. Tan, S.C. Ng, H.S.O. Chan, G.Q. Xu, T.S.A. Hor, *Chem. Mater.* **10** (1998) 718.
31. T. Frelink, W. Visscher, and J.A.R. van Veen, *Surf. Sci.* **335** (1995) 353.
32. Ki Chul Park, Takuya Hayashi, Hiroshi Tomiyasu, Morinobu Enbo, and Mildred S. Dresselhaus, *J. Mater. Chem.* **15** (2005) 407.
33. 汪建民，材料分析，中國材料學會，台灣新竹 (1998).
34. L.Q. Jiang, L. Gao, *Carbon* **41** (2003) 2923.
35. B. Rohland, Marlies Pietrzak, S. Moller, Mihaela-C. Bunescu, Marion Wienecke and T. Barfels, *Fullerenes, Nanotubes, and Carbon Nanostructures* **13** (2005) 511.
36. H.J. Wang, H. Yu, F. Peng, P. Lv, *Electrochem. Commun.* **8** (2006) 499.
37. Yong-Tae Kim, Tadaoki Mitani, *J. Catalysis* **283** (2006) 394.
38. T.I.T. Okpalugo, P. Papakonstantinou, H. Murphy, J. McLaughlin, N.M.D. Brown and T. McNally, *Fullerenes, Nanotubes, and Carbon Nanostructures* **13** (2005) 477.
39. T. Teranishi, M. Hosoe, T. Tanaka, and M. Miyake, *J. Phys. Chem. B* **103** (1999) 3818.

40. 衣寶廉，燃料電池-原理與應用，五南圖書出版公司 台灣 (2004).
41. Min Chen and Yangchuan Xing, *Langmuir* **21** (2005) 9334.
42. Woods, R. *Electroanal. Chem.* **9** (1976) 1.
43. B.E. Warren, *X-ray Diffraction*, Addison-Wesley, Reading, MA, 1996.





## 個人簡歷

姓名：莊方慈

性別：男

出生日期：民國 71 年 2 月 16 日

籍貫：台北市

住址：台北市北投區知行路 91 巷 5 號 3 樓

學歷：國立清華大學材料科學與工程學系學士 (89.9-93.6)

國立交通大學材料科學與工程學系碩士 (93.9-95.6)

碩士論文題目：

奈米碳管化學表面改質應用於直接甲醇燃料電池陰極電極之研究

Study of Chemical Surface Modifications of CNTs as cathode electrode for DMFC

